Measuring and modeling canopy photosynthesis of olive orchards

Alejandro Morales Sierra

MSc Thesis Plant Production Systems

PPS-80439

June 2012

Title:

Measuring and modeling canopy photosynthesis of olive orchards

Author:

Alejandro Morales Sierra

Thesis:

MSc Thesis Plant Production Systems

PPS-80439

Date:

April 2012

Supervisors:

Peter Leffelaar, Plant Production Systems, Wageningen University (The Netherlands)

Francisco Villalobos, Agronomy Department, University of Cordoba (Spain)

Examiners:

Xinyou Yin, Centre for Crop Systems Analysis, Wageningen University (The Netherlands)

Table of contents

Figures

Tables

1. Introduction

Olive trees (*Olea europaea* L.) represent an extended horticultural crop in regions with Mediterranean climate, reaching 9.5 Mha worldwide in 2010 (FAO Statistics Division, 2012). The impact of this crop on the regional carbon balance is important, especially in countries were the cultivation of olives is done in extensive surfaces such as Spain, Italy or Greece. Olive cropping systems, which include agroforestry systems, traditional groves and intensive orchards, at high and super-high densities, are of enormous relevance from the economic and ecological perspective. Super-high density olive orchards are planted at a density of 1500-2000 trees ha^{-1} in order to obtain high yields during the first years of establishment and they are pruned to generate a structure suitable for mechanizing all operations (Gomez-del-Campo, 2010). In these orchards, each tree consists of a single main stem and fruits are harvested with modified grape harvesters. When the orchards reach their maximum dimension, the crowns of the trees merge, forming continuous, parallel hedgerows. Due to the very recent implementation of this system (Vossen, 2007), the experimental information is scarce and no measurements or models of canopy photosynthesis have been published, to the knowledge of the author. To fill this gap, the present study focuses on the measurement and modeling of canopy photosynthesis in super-high density olive orchards using as a case study a modern orchard located in Cordoba (Spain). The conclusions obtained from the analysis of the measurements and the proposed model can be easily extended (or applied directly) to other types of irrigated olive orchards.

It is not possible to measure directly photosynthesis at the canopy level and the different methodologies quantify only the net exchange of CO_2 between the canopy or the ecosystem and the atmosphere, which includes respiration fluxes that need to be calculated or measured independently in order to obtain the photosynthetic flux. The accuracy and precision of those independent measurements or calculations needs to be taken into account. The first chapter of this document focuses on the different issues associated to measurements of canopy photosynthesis in fruit trees orchards using micrometeorological techniques including eddy covariance (Baldocchi, 2003) and closed chambers (Reicosky, 1990). The analysis is made for measurements taken during the year 2011 in a super-high density olive orchard in Cordoba, Spain. There are two common strategies to calculate canopy photosynthesis using micrometeorological techniques (Lavigne et al., 1997):

1. Measurement of ecosystem respiration during the night with the an eddy covariance system and extrapolation into daytime through the use of statistical models describing the response of respiration to environmental variables. This respiration is added to daytime measurements of net CO_2 ecosystem exchange to obtain canopy photosynthesis.

2. Measurement of soil respiration (including heterotrophic and autotrophic respiration) and canopy respiration during daylight with closed chambers in different locations on the orchard, averaging these fluxes in space and interpolating in time in order to obtain a continuous time series of field-level soil respiration. These two respiration fluxes are added to daytime measurements of net CO_2 ecosystem exchange to obtain canopy photosynthesis.

It is not clear from the existing scientific literature which is the best strategy *a priori* and both can suffer from strong biases. In strategy 1 the bias is generated by an underestimation of nighttime fluxes due to non-turbulent transport of CO_2. In strategy 2 the bias is generated by sampling error of soil respiration measurements due to the spatial heterogeneity of the soil. To the knowledge of the author, the two strategies have never been compared in detail for fruit tree orchard systems, which have a very different canopy structure compared to crops, forest and grasslands. This different structure also generates different gradients of soil physical properties.

The second chapter focuses on the simulation of canopy photosynthesis, by considering the three-dimensional structure of the canopy and how this affects the scaling of photosynthesis from the leaf to the canopy level. Abundant information exists regarding photosynthesis of olive trees at the leaf scale, but the scaling of this information to the canopy level is not straightforward as the canopy of an olive orchard is not uniform and horizontally continuous. An accurate simulation of radiation profiles within the canopy are needed in order to determine the local conditions in which each leaf performs photosynthesis.

Since the structure of olive canopies varies considerably with planting density, pruning strategy and the age of the plantation, a generic 3D model of radiation interception and photosynthesis (which facilitates its application to other orchards) was preferred to simpler models that are optimized for specific types of structures (e.g. models for row crops). Also, since olive trees are perennial, evergreen plants, the leaves perform photosynthesis under a wide range of environmental conditions and a general, comprehensive, mechanistic model of photosynthesis is desired to describe adequately the behavior of leaves under all these different conditions.

The model Maestra (Luo et al., 2001) is a comprehensive 3D model of canopy radiation interception, transpiration and photosynthesis that has been used extensively for ecophysiological studies in forest science and agroforestry and can be applied to olive orchards, once calibrated. All the necessary experimental information required for its calibration is available in the existing scientific literature, so that the data obtained in the experiment analyzed in first chapter was directly used to test the predictions of the model. A sensitivity analysis was performed to identify those parameters that need to be determined with highest accuracy in future recalibrations. This sensitivity analysis also gives us directions on possible ways to simplify the model if needed.

2. Comparison of two methods to calculate canopy photosynthesis in a super-high density olive orchard

Summary

Net CO_2 ecosystem exchange was measured with an eddy covariance system, in a super-high density olive orchard in Cordoba (Spain). Soil respiration was measured in different locations of the orchard using closed chambers. Several models of ecosystem and soil respiration were fitted to the data and compared using the corrected Akaike Information Criterion. The effect of spatial variability on the parameters of the models of soil respiration was considered explicitly. Canopy respiration was calculated with a published model that required an allometric-based estimation of biomass. Then, canopy photosynthesis was calculated following two strategies: (i) as the sum of net ecosystem exchange and ecosystem respiration and (ii) as the sum of net ecosystem exchange, soil respiration and canopy respiration. For the same environmental conditions, nighttime ecosystem respiration was, on average, 5 µmol CO_2 m^{-2} ground s^{-1} lower than daytime soil respiration. As a result, daily average canopy photosynthesis following strategy 1 varied in the range 7.1-15.9 µmol CO_2 m^{-2} ground s^{-1} but the range for strategy 2 was 15.3-27.7 µmol CO_2 m^{-2} ground s^{-1}. This indicates that at least one of the strategies is strongly biased. The total uncertainty in the calculations was quantified, considering the effect of model error, parameter and model selection uncertainty, using the plugin method, derived from a simplification of Bayesian theory, resulting in an average standard error of 1.8 µmol CO_2 m^{-2} ground s^{-1}. The methodology presented in this study is generic and can be extended to any type of vegetation.

Keywords: Eddy covariance, soil respiration, ecosystem respiration, net ecosystem exchange, Akaike Information Criterion, Bayesian, Likelihood, model selection, olive, *Olea europaea*, superintensive olive, super-high density olive.

2.1. Introduction

The assimilation of CO_2 through photosynthesis is the main process that determines the growth and productivity of plants (Goudriaan and van Laar, 1994) and it is an important flux in the global CO_2 cycle (Cox et al., 2000). Photosynthesis is a well-known process under conditions of no water stress or nutrient deficiency and the use of leaf-level models has been key in ecophysiological studies (Farquhar et al., 2001). However, the environmental conditions within a canopy[1] are not uniform (Goudriaan, 1977) and this affects the scaling of leaf photosynthesis to the canopy level (Leuning et al., 1995). In order to evaluate the different scaling methods, measurements of canopy photosynthesis are required.

[1] By canopy it is meant the above-ground part of a community of plants, including the photosynthetic and non-photosynthetic organs of all individuals. Variables at the canopy level are quantified per unit of ground surface.

These measurements are also needed to quantify the components of the carbon budget associated to different land uses (Baldocchi et al., 2003).

Olive trees (*Olea europaea* L.) represent an extended horticultural crop in Mediterranean regions, reaching 9.5 Mha worldwide in 2010 (FAO Statistics Division, 2012). The impact of this crop on the regional carbon balance is important, especially in countries were the cultivation of olives is done in extensive surfaces such as Spain, Italy or Greece. Olive cropping systems, which include agroforestry systems, traditional groves and intensive orchards, at high and super-high densities, are of enormous relevance from the economic and ecological perspective. Super-high density olive orchards are planted at a density of 1500-2000 trees ha^{-1} in order to obtain high yields during the first years of establishment and they are pruned to generate a structure suitable for mechanization of all operations (Gomez-del-Campo, 2010). In these orchards, each tree consists of a single main stem and fruits are harvested with modified grape harvesters. When the orchards reach their maximum dimension, the crowns of the trees merge, forming continuous, parallel hedgerows. Due to the very recent implementation of this system (Vossen, 2007), the experimental information is scarce and no measurements of canopy photosynthesis are available.

The net exchange of CO_2 between an ecosystem and the atmosphere is composed of gross primary production (i.e. CO_2 fixed by the ecosystem) and ecosystem respiration (i.e. CO_2 released by the ecosystem) which itself is divided into soil and canopy respiration. In the absence of weeds or green covers, canopy photosynthesis in an olive orchard is equal to gross primary production. The most extended method to measure net CO_2 ecosystem exchange is the eddy covariance method (Baldocchi et al., 2003), which measures the average flux of CO_2 for every period of 30 minutes and averaged for a certain surface (i.e. the "footprint" surface) which should be contained within the canopy under study. However, since photosynthesis and respiration occur simultaneously, canopy photosynthesis cannot be extracted directly from the eddy covariance measurements. Thus, an independent measurement of ecosystem respiration is needed. Ecosystem respiration can be measured during the night with the same eddy covariance method, and extrapolated into the day (Baldocchi et al., 2003), using statistical models. However, nighttime measurements by eddy covariance tend to underestimate the fluxes (Aubinet, 2008), which would introduce a bias in the calculations of canopy photosynthesis.

An alternative strategy consists in measuring both soil and canopy respiration. Soil respiration can be measured with closed chambers (Reicosky et al., 1990) and the measurements are performed during the day, so that, in principle, no extrapolation would be needed. However, the variability of soil characteristics generates a spatial variability in soil respiration, which can introduce a bias in the calculations, so that the measurements need to be done in several locations and aggregated. Also, no automatic system is generally available to measure soil respiration and, even when it is available, several measurements have to be rejected due to low quality (Savage et al., 2008), so it is necessary to interpolate in time from the set of measurements performed in the field. Canopy respiration can be measured with opaque chambers that surround a representative portion of the canopy (e.g. a individual tree). Perez-Priego et al. (2012, submitted) measured canopy respiration of irrigated olive trees and proposed a model of specific respiration (i.e. respiration per unit of biomass) as a function of

temperature. In this study, the biomass of the trees was deduced from leaf area and allometric ratios and the model was applied to calculate canopy respiration.

Comparisons of these two approaches in the past have shown mixed results, as in some cases they produced similar estimations (Granier et al., 2000; Wohlfahrt et al., 2005), whereas in other cases there were important differences (Goulden et al., 1996; Lavigne et al., 1997; Law et al., 2001). It is not possible to know *a priori* which approach will be more adequate, as the different sources of error depend on the structure of the canopy, meteorological conditions and soil variability, so that a site-specific comparison of their accuracy and precision is needed.

Statistical models are generally used to predict[2] ecosystem and soil respiration (Desai et al., 2008), but a high variety of different expressions have been proposed and no model has been proven to be superior to the rest (Desai et al., 2008; Richardson et al., 2006). Complex models[3] may predict the data used for calibration very accurately but fail to make accurate predictions under new situations as they incorporate part of the measurement error as information during the calibration process (Zucchini, 2000). To avoid this "overfitting" of the model, several model comparison criteria exist to evaluate the tradeoff between goodness of fit and model complexity. Information criteria (Burnham and Anderson, 2002) are useful model comparison criteria, due to their simplicity, generality and strong theoretical basis. As these criteria are based on the method of maximum likelihood (Bolker, 2008) they are compatible with any error distribution, which is important as non-Normal distributions have been reported for eddy covariance and soil respiration measurements (Richardson et al., 2008; Savage et al., 2008).

There are several sources of uncertainty that will reduce the accuracy and precision of the predictions and they have to be properly combined (Draper, 1997). Any measurement contains errors which, combined with the variability unexplained by the model results in a model error or residual. This error generates a first source uncertainty in the predictions of the model. The fact that the values of the parameters are not known but have to be estimated from the data is a second source of uncertainty (i.e. parameter uncertainty) and the necessity to select a model out of a series of alternative candidate models represents a third source of uncertainty (i.e. model selection uncertainty). Different methodologies will result in different calculations of predictive uncertainty (Richardson & Hollinger, 2005) due to their different assumptions, but, to the knowledge of the author, the only generic methodology that integrates all the sources of uncertainty described in the above is Bayesian method (Draper, 1997). It will be shown that adopting this method does not increase substantially the technical complexity of the study as, under the assumption of asymptotic conditions (which are reasonable given the size of the samples obtained in the experiment), the Bayesian posterior distribution can be

[2] In this study, the term prediction does not refer to forecasts of the future, but rather to interpolations in time. Since an interpolation calculates a variable when it is unknown, it is not statistically different from a prediction. This terminology enables the comparison with the standard statistical literature.

[3] In this study, the complexity of a model is characterized by the number of free parameters. Other aspects like the nature of the mathematical expression or the interdependence of the parameters are not considered.

approximated by the likelihood function (Walker, 1967) without having to choose any prior distribution (Bolker, 2008).

In this study, a comparison of the two strategies to estimate canopy photosynthesis is presented using flux measurements in a super-high density olive orchard in Cordoba (Spain) during Spring and Summer 2011. Several statistical models were proposed to capture the response of respiration to environmental variables and their relative performance was evaluated with the corrected Akaike Information Criterion (Burnham and Anderson, 2002). The effect of spatial variability on soil respiration was included by measuring at different locations in the orchard and by including the effect of this variability explicitly in the parameters of the model. The uncertainty in the predictions of canopy photosynthesis following both strategies was calculated with a simplified Bayesian approach. The methodology presented in this study is generic and can be applied to any experiment where flux measurements are available.

2.2. Materials & Methods

2.2.1. Site description

The experiment was performed in the farm "La Harina" located in Cordoba, Spain (37° 44' N, 4° 36' W, altitude 170 m) in the Spring and Summer of 2011. The system studied was a 21.5 ha olive orchard (*Olea europaea* L. cv. "Arbequina") planted in 2005, spaced at 4 x 1.5 m, with rows oriented on the NNW-SSE axis (figure 1.1B). The soil is a Xerofluvent (IGN, 2011) with vertic properties as described by the Soil Taxonomy classification system (NRCS, 2006). The climate in the area is typically Mediterranean, with an average annual rainfall of 600 mm, with almost no rain in the summer, and an average annual reference evapotranspiration of 1390 mm.

The orchard was drip-irrigated with two emitters per tree (total discharge rate of 4.4 l h^{-1} $tree^{-1}$). Irrigation was applied twice every week, with an extent of 7 hours per application. The trees were pruned every two years, with a mechanical topping that reduced height to 2.5 m and lateral, manual pruning. During the experiment, the height of the canopy was 3 m. The pruning residues were chipped and spread over the soil surface. Weeds in the rows were controlled chemically. No tillage was performed and, during winter, a green cover was allowed to grow in the alleys between the planted rows, being eliminated in spring by mowing. However, due to the rainfall in Spring 2011, the green cover grew again, occupying the alleys, and was not eliminated until the day 172 of the year (i.e. mid-June).

2.2.2. Experiment – Soil respiration

Soil respiration was measured with a closed chamber (Luo and Zhou, 2006), using a chamber of 0.118 m^2 of basal surface and 0.032 m^3 of volume. In every measurement, the air inside the chamber was mixed with a fan and the increasing concentration of CO_2 was measured during 90 s at a frequency of 1 Hz by an infrared gas analyzer (model LI–820, LI–COR Biosciences, Lincoln, Nebraska, USA). To avoid the dilution of CO_2 due to the increase of water vapor inside the chamber, the air was dried by forcing it through a glass tube filled with silica gel. Air temperatures inside the chamber were measured with a thermocouple (type k or chromel–alumel) at the start, middle and end of the measurement and

interpolated linearly. A tube with a small diameter on the top of the chamber allowed the equilibration of the air pressure inside the chamber with the atmosphere.

The Rate Regression Method (Reicosky et al., 1990) was applied to derive the flux of CO_2. In this method, a parabola is fitted to each series of CO_2 concentration versus time and the flux (F_{CO2}, µmol CO_2 m^{-2} ground s^{-1}) is obtained from the first derivative of the parabola evaluated at time = 0:

$$F_{CO_2} = \left.\frac{d\left(CO_2(t)273.15 \Big/ \left(T_{air}(t)V_{mol,0}\right)\right)}{dt}\right|_{t=0} \frac{V}{A} \qquad (1.1)$$

Where CO_2 is the measured molar concentration (µmol CO_2 mol^{-1} air), T_{air} is air temperature inside the chamber (K), $V_{mol,0}$ is the molar volume of air at an air temperature of 273.15 K (22.4 10^{-3} m^3 air mol^{-1} air), V is the volume of the chamber (m^3) and A is the basal area of the chamber (m^2). All measurements where the parabola had a coefficient of determination (R^2) lower than 0.9 were rejected, as recommended by Savage et al. (2008).

The use of collars to attach the chamber to the surface of soils with vertic properties under Mediterranean conditions faces several problems including the high level of compaction of the upper layers when the soil is dry and the formation of cracks in the soil due to shrinkage in the process of drying. Thus, no collar was used and the chamber was placed directly on the soil surface, but weight was applied on its top to ensure proper contact between soil surface and the chamber. Each location where soil respiration was measured was marked with paint on the border. The chamber was covered by aluminum foil to minimize heating during the measurements.

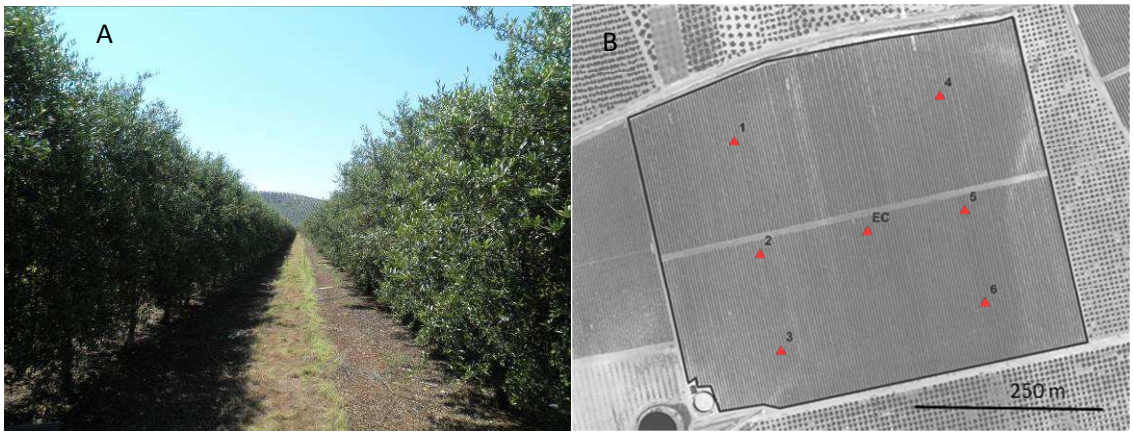

Figure 1.1: Example of an alley in the super-high density olive orchard (A) and a sketch of different locations (red triangles with numbers) where soil respiration was measured (B). The triangle in the center indicates the position of the eddy covariance system (EC) and the black solid represents the borders of the orchard. North–South axis corresponds to the vertical axis of the image. The sketch (B) was drawn on an orthophotograph of the area taken in 2009 (Infraestructura de Datos Espaciales de Andalucia, Seville, Spain). The photograph of the alley (A) was taken by the author during the experiment.

In order to calculate the average soil respiration at the field level, it was necessary to consider the effect of the spatial variability of the soil. The use of chambers with a high basal area allows integrating the small scale variability (in the order of centimeters). To capture the variability at the scale of meters, six areas of the orchard were chosen in a systematic distribution, symmetric with respect to the location of the eddy covariance system (figure 1.1B).

The canopy was discontinuous as the trees were organized in parallel hedgerows (figure 1.1A). Irrigation was also discontinuous in space as it was applied locally with drippers close to the base of the trees. Such spatial arrangement generated important gradients of soil temperature, water content and root density, which would induce a gradient in soil respiration (Tang and Baldocchi, 2005). To include this gradient, for every area where soil respiration was measured (figure 1.1B) two locations were chosen, one beneath the canopy and one in the center of the alley, for a total of 12 locations in the orchard.

In every location, soil temperature and water content were measured using thermocouples (type k) buried at 7.5 cm and capacitance probes (model 10HS, Decagon Devices Inc., Pullman, Washington, USA) buried at 5 cm, respectively. The apparent sensitivity of soil respiration to temperature varies with the depth at which temperature is measured (Phillips et al., 2011) and diurnal cycles may show a hysteresis behavior due to the time lags in soil temperature at different depths. Savage et al. (2009) reported a minimum hysteresis effect at 5 cm, though Gaumont-Guay (2006) reported that this depth varied seasonally. In addition, four sensors measured continuously, every 30 minutes, the water content and temperature beneath the canopy and in the alley next to the eddy covariance system (figure 1.1B).

The temporal variation of soil respiration is characterized by different timescales (Savage et al., 2009), but the ones relevant to this study were the diurnal and seasonal scale. Thus, measurements were taken approximately every 10 days, with 4-6 measurements per location and day (evenly distributed between 600 and 1800 GMT). Measurements of soil respiration started on mid-May (DOY 140) and finished at the end of July (DOY 210). Since the green cover was present during the first 30 days of the experiment, the grass was removed at each location. Although those measurements were not representative of the soil respiration in the orchard during those days, the data were used to calibrate the models and the interpolation was performed only after DOY 172, once the green cover had been removed.

2.2.3 Experiment – Eddy covariance and auxiliary measurements

An eddy covariance system was installed in the center of the orchard (figure 1.1B). The system measured continuously from 20 May 2011 until 24 October 2011 (DOY 140 - 297) and it consisted of a three-dimensional sonic anemometer (model CSAT3, Campbell Scientific Inc., Logan, Utah, USA) and an open path CO_2/H_2O analyzer (model LI7500, LI-COR Biosciences, Lincoln, Nebraska, USA). Both sensors were placed 6 m above the ground and separated horizontally by 20 cm. Air temperature and relative humidity were measured at the same height as wind velocity with a combined probe (model CS215, Campbell Scientific Inc., Logan, Utah, USA). All the sensors were connected to a datalogger (model CR1000, Campbell Scientific Inc., Logan, Utah, USA), that registered the measurements with a sampling rate of 10 Hz. The instruments and dataloggers were mounted on a mast to avoid distortions of the air flow.

During nighttime, CO_2 concentration was measured at two heights (0.3 and 3.0 m) with a closed-path CO_2 analyzer (model LI-820, LI-COR Biosciences, Lincoln, Nebraska, USA). Canopy temperature was measured with an infrared[4] thermometer (model IRTS-P, Apogee Instruments, Inc., Logan, Utah, USA) mounted on a pole at a height of 4 m and the data was registered each 15 min in a datalogger (model CR1000, Campbell Scientific Inc., Logan, Utah, USA). The measurements were corrected for the reflection of sky-emitted infrared radiation (Verhoef, 1995).

The eddy covariance technique calculates the net CO_2 ecosystem exchange (NEE, μmol CO_2 m^{-2} soil s^{-1}) from the covariance between the fluctuating components of vertical wind velocity (ω', m s^{-1}) and CO_2 mixing ratio (c', μmol CO_2 mol^{-1} air) obtained from Reynolds decomposition[5] (Baldocchi, 2003):

$$NEE = \overline{\rho_a}\ \overline{\omega' c'} \qquad (1.2)$$

Where ρ_a is the air density (mol air m^{-3} air). Equation 1.2 is only valid under the following assumptions:

1. The system is in a steady state and turbulence is well developed;
2. The surface under study is homogenous;
3. There is no advection;
4. There is no storage or depletion of CO_2 between the measurement height and the ground;
5. The mean wind flow is parallel to the local horizontal plane of the anemometer.

These assumptions describe an ideal system and any measurement performed under conditions that deviate excessively from these assumptions should be rejected or corrected. In this study, deviations from assumptions 4 and 5 were corrected using published values whereas deviations from assumptions 1-2 were quantified and fluxes were rejected if these deviations were excessive, using published quality tests (Foken et al., 2004; Gockede et al., 2008). In addition, corrections were applied to the raw data due to the physical limitations of the measuring system (see below for details). The only assumption that was not corrected or used to filter data was advection, as it requires a more complex experimental setup with multiple sonic anemometers (Aubinet, 2008). Not taking into account advection may generate underestimations of nighttime fluxes. All the calculations, corrections (except storage correction) and quality tests described below were performed with the software Turbulent Knight 3 (Mauder and Foken, 2011). In the following paragraphs, the different corrections and filters are described in more detail.

The time averages were defined for periods of 30 minutes. Spikes in the signal generated by the electrical noise were eliminated using the algorithm of Vickers and Mahrt (1997). The fact that the anemometer and the CO_2 sensor were separated by 20 cm introduced a time lag in the measurements, which was corrected by cross-correlation. The maximum sampling frequency was limited to 10 Hz and

[4] Here, infrared radiation refers to the radiation emitted by bodies on the surface of the Earth. Thermal radiation is a synonym. This is not to be confused with the near infrared radiation that is part of the solar spectrum.

[5] Any variable C measured during a certain period of time in a turbulent flow can be decomposed into $c = \overline{c} + c'$ where $\overline{c}$ is the time average and c' is the fluctuation or deviation between each measurement and the time average.

the minimum was imposed by the averaging period (1/30 min = 5.5 10^{-4} Hz). Thus, low and high frequencies in the turbulent spectrum were being filtered by the measurement system, underestimating the real flux. This was corrected using transfer and gain functions as defined by Moore (1986), based on the theoretical spectral models of Kaimal et al. (1972) and Højstrup (1981). Fluctuations in air temperature and water vapor modify air density and this was taken into account with the method of Webb et al. (1980). The angle between the local horizontal plane of the anemometer and the mean wind flow was corrected by the method of the planar fit (Wilczak et al., 2001).

The first quality test evaluated the stationarity of the system, by dividing each period of 30 minutes into six sub-periods of 5 minutes and calculating the covariance for each sub-period. The relative difference between the covariance for the whole period and the average covariance from the six sub-periods is a measure of stationarity (Foken et al., 2004). Fluxes with relative differences larger than 30% were rejected, as recommended by Ruppert et al. (2006).

The second quality test evaluated if the turbulent regime was well developed. The similarity theory for the surface-layer turbulence (Monin and Obukhov, 1954 in Foken et al., 2004) was used to evaluate the turbulent regime in each measurement. The concept of similarity implies that the ratio between the standard deviation of a turbulent variable and its turbulent flux is a function of atmospheric stability (Foken, 2008). The ratios were calculated for CO_2 and whenever they deviated from the theoretical values by more than 30%, the measurement was rejected, as recommended by Ruppert et al. (2006).

The third quality test evaluated if the measured fluxes were being generated from within the orchard. The test uses the footprint function of Kormann and Meixner (2001). The footprint function is a continuous bi-dimensional function that calculates, for any surface (S), the fraction of the total flux measured by the eddy covariance that was generated in S[6]. This footprint function is analytical and uses the advection-diffusion equation to simulate the transport in the direction of the wind and a Normal density function for the transport in the direction perpendicular to wind (Kormann and Meixner, 2001). A raster matrix was created using an orthophotograph of the orchard (figure 1.1B) where each pixel represented a square grid cell of 0.5 m^2. The matrix was recoded into binary values where pixels located inside of the orchard had a value of 1 and pixels located outside had a value of 0. For every measurement, a raster matrix with the same dimensions and resolution was created and the footprint function was calculated for each pixel. The values of both matrices for each pixel were multiplied and then added to obtained the total fraction of the flux that had been generated from within the orchard. If more than 20% of the flux had been generated outside the orchard, the flux was rejected, as recommended by Gockede et al. (2008).

During nighttime, the average rate of change of the amount of CO_2 stored between the surface and the eddy covariance measurement height was calculated from the vertical profiles of CO_2 concentration, for every period of 30 minutes, and added to the eddy covariance measurement. However, if the correction in the flux is larger than 30%, the measurement was rejected. This is justified as there was no quality

[6] Another way to interpret the footprint function is as the bivariate probability density that a particle on the ground at point $A(x_A,y_A,0)$ will be transported to point $B(x_B,y_B,z_B)$ where the eddy covariance measurement is taken.

control of the measurements of the CO_2 profile, and large rates of change could be related to errors in the measurement of the profiles. The vertical profiles of CO_2 were not measured during daytime as it was assumed that the canopy was well ventilated and coupled to the upper atmospheric layers (Villalobos et al., 2000).

2.2.4. Modeling

2.2.4.1. Statistical models of soil and ecosystem respiration

Several types of models have been proposed to predict ecosystem and soil respiration obtained by eddy covariance and soil respiration chamber measurements, including nonlinear regressions, lookup tables and artificial neural networks (Desai et al., 2008). Several comparisons have been published (Desai et al., 2008; Falge et al., 2001; Richardson et al., 2008), but there is no evidence that any model is superior to the rest. In this study, respiration was described using simple non-linear regression models that were compared using information criteria (see section 2.2.4.3.2) to quantify model selection uncertainty (Burnham and Anderson, 2002).

2.2.4.1.1. Modeling soil respiration

To calculate photosynthesis following strategy 2, soil respiration needs to be calculated. The simplest approach to describe soil respiration is the model proposed by van't Hoff (1898) from which the rest of empirical models can be deduced:

$$R_T = R_{ref} e^{b(T-T_{ref})} \quad (1.3)$$

where R_T (µmol CO_2 m^{-2} ground s^{-1}) is respiration at temperature T (°C), R_{ref} is respiration at reference temperature T_{ref}, and b is an empirical parameter describing the response to temperature ($°C^{-1}$). The effect of other environmental factors can be included as modifications of either the reference respiration (equivalent to the assumption that the effects are independent) or the sensitivity to temperature. Soil respiration in the alleys and beneath the canopy were modeled independently, but the list of candidate of models was the same for both types of locations.

Table 1.1: Models of soil respiration. T is soil temperature (°C), θ is the soil water content (cm^3 water cm^{-3} soil), D is the day of year in radians (2π = 365 days) and β_i are empirical parameters. Each model is identified by a unique ID.

Model ID	Expression
m_1	$\beta_1 \exp\left\{\beta_2\left[(293.15-\beta_3)^{-1}-(T+273.15-\beta_3)^{-1}\right]\right\}$
m_2	$\beta_1(\beta_2+\beta_3\sin D+\beta_4\cos D)^{(T-20)/10}$
m_3	$\beta_1 \exp\left\{\left[\beta_2+\beta_3(\theta-0.2)\right]\left[(293.15-\beta_4)^{-1}-(T+273.15-\beta_4)^{-1}\right]\right\}$
m_4	$\left(\beta_1+\beta_2\theta+\beta_3\theta^2\right)\beta_4^{(T-20)/10}$
m_5	$\left(\beta_1+\beta_2\sin D+\beta_3\cos D\right)\beta_4^{(T-20)/10}$
m_6	$\left(\beta_1+\beta_2\sin D+\beta_3\cos D\right)\exp\left\{\left[\beta_4+\beta_5(\theta-0.2)\right]\left[(293.15-\beta_6)^{-1}-(T+273.15-\beta_6)^{-1}\right]\right\}$

Six alternative models of soil respiration (table 1.1) were proposed:

- Model 1: Lloyd and Taylor (1995) observed that the sensitivity to temperature of soil respiration decreased with increasing soil temperatures and proposed a modified version of the Arrhenius equation where the activation energy decreased as temperature increased.

- Model 2: Long-term experiments have shown that the temperature sensitivity of soil respiration varies seasonally (Reichstein and Beer, 2008) which includes the effects of soil water content, phenology and modifications of the composition of soil biota. Richardson et al. (2008) proposed a model based on first-order Fourier series to describe the variation of respiration with respect to the day of year.

- Model 3: Among other effects, low soil water content reduces biological activity in the soil through cell dehydration whereas high soil water contents reduce the amount of oxygen available for respiratory processes (Luo & Zhou, 2006). These effects can be interpreted as a modification of the sensitivity to temperature and the equation proposed by Reichstein et al. (2002) was used.

- Model 4: Soil water content also affects the diffusivity of gases in the soil and may alter the specific composition of the soil biota as some species enter into a dormant state at low soil water contents (Luo & Zhuo, 2006). These effects can be translated into a modification of the reference soil respiration. To account for these effects, a parabolic function was proposed.

- Model 5: The seasonal variability may also induce changes in reference respiration, through root mortality, changes in allocation of assimilates to roots or changes in the composition of soil biota. A model based on first-order Fourier series was proposed.

- Model 6: In this model it was assumed that soil water content affected the temperature sensitivity whereas seasonal effects were related to the reference respiration. Thus, models 3 and 5 were combined into one single model.

For every model, 4 variants were proposed, based on how the spatial variability was being taken into account. The identification of the variant was done by adding a numeric suffix to the model ID (table 1.1):

- Variant 1: Variant in which the spatial variability was not included in the parameters of the model. This means that the model predicted soil respiration already averaged for the different locations.

- Variant 2: Variant in which the spatial variability was incorporated in one of the parameters describing reference respiration, that is, β_1 for all the models. This means that a different β_1 value was estimated for each location, whereas the rest of the parameters were assumed “global” and estimated with the data pooled from all locations.

- Variant 3: Variant in which the spatial variability was incorporated in one of the parameters describing the sensitivity to temperature (for models 1 through 4) or seasonal variability of the

reference respiration (for models 5 through 6). This means the parameter β_2 in all models except for model 4, for which the location-specific parameter was β_4.

- Variant 4: Variant in which the effect of spatial variability on reference respiration and the sensitivity to temperature or seasonal dynamics (depending on the model) was included. In corresponds to the combination of variants 2 and 3, that is, location-specific β_1 and β_2 for all models except for model 4 (β_1 and β_4).

For example, the respiration at location i based on model m43 is calculated as $\left(\beta_1+\beta_2\theta_i+\beta_3\theta_i^2\right)\beta_{4,i}^{(T_i-20)/10}$ where parameters β_1 through β_3 are the same for all locations but parameter β_4 has a different value for each location i. This means that model m43 has a total of 9 parameters, because β_4 is location-specific. The author is not aware of any published work in which spatial variability of soil respiration is incorporated via location-specific parameters. This method is completely deterministic and is not to be confused with hierarchical Bayesian models that have been used in studies of soil respiration (e.g. Cable et al., 2011), where the parameters are substituted by probability distributions that capture the spatial variability.

In variants 2-4, the predictions of soil respiration were calculated for each location and then aggregated to the field level. In variant 1, the model predicted directly the field-level aggregated soil respiration. For variants 2-4, local temperature and soil water content were estimated from the continuous measurements assuming a linear relationship that was calibrated with the samples taken at the same time as soil respiration using robust linear regression models based on iterative re-weighted least squares (Venables and Ripley, 2002).

Soil respiration was aggregated to the field-level assigning weights to soil respiration in the alleys and beneath the canopy. In order to determine these weights, it is necessary to characterize the fraction of the orchard that belongs to each type of location, based on the gradients of environmental conditions and sources of CO_2. The surface wetted by the drippers formed a strip of 50 cm wide, but the extension of the wet bulbs below the soil surface was unknown. The root distribution was also unknown, but Fernandez et al. (1991) reported for olive trees that roots grew mainly within the wet volumes affected by the drippers and Searles et al. (2009) observed that most of the roots were located within 1 m from the line of drippers for different types of olive orchards. It was then assumed that stripe of 1 m wide centered at each line of drippers was representing the same conditions as in the locations beneath the canopy. This means that measurements in the alley and beneath the canopy were weighted by 0.75 and 0.25.

2.2.4.1.2. Modeling ecosystem respiration

To calculate photosynthesis following strategy 1, ecosystem respiration needs to be calculated. Ecosystem respiration is the sum of soil respiration and canopy respiration, but, unless both sources of CO_2 are measured independently, it is not possible to distinguish them. Testi et al. (2008) showed that the ratio of soil to ecosystem respiration in an olive orchard decreased from 1 to 2/3 as the orchard

grew up to a leaf area index of 1.5. Davidson et al. (2005) reported that the ratio of soil to ecosystem respiration varied seasonally in a spruce forest from 0.45 to 0.80.

Assuming that soil respiration was the main source of CO_2 during the experiment, ecosystem respiration was modeled using the same models proposed for soil respiration (table 1.1), but always using the first variant as the spatial variability in measurements with eddy covariance was not considered. This choice implies that, whatever the actual ratio between soil and ecosystem respiration is, the changes in ecosystem respiration are assumed to be correlated with changes in soil temperature, water content and day of year. During the night, both the canopy and the soil were cooling down so that the dynamics of canopy and soil temperature are similar. However, during daytime, their dynamics will differ, which could affect the accuracy of the method if the ratio between soil and ecosystem respiration happens to be low. The continuous sensors of temperature and water content were used in the calculation of ecosystem respiration, by weighting each sensor with the same weights used for aggregating soil respiration in the alleys and beneath the canopy.

2.2.4.1.3. Calculation of plant respiration

To calculate photosynthesis following strategy 2, the respiration of the canopy needs to be calculated. As it was not measured during the experiment, it had to be calculated from an existing model (Perez-Priego et al., submitted). Using allometric coefficients and the biomass of leaves, it was possible to estimate the biomass of the rest of the organs. The biomass of leaves was deduced from the specific leaf area. Two samples of 100 leaves were taken, choosing fully expanded leaves distributed throughout the entire canopy. They were sealed into a refrigerated plastic bag to avoid dehydration in the transport and their surface were measured with an area meter (model LI-3000, LI-COR Biosciences, Lincoln, NE). They were dried in an oven for 48 h and weighted again to obtain the dry matter content. The result was a specific leaf area of 50.0 (2.2) 10^{-4} m^2 g^{-1} DM.

The biomass stored in the wood of the trees was deduced assuming a wood:leaf ratio of 0.7:0.3 based on the data published by Mariscal et al. (2000b) and Villalobos et al. (2006). Out of the total woody tissue, 85% was considered tissue with low metabolic activity and 15% tissue with high metabolic activity (Perez-Priego, submitted). The respiration of these tissues was simulated using the model of Lloyd and Taylor (1994) with the parameters obtained by Perez-Priego et al. (submitted) from chamber measurements:

$$R_{wood} = W_{wood} R_{w,18} \exp^{E_0\left(\frac{1}{291.15-T_0} - \frac{1}{T+273.15-T_0}\right)} \quad (2.4)$$

Where R_{wood} is the respiration of wood material (µmol CO_2 m^{-2} ground s^{-1}), W_{wood} is wood biomass (kg DM m^{-2} ground), $R_{w,18}$ is respiration per unit of biomass at 18 °C (µmol CO_2 kg DM s^{-1}), and E_0 and T_0 (K) are empirical parameters. $R_{w,18}$ was 0.06 and 0.95 µmol CO_2 s^{-1} kg^{-1} DM for low and high activity tissues, E_0 was 200 and 166 K and T_0 was 247 and 256 K, respectively.

2.2.4.2. Likelihood functions

Since measurements always contain errors and models are simplifications of reality, there would always be deviations or residuals between the predictions of a model and the data. These residuals (i.e. model error) generate an uncertainty about which model will best predict the system (parameter and model selection uncertainty) and how accurate the predictions of that model will be (predictive uncertainty). The first step to account for the different sources of uncertainty is to build a probability model (p) with a mean equal to the predictions of the descriptive model (m), and a variance component that describes the dispersion of the residuals (Bolker, 2008). In its simplest form, as used in this study, the probability model lumps all the sources of model error in a single function (Brown, 2010). If only measurement error was included, the probability model would be incomplete.

The use of a probability model does not imply that the data was collected with a random procedure nor that the process is stochastic, as the causes of the deviations could all be deterministic, but since we do not know those causes, we may use probability theory to describe our lack of information (Jaynes, 2003). Indeed, the data in this study was not collected randomly and soil and ecosystem respiration were assumed to be entirely deterministic.

The likelihood function (L) for continuous probability models is equal to the product of the probability density (p) of each individual datum, x_i (Fisher, 1922):

$$L(\beta \mid x) = \prod_{\forall i} p(x_i \mid \beta) \qquad (1.5)$$

Where β is the vector of parameters of the probability model and x_i is each datum. The vertical bar separates variables (on the left) and parameters or fixed quantities (on the right). In the probability model, β is fixed and x is variable, whereas in the likelihood function the x is fixed and β is variable. β includes the parameters of the deterministic model (m) and the variance of the probability model. Since the probability model describes the distribution of residuals, it depends on both the measurement error and the variability in the data not captured by the model and it cannot be determined *a priori* which probability distribution is most adequate. The function p is a conditional probability density, that evaluates the probability density of x_i conditional on β. The function L is not a probability function (it does not integrate up to 1) but an analogous notation is used to indicate that the likelihood of β is conditional on the data, x.

Richardson et al. (2008) reported that the residuals of a model that predicted CO_2 fluxes with respect to measurements with eddy covariance were symmetric, with a higher kurtosis than expected from a Normal distribution and with a variance that increased with the flux. Several studies have shown similar properties for the measurement error in eddy covariance and soil respiration (Hollinger and Richardson, 2005; Richardson et al., 2006; Savage et al., 2008; Stauch et al., 2008). The choice of probability model affects the estimation of the parameters of the model (van Wijk et al., 2008) so it is important to use the most adequate probability model. Two main probability models can be proposed based on the literature:

1. A Laplace distribution where the scale parameter is linearly related to the flux (Richardson et al., 2006, 2008; Savage et al., 2008). The probability model corresponds to:

$$p(x|\beta) = HeL_i(x|\beta) = \frac{1}{2\left(\beta_{p,1} + \beta_{p,2} m_i(\beta_d)\right)} \exp\left(-\frac{|x - m_i(\beta_d)|}{\beta_{p,1} + \beta_{p,2} m_i(\beta_d)} \right) \quad (1.6)$$

Where $\beta_{p,1}$ and $\beta_{p,2}$ are the parameters related to the variance of the residuals, m_i is the mean of the distribution and represents the deterministic component (see section 2.2.4.1.1) and β_d is the vector of parameters of this deterministic component. The suffix HeL substitutes the "m" in the identification code of each model to indicate that the deterministic component is combined with a Laplace probability model with heterogeneous variance. For example, the model "m42" is associated to the probability model "HeL42".

2. A Normal distribution with a standard deviation linearly related to the flux (Hollinger and Richardson, 2005; Stauch et al., 2008). The probability model corresponds to:

$$p(x|\beta) = HeN_i(x|\beta) = \frac{1}{\sqrt{2\pi\left(\beta_{p,1} + \beta_{p,2} m_i(\beta_d)\right)^2}} \exp\left(-\frac{\left(x - m_i(\beta_d)\right)^2}{2\left(\beta_{p,1} + \beta_{p,2} m_i(\beta_d)\right)^2} \right) \quad (1.7)$$

Where the parameters have the same meaning as in equation 1.5. The suffix HeN is used in the same way as discussed for the Laplace model. In some of the sites studied by Richardson et al. (2008), the linear coefficient of the variance ($\beta_{p,2}$) was small, which suggests that it could be simplified and assumed equal to zero. Thus, two additional types of distribution were proposed (HoL and HoN) that are equivalent to equations 1.5 and 1.6 but assuming $\beta_{p,2}$ = 0. That is, in those probability models the variance is homogeneous.

Note that the methodology has resulted into 6 descriptive models, with up to 4 variants and 4 probability distributions. Accounting for all the respiration fluxes, it amounts to a total of 216 expressions. On the one hand, it does not seem reasonable to fit all these expressions, but on the other hand, all the aspects discussed in the above need to be considered rigorously. Therefore, a strategy with minimal assumptions is presented to simplify the implementation of the method. This strategy assumes that the choice of probability model does not have a major impact of each descriptive model (i.e. if one descriptive model is better than another, this will hold for all probability distributions as long as they are both estimated with the same probability distribution). The strategy contains of four steps:

1. The parameters of the different deterministic models were estimated using a Normal probability model with constant variance. This is described in section 2.2.4.3.1.

2. All the models were compared using an information criterion. This is described in section 2.2.4.3.2.

3. For a small subset of the best performing models, the four alternative probability models are estimated and compared with the same information criterion. The different sources of uncertainty are quantified for the best performing models. This is described in section 2.2.4.3.2.

4. The model-weighted uncertainty in the predictions of respiration is calculated for the best performing models using the values generated in the previous step. This is described in section 2.2.4.3.3.

2.2.4.3. Parameter estimation, model selection and uncertainty in predictions

The information-theoretic[7] methodology described by Burnham and Anderson (2002) was used to quantify and estimate the different sources of uncertainty. The uncertainty in the predictions will be calculated using Bayesian integration (Koch, 2007), by approximating the posterior distribution of the parameters by a Normal distribution (Walker, 1967). The information-theoretic approach to modeling assumes that all models are approximations to reality and the goal is not to find the "true model"[8] or the "true value" of a parameter, but rather the model and parameter values that best predict the observed reality. The degree of closeness to reality is not evaluated in absolute terms but relative to the set of alternative candidate models and it is found by minimizing a relative discrepancy function (Kullback and Leibler, 1951) as proposed by Akaike (1973). A brief description of the theory is presented in the following sections, but the reader is referred to Burnham and Anderson (2002) for a more detailed discussion.

In the following, f will denote reality, indexed by x (i.e. x represents every position in space and instant in time that are relevant to the experiment) and p is the model. The Kullback-Leibler information divergence (Kullback and Leibler, 1951) between reality and the model is

$$D\left(f, p(\cdot|\beta)\right) = \int f \log\left(\frac{f}{p(\cdot|\beta)}\right) dx \qquad (1.8)$$

The symbol "·" indicates that the discrepancy is averaged over the reality of the experiment. For a given experiment, reality is fixed and unknown, so the equation can be transformed into:

$$D\left(f, p(\cdot|\beta)\right) = E_f\left[\log\left(f\right)\right] - E_f\left[\log\left(p(\cdot|\beta)\right)\right] = C - E_f\left[\log\left(p(\cdot|\beta)\right)\right] \qquad (1.9)$$

Where C is an arbitrary constant common to all models and E_f represents the expectation operator over reality. Given a model p, the information-theoretic approach estimates the value of β that maximizes the last term in equation 1.8, once β has been estimated using the data, the relative divergence of the calibrated model (i.e. $D\left(f, p(\cdot|\hat{\beta})\right)$ where $\hat{\beta}$ is the optimal value of β) is used to select the best performing

[7] The term "information-theoretic" refers to the fact that the methodology is derived from applying the concepts of information theory (Shannon, 1948; Kullback and Leibler, 1951) to statistical inference. The approach in this study refers exclusively to the paradigm described by Burnham and Anderson (2002) as information theory has other applications in statistics (e.g. Jaynes, 1957; Bernardo and Smith, 1994; Caticha and Preuss, 2004).

[8] For simplicity, in this section, by model it is meant the probability model as described in section 2.2.4.2 and not the deterministic model as described in section 2.2.4.1.

model (Burnham and Anderson, 2002). Note that this information divergence is unknown and has to be estimated from the data, as described in the following sections.

2.2.4.3.1. Parameter estimation

In this section, it is described how to choose the value of $\hat{\beta}$. For a given model p, the vector β_0 is defined as the vector that minimizes the relative divergence:

$$\beta_0 = \underset{\beta \in B}{\arg\min}\left(D\left(f, p(\cdot|\beta)\right)\right) \tag{1.10}$$

This is a desirable value for β, but we cannot evaluate it as we cannot calculate the divergence. However, the maximum likelihood estimator (Fisher, 1922), $\hat{\beta}$, converges asymptotically to β_0 (Burnham and Anderson, 2002; Lele, 2004), with an stochastic error in the approximation that decreases with the amount of data used in the estimation. $\hat{\beta}$ is defined as:

$$\hat{\beta} = \underset{\beta \in B}{\arg\max}\left(L\left(\beta|x\right)\right) \tag{1.11}$$

Where the function L is the likelihood function described in section 2.2.4.2. Thus, the maximum likelihood method is an optimal information criterion to estimate the parameters of model p. An example of what is meant by asymptotic convergence is shown for model HoN_5 of ecosystem respiration in figure AI.3 of Appendix I.

As the error in the approximation is stochastic, there is an uncertainty about the value of β_0 and this uncertainty can be described by a multivariate Normal distribution, where the mean is $\hat{\beta}$ and the variance-covariance matrix (V) is estimated from the curvature of the logarithm of the likelihood function evaluated at the maximum likelihood estimation (Bolker, 2008):

$$V \approx I = \left[-\frac{\partial^2 \log\left(L\left(\hat{\beta}|x\right)\right)}{\partial \beta^2} \right]^{-1} \tag{1.12}$$

Where I is the observed information matrix (Fisher, 1922). Since the logarithm is a monotonic function, the maximum of both the likelihood function and its logarithm are found for the same β (Bolker, 2008). Thus, to facilitate the calculation of V, the log likelihood was maximized instead of the likelihood. The optimization was done in two steps:

1. A first global optimization was performed using the simulated annealing algorithm with logarithmic cooling schedule (Belisle, 1992) and 200,000 iterations.

2. Starting at the solution of the global optimization, a local optimization was performed using the Nelder-Mead algorithm (Press, 2007).

All the calculations were performed using the "bbmle" R package (Bolker and R Development Core Team, 2012).

For some models (especially in the variants with location-specific parameters), the log-likelihood function was not smooth and the second partial derivative was not a good approximation to the information matrix. In that case, log-likelihood profiles for each parameter were built (Bolker, 2008), a parabola was fitted to each profile (as the logarithm of a Normal distribution is a parabola) and the second derivative of the parabola was used to quantify the variance. An example comparing the two approaches is presented in figure A1.4 of Appendix I.

2.2.4.3.2. Model selection

The expected relative information divergence for the calibrated model can be approximated by the expression (Akaike, 1973):

$$D\left(f, p\left(\cdot \mid \hat{\beta}\right)\right) = C - E_f\left[\log p(\cdot \mid \hat{\beta})\right] \approx C - E_y E_x\left[\log p(x \mid \hat{\beta}(y))\right] \quad (1.13)$$

Where x is the sample of reality measured in the experiment and y represents any other independent sample from the same reality. The double expectation at the end of equation 1.12 can itself be approximated by an information criterion (IC) which has the following general form (Akaike, 1973):

$$E_y E_x\left[\log p(x \mid \hat{\beta}(y))\right] \approx IC = \log\left(L\left(\hat{\beta} \mid x\right)\right) + bias \quad (1.14)$$

Where bias is an expression that will vary for the different information criteria. Following the recommendations of Burnham and Anderson (2002), the corrected Akaike Information Criterion (AIC_c) was used in this study (Sugiura, 1978):

$$AIC_c = -2\log\left(L\left(\hat{\beta} \mid x\right)\right) + 2k\frac{n}{n-k-1} \quad (1.15)$$

Where n is the number of elements in x (i.e. the sample size) and k is the number of free parameters in the model. Note that the criterion has been multiplied by -2 as proposed by Akaike (1973) so that the first term of equation 1.14 is equivalent to the sum of the squares of the residuals in the case of Normal probability models. Since AIC_c is a relative measure (i.e. only the differences are useful, see equation 1.8), it can be multiplied by any arbitrary integer (Burnham and Anderson, 2002). The model with the lowest AIC_C will be the model that has the minimum relative Kullback-Leibler information divergence (equation 1.8). When n is large, the second term in equation 1.14 converges to 2k, and AIC_c will be equivalent to the classic Akaike Information Criterion (Akaike, 1973).

Note that when the variants 2-4 of models of soil respiration are used (see section 2.2.4.1.1) it is not clear which is the sample size, as some parameters are being estimated with all the data pooled from all locations whereas other parameters are being estimated with the data obtained at each individual location. Because those variants were used to predict soil respiration at each location and then aggregated to the field level, the sample size was assumed equal to the number of measurements taken at each location (i.e. n = 60) This choice favors simpler models, as the importance of k in equation 1.14 increases as n decreases.

The uncertainty in model selection can be quantified by "Akaike weights" or model probabilities (Burnham and Anderson, 2004), which, for AIC_c, are defined as:

$$w_i = \frac{\exp\left(-\Delta AIC_{c,i}/2\right)}{\sum_{j=1}^{h}\exp\left(-\Delta AIC_{c,j}/2\right)} = \frac{L_i(\hat{\beta}|x)}{e^{k_i n/(n-k_i-1)}} \frac{\sum_{j=1}^{h} e^{k_j n/(n-k_j-1)}}{\sum_{j=1}^{h} L_j(\hat{\beta}|x)} \quad (1.16)$$

Where w_i is the probability that the estimated model i is the one with the lowest information divergence, ΔAIC_c is the difference in AIC_c values with respect to the best model and h is the number of models in the set. Note that the sum of w_i for all models is 1.

In order to provide an absolute measure of goodness of fit, the root mean square error (RMSE) was used

$$RMSE = \frac{1}{n}\sqrt{\sum_{i=1}^{n}\left(o_i - p_{r,i}\right)^2} \quad (1.17)$$

Where o_i is each observation i and $p_{r,i}$ is the prediction by the model of that observation i.

2.2.4.3.3. Uncertainty in predictions

Any estimation of predictive uncertainty is over-optimistic as every source of uncertainty may not be quantified or known (Brown, 2010). Therefore, the uncertainty is calculated conditional on the set of alternative candidate models, the data and the assumption that the system behaves in the same way during the calibration and prediction stages. Every prediction will be associated to an estimated probability distribution, which is obtained by integrating the probability model, for all models and parameter weighted by their probabilities (Draper, 1997):

$$p(x|B,h) = \sum_{i=1}^{h} w_i \int_{\beta\in B} p_i(x|\beta)\, p_i(\beta)\, d\beta \quad (1.18)$$

Where p (x |B,h) is the probability of observing a flux x conditional on all parameters (B) and models (h), w_i is the Akaike weight of model i, p_i (x|β) is the probability of observing a flux x conditional on model i and the vector of parameters β (this coincides with the probability model, see section 2.2.4.2) and p_i (β) is the posterior probability of the parameters of model i. This probability will be calculated for each location in the case of variants 2 through 4 and then aggregated to the field level. Note that the model error is contained within the probability model, so that equation 1.17 integrates all the (known) sources of uncertainty in the prediction. If the uncertainty in the parameters is small, equation 1.17 maybe simplified to:

$$p\left(x|\hat{\beta},h\right) = \sum_{i=1}^{h} w_i\, p_i\left(x|\hat{\beta}_i\right) \quad (1.19)$$

Where $\hat{\beta}_i$ is the maximum likelihood estimation of the parameters in model i. This simplification is also known as "plug-in" method (Smith, 1998), averaging with Akaike weights and it should only be used when the uncertainty in the parameter has indeed a small effect in the total predictive uncertainty. Note

that equation 1.17 or 1.18 need to be applied to every period of 30 min where a measurement of net CO_2 ecosystem exchange has been made. In order to evaluate if the simplification was adequate, a sample of 30 measurements was selected and the 95% probability intervals were calculated using equation 1.17 and 1.18 (for equation 1.17 a Monte Carlo approach was used). This was repeated for predictions of soil and ecosystem respiration. In the case of ecosystem respiration, differences between the 95% quantiles were below 2.5% and in the case of soil respiration, differences were below 4.5%. Therefore, it was concluded that the simplified approach was adequate and was applied to all the predictions.

Note that the estimation of uncertainty in the predictions of canopy photosynthesis following strategy 2 do not include the uncertainty in the calculations of canopy respiration as it was not possible to calculate it from the information available. Therefore, the values generated for the second strategy are underestimated by the amount of uncertainty generated by the predictions of canopy respiration.

2.2.4.4. Estimation of canopy photosynthesis and net canopy exchange

The gross primary production (GPP) of an ecosystem is the sum of net ecosystem exchange (NEE) and ecosystem respiration (R_{eco}). When the trees and soil are the only significant sources and sinks of CO_2, canopy photosynthesis (P) is equivalent to gross primary production:

$$P = NEE + R_{eco} \quad (1.20)$$

The gross primary production (GPP) of an ecosystem can also be calculated as the sum of net CO_2 ecosystem exchange, soil respiration (R_{soil}) and canopy respiration (R_{canopy}):

$$P = NEE + R_{soil} + R_{canopy} \quad (1.21)$$

During the first days of the experiment, before DOY 172, the alleys were covered by a green cover, which means that the approximation of canopy photosynthesis by gross primary production was not valid. Therefore, all calculations were done with the data collected after that day.

These two strategies are based on the following assumptions:

1. Extrapolation of nighttime ecosystem respiration (equation 1.19):
    a. The dynamics of the autotrophic component of soil respiration was not affected by the transport of assimilates (Baldocchi et al., 2006).
    b. Canopy respiration was not affected by leaf water potential (Hsiao, 1973).
    c. Photosynthesis and substrate limitations did not affect canopy respiration (Amthor, 2000).
    d. The occurrence of advection during nighttime did not generate any systematic bias in the measurements of ecosystem respiration (Aubinet, 2008).
2. Aggregation of soil respiration (equation 1.20):
    a. The stratification into alley and beneath the canopy was representative of the entire orchard.

b. CO_2 emitted by the soil surface was not used for photosynthesis by the trees, as the canopy was assumed to be well ventilated, avoiding the formation of CO_2 profiles.

The uncertainty in the predictions of canopy photosynthesis was affected by the errors in the measurements of NEE during daytime and the uncertainty in the predictions of the soil and ecosystem respiration (see section 2.2.4.3.3).

As the eddy covariance technique involves several measurements and assumptions, different methodologies have been proposed to calculate the total error in its measurements (Billesbach, 2011). The method of "paired differences" proposed by Hollinger and Richardson (2005) will be used to quantify the uncertainty in the measurements of daytime NEE. This method estimates the error by comparing two independent series of measurements where each pair of corresponding elements (F_1, F_2) represents two measurements of the same flux. Defining F_d as

$$F_d = F_1 - F_2 \tag{1.22}$$

The variance of F_d depends on the variances and covariance of F_1 and F_2 ($\sigma^2_{Fd} = \sigma^2_{F1} + \sigma^2_{F2} - 2\sigma_{F1F2}$). Since F_1 and F_2 are independent and identically distributed random variables, the third term is null. Assuming that the error distributions of F_1 and F_2 are the same, $\sigma_{F1} = \sigma_{F2} = \sigma_\varepsilon$, where σ_ε is the standard deviation of the measurement error

$$\sigma_\varepsilon = \frac{\sigma_{Fd}}{\sqrt{2}} \tag{1.23}$$

The time series was created by choosing pairs of measurements under similar conditions environmental conditions. The criteria proposed in Richardson et al. (2008) were used. Two measurements were assumed to refer to the same real flux if:

1. The measurements were performed exactly 24 hours apart;
2. Differences in incoming PAR were less than 75 µmol photons m^{-2} ground s^{-1};
3. Differences in air temperature were less than 3 °C;
4. Differences in vapor pressure deficit were less than 0.2 kPa.

The different candidate probability distributions for the measurement error in eddy covariance were the same as the ones described in section 2.2.4.2 ad they were compared with the corrected Akaike Information Criterion. Then, the uncertainty generated in the predictions of respiration was added to this measurement error to generate the total uncertainty in the values of canopy photosynthesis following both strategies.

2.3. Results

2.3.1. Soil respiration

In general, curves of CO_2 concentration versus time were curvilinear (figure 1.2) confirming the need to use a parabola to derive the initial slope. The correction of the molar volume by the temperature of the air had a negligible effect on the shape of the curves but it affect the scale of the y-axis (figure 1.2) and thus affected the flux derived as the initial slope.

The diurnal curves of soil respiration followed two main types of patterns, either increasing up to a maximum around 1200 – 1400 GMT and then decreasing, or without a clear trend throughout the day. Although both patterns were observed in all locations, measurements in the alley generally followed the first pattern whereas measurements beneath the canopy tend to follow the second pattern.

The dynamics of soil respiration beneath the canopy and in the alley were different, although the fluxes were similar in both types of locations at the beginning of the experiment. The seasonal dynamics of soil respiration beneath the canopy followed a very similar pattern for all locations (figure 1.3) with a peak on DOY 172 and another peak on DOY 209. Values of soil respiration on DOY 209 varied from 4.0 to 10.5 µmol CO_2 m^{-2} ground s^{-1}, whereas the minimum values occurred on DOY 200, varying from 1.5 to 3 µmol CO_2 m^{-2} ground s^{-1}.

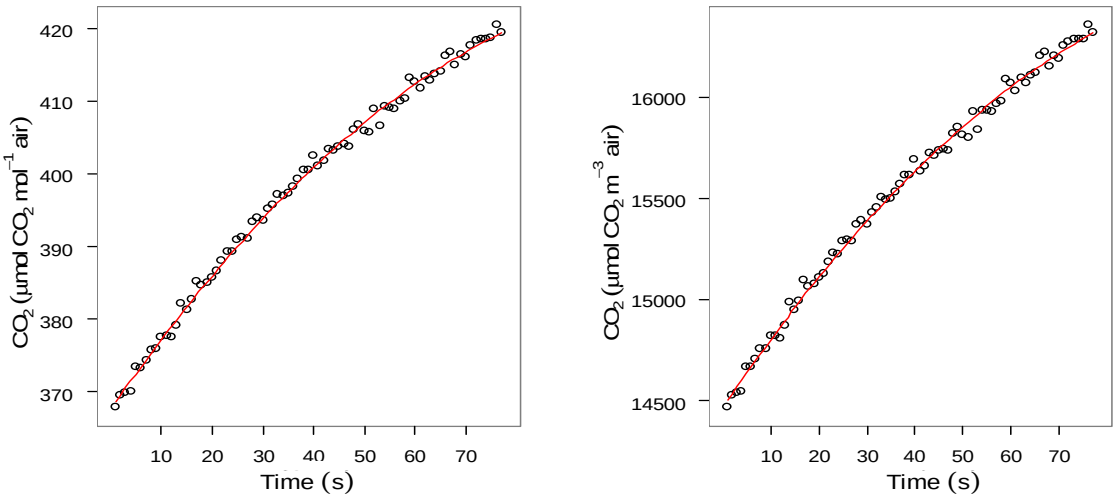

Figure 1.2: Example of CO_2 concentration versus time from a measurement of soil respiration, showing the raw data (left) and the data corrected for air temperature and molar volume (right). Each dot represents a measurement of CO_2 concentration and the line represents the parabola fitted to the data.

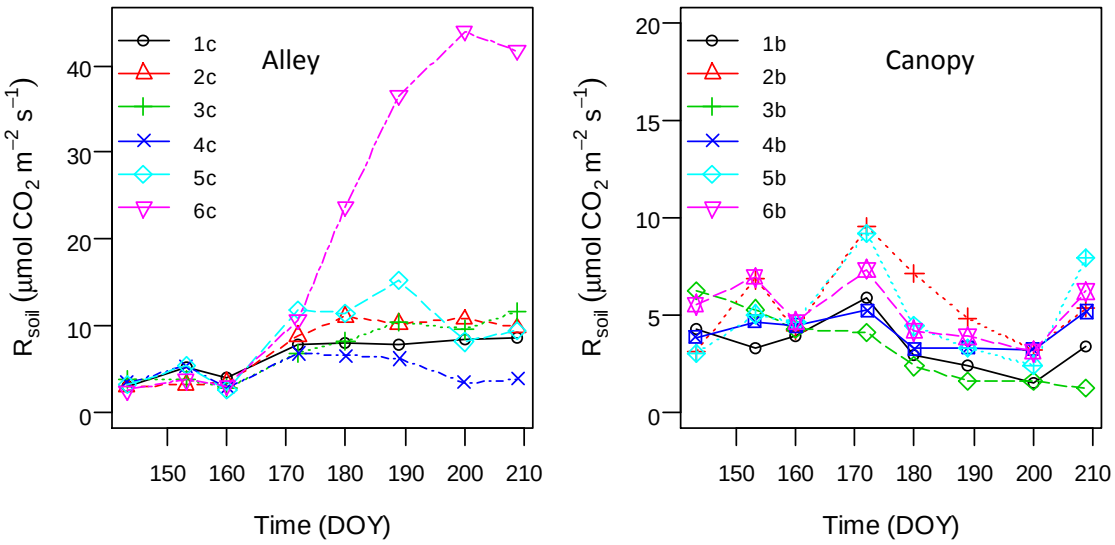

Figure 1.3: Average diurnal soil respiration of all the points in the alley (left) and beneath the canopy (right).

The diurnal average soil respiration in the alley increased between DOY 160 and 170, but was very stable before and after this period, except for location 6 where respiration increased continuously during the second half of the experiment reaching values much higher than in any other location in the orchard. Soil respiration in location 6 (alley) reached a maximum value of 45.0 µmol CO_2 m^{-2} ground s^{-1}, compared to an initial value of 2.7 µmol CO_2 m^{-2} ground s^{-1}. The rest of the locations increased from approximately 2.7 up to 11.4 µmol CO_2 m^{-2} ground s^{-1}, although a decrease was observed in location 4 at the end of the experiment.

The application of the quality tests during the night rejected 69% of the eddy covariance fluxes (table 1.2). Almost half of the fluxes did not pass the tests on stationarity and turbulent regime, indicating that turbulence was very weak and intermittent at night. The test of footprint fraction within the orchard eliminated an additional 16% of fluxes whereas rejections due to excessive flux corrections based on storage of CO_2 were only responsible for an additional 8%. The filters eliminated data from the entire range of friction velocity values, but a higher proportion of rejected fluxes occurred at low friction velocities. Also, most fluxes were rejected at the end of the night (see Appendix I for additional figures and tables).

During daytime, the percentage of rejected fluxes was much smaller, with only 15% of the fluxes not passing the tests on stationarity and turbulent regime and a small additional 2% filtered due to tests based on the footprint function. Most of the rejected fluxes occurred at sunset and sunrise (figure A1.2 in Appendix I). This allowed retaining most of the diurnal patterns. Net ecosystem exchange followed an asymmetric pattern throughout each day, with a peak between 800 and 1000 GMT and a constant decrease during the rest of the day or a flattening of the flux at noon. Net ecosystem exchange varied at night between 0.6 and 9.1 µmol CO_2 m^{-2} ground s^{-1}. During the day, it varied between -20.7 and +3.8 µmol CO_2 m^{-2} ground s^{-1} (negative values indicate net uptake of CO_2, positive values indicate net release of CO_2), indicating that at sunrise and sunset the ecosystem behaved as a net source of CO_2 and ecosystem respiration was larger than photosynthesis.

Table 1.2: Effect of different filters on the eddy covariance measurements, with the cumulative percentage and cumulative number of measurements rejected by application of each additional test. SS refers to steady state quality test and ITC to integral turbulence quality test. Footprint refers to quality test based on footprint function and storage is the filter based on excessive flux correction by storage.

Nighttime			Daytime		
Filter	**Cum. %**	**No. measurements**	**Filter**	**Cum. %**	**No. measurements**
SS + ITC	45	474	SS + ITC	15	296
Footprint	61	641	Footprint	17	336
Storage	69	721			

2.3.2. Soil water content and temperature

Soil temperature varied at the daily and seasonal scale (figure 1.4A), with higher temperatures achieved in the alley at the end of the experiment, but similar values in both types of locations at the beginning. The minimum soil temperature was generally reached around 700 GMT (2 hours after sunrise) whereas the maximum value differed for locations beneath the canopy and in the center of the alley. Beneath the canopy, there was a relative maximum around 1000 GMT and the absolute maximum value of the day occurred at 1700 GMT. Between these two moments, the soil beneath the canopy was shaded by the canopy. In the center of the alley there was a single maximum around 1500 GMT. Minimum daily soil temperature was similar in both locations but the maximum was higher in the alley.

Soil water content was high at the beginning of the experiment in all locations (figure 1.4B), and then the soil dried gradually in the alley and varied in a more complex way beneath the canopy. Sensors below locations 1 and 3 showed a different behavior compared to the rest of the sensors and reached unrealistically low levels at the end of the experiment, although they were within the range of values that can be detected reliably by this type of sensor (Mittelbach et al., 2011). Air gaps between the soil and the sensors could explain this phenomenon. For the locations were the measurements were deemed correct, soil water content decreased from an initial average of 0.34 cm^3 water cm^{-3} soil to a final average of 0.16 cm^3 water cm^{-3} soil. Since differences among these sensors were small and within the expected measurement error, their average values were used to substitute the two sensors that had failed. In the locations beneath the canopy, soil water content varied due to irrigation (figure 1.4B) and the spatial variability was much higher than in the alley. Such spatial variability allowed locations 1 and 5 to reach soil water contents as low as the one observed in the center of the alley at the end of the experiment and the cause of such unusual values is unknown.

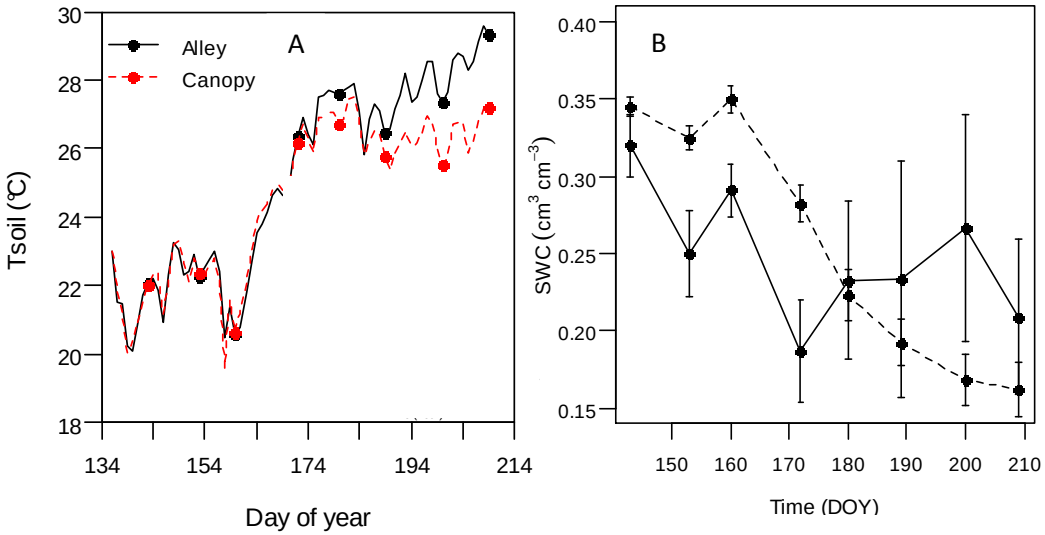

Figure 1.4: Seasonal variation of soil temperature (A) retrieved from the continuous sensors and seasonal variation of soil water content (B) averaged for each group of locations (dashed line – alleys; solid lines – beneath the canopy), indicating twice the standard deviation with vertical bars.

2.3.3. Modeling

2.3.3.1. Parameter estimation and model selection

Model uncertainty was negligible for soil respiration and both types of locations where model HoL64 reached a model probability of 1.00 (table 1.3). This model was the most complex in the list of candidate models, with 17 free parameters in total. Model uncertainty in ecosystem respiration was small, where model 5 had a model probability of 0.88 and model 3 had a model probability of 0.08. The root mean square error of the best models differed with the type of flux being described (table 1.4) being smaller for ecosystem respiration than for soil respiration. In the models of soil respiration, the residuals are calculated for each location, so the values represented in table 1.4 are a mean RMSE for all locations. Location 6 in the alley had a very high RMSE, increasing by 33% the mean RMSE of the model (table 1.4).

The uncertainty in the parameters was, in most cases, very small (table 1.4). The Normal approximation was adequate for all parameters except for some values of β_1 in the models of soil respiration in the alley, as the likelihood function was strongly asymmetric for those parameters. The residuals of the best model of ecosystem respiration were best described by a Laplace distribution with constant variance, but the model probability was only 0.60, indicating a high uncertainty in the selection of this model (table 1.5) whereas visual analysis of the histogram confirmed that the Normal distribution was also a reasonable choice (figure 1.5). For simplicity, the Normal probability model was selected. In the case of soil respiration, the Laplace distribution was also the best model in describing the residuals, but in this case the uncertainty about this choice was much smaller (table 1.5), which agrees with the presence of long tails in the histograms (figure 1.5). Thus, model 64 was re-estimated using a Laplace probability model for both types of locations of soil respiration (table 1.3).

Table 1.3: Comparison of models of soil and ecosystem respiration using the corrected Akaike Information Criterion. Models are identified by their ID (section 2.3.2). w_i is the model probability or Akaike weight and ΔAICc is the difference in the information criterion with respect to the best performing model. The number of observations used in soil respiration and ecosystem respiration were 60 and 746, respectively. Only the first 5 models of each list are shown.

Model	**w_i**	**ΔAIC_c**	**Model**	**w_i**	**ΔAIC_c**	**Model**	**w_i**	**ΔAIC_c**
Alley			**Canopy**			**Ecosystem**		
HoL64	1.00	0.0	**HoL64**	1.00	0.0	**HoN5**	0.88	0.0
HoN62	0.00	79.9	**HoN64**	0.00	36.11	**HoN3**	0.08	4.8
HoN54	0.00	126.7	**HoN24**	0.00	89.34	**HoN2**	0.04	6.3
HoN34	0.00	243.7	**HoN62**	0.00	94.59	**HoN6**	0.00	26.7
HoN52	0.00	325.8	**HoN23**	0.00	98.14	**HoN4**	0.00	37.8

In all the models, there was no evidence of heterogeneity in the variance of the residuals. However, the value of ΔAIC_c increased only 2 units for each distribution where heterogeneity was assumed. All models with heterogeneous variance had a negligible linear coefficient of the variance component (e.g. $\beta_{p,2}$ of the Normal model of ecosystem respiration was $-1.5 \cdot 10^{-7}$), meaning that they were actually describing a very homogeneous variance in the residuals. This is explained by the fact that both types of models (i.e. with homogeneous and heterogeneous variance) had the same log-likelihood (as they predicted the data equally well) but a difference in the number of parameters of 1. For large samples, the bias term in AIC_c approaches 2k, which explains the difference of 2 units for a difference of 1 parameter.

This aspect needs to be taken into account when interpreting the results of the corrected Akaike Information Criterion for nested models, as it may seem at first sight that assuming heterogeneity in the variance could be justified with a model probability of 0.27 (for soil respiration in the alley). However, the fact that the models are nested and AIC_c increases only by 2 implies that there is no improvement in assuming heterogeneity in the variance. Thus, special caution is needed when interpreting the comparison of nested models using information criteria.

In the case of soil respiration, the most complex model was selected as the best model, but that was not the case for ecosystem respiration (table 1.3). When all the models of soil respiration are analyzed (results not shown) the rank of the models sorted by AIC_c does not coincide with the rank based on number of parameters, indicating that, in models of intermediate complexity, there is tradeoff between goodness of fit and complexity.

Table 1.4: Parameters of the soil (R_{soil}) and ecosystem (R_{eco}) respiration models with lowest AIC_c. βd are the different parameters of each descriptive model and β_p are the parameters associated to the variance of the error. The standard deviation of each parameter, based on the Normal approximation, is shown in brackets. RMSE (μmol CO_2 m^{-2} ground s^{-1}) is the root mean square error of each model. HoN5 is model 5 with Normal probability model and homogeneous variance. HoL64 is model 6 with Laplace probability model, homogeneous variance and location-specific parameters β_1 and β_2. For soil respiration in the alleys, the value of RMSE when the residuals from location 6 are not included is shown in brackets. The number of observations used in soil respiration and ecosystem respiration were 60 and 746, respectively.

Models	**R_{soil} HoL64 (Alley)**	**R_{soil} HoL64 (Canopy)**	**R_{eco} HoN5**
$\beta_{d,1}$	[-5.09,-2.34,-3.86,-5.00,-1.88,9.59] (0.20,0.31,0.23,0.27,0.36,0.39)	[8.50, 11.30, 8.54, 10.51, 9.15, 10.33] (0.09, 0.18, 0.12, 0.14, 0.11, 0.11)	3.76 (0.17)
$\beta_{d,2}$	[0.001,-3.68,-2.18, 2.71,-3.27,-2.92] (0.07,0.82,0.68,0.78,0.91,0.88)	[2.98, 0.02, 3.80, 0.33, 3.34, 1.80] (0.44, 0.14, 0.38, 0.26, 0.51, 0.39)	1.36 (0.16)
$\beta_{d,3}$	-9.36 (0.09)	6.87 (0.03)	0.68 (0.21)
$\beta_{d,4}$	51.78 (0.96)	26.18 (0.23)	1.43 (0.11)
$\beta_{d,5}$	-134.56 (5.84)	-89.22 (1.04)	-
$\beta_{d,6}$	272.44 (0.41)	285.80 (0.14)	-
$\beta_{p,1}$	2.36 (0.02)	1.18 (0.06)	0.91 (0.02)
RMSE	3.35(2.5)	1.60	0.91

Table 1.5: Model comparison using the corrected Akaike Information Criterion for different probability models, estimated from the residuals of the best performing models of ecosystem and soil respiration. w_i is the model probabilities and ΔAIC_c the difference in the information criteria with respect to the best model. HoL and HoN refer to Laplace and Normal distribution with homogeneous variance and HeL and HeN for the case of heterogeneous variance. The number of observations used in soil respiration and ecosystem respiration were 60 and 746, respectively.

Model	**w_i**	**ΔAIC_c**	**Model**	**w_i**	**ΔAIC_c**	**Model**	**w_i**	**ΔAIC_c**
Alley (model 64)			**Canopy (model 64)**			**Ecosystem (model 5)**		
HoL	0.73	0.0	**HoL**	0.70	0.0	**HoL**	0.60	0.0
HeL	0.27	2.0	**HeL**	0.26	2.0	**HeL**	0.22	2.0
HoN	0.00	60.9	**HoN**	0.03	6.5	**HoN**	0.13	3.0
HeN	0.00	63.0	**HeN**	0.01	8.6	**HeN**	0.05	5.0

Table 1.6: Comparison of different probability models characterizing the measurement error of diurnal net CO_2 ecosystem exchange using the corrected Akaike Information Criterion. w_i is the probability model and ΔAICc the difference in the information criterion with respect to the best model. HoL and HoN refer to Laplace and Normal distribution with homogeneous variance and HeL and HeN for the case of heterogeneous variance. The sample size was 466.

Model	**HeN**	**HeL**	**HoL**	**HoN**
w_i	1.00	0.00	0.00	0.00
ΔAIC_c	0.00	14.00	58.90	84.40

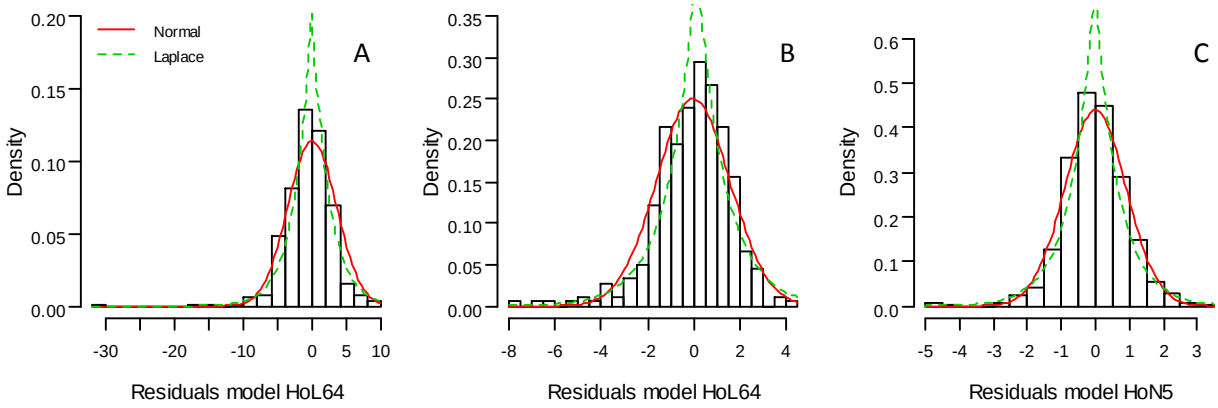

Figure 1.5: Density histogram of the residuals of the models of soil respiration in the alleys (A), beneath the canopy (B) and ecosystem respiration (C). HoN and HoL stand for Normal and Laplace probability models with homogeneous variance. 64 and 5 stand for descriptive models 6 with spatial variation in $\beta_1$and β_2 and deterministic model 5. Green, dashed lines and red, solid lines correspond to the probability densities of the Laplace and Normal models with homogeneous variance.

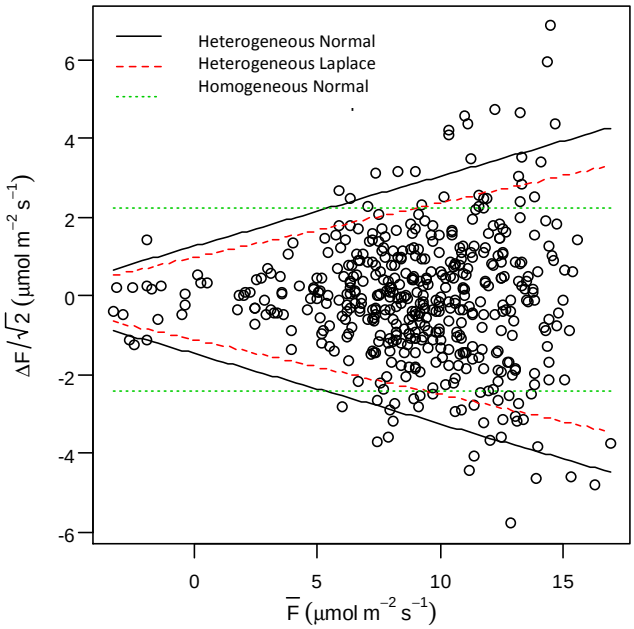

Figure 1.6: Paired differences of daytime net ecosystem exchange versus the average of each pair of fluxes. The different lines represent the 95% probability intervals generated by the different probability models. Negative values of the flux correspond to net respiration.

The model 64 of soil respiration showed a high variability in the values of the parameters, especially for the location-specific parameters (table 1.4). Note that these parameters do not have a direct physical interpretation as they describe an empirical trigonometric function of time, but their higher predictive accuracy makes them attractive models for the purpose of interpolating the measurements. The predictions with the models should not be applied outside the period of calibration and, indeed, the model of soil respiration in the alley predicted fluxes that were not physically possible when extrapolating to the entire year (results not shown).

2.3.3.2. Canopy photosynthesis (Strategy 1)

The variance of the paired differences in the measurements of net CO_2 ecosystem exchange (NEE) was clearly heterogeneous and increased linearly with the magnitude of the flux (table 1.6, figure 1.6) and the Normal distribution was a better description than the Laplace distribution. The optimal values of the parameters (and their standard deviations) associated with the variance of the paired differences, (i.e. $\sigma_\varepsilon = \beta_{p,1} + \beta_{p,2}|NEE|$) were 0.7 (0.05) and 0.09 (0.006). Thus, σ_ε varied between 0.70 and 2.05 µmol CO_2 m^{-2} ground s^{-1} as NEE increased from 0.00 to 15.00 µmol CO_2 m^{-2} ground s^{-1}. The mean paired difference was -0.10 (0.07) µmol CO_2 m^{-2} ground s^{-1}, indicating that the bias in the methodology for selecting fluxes was minimal. The Laplace distribution with heterogeneous variance underestimated the spread of the paired differences around the mean, as the 95% probability region contained only 87% of the observed differences, whereas in the Normal distribution with heterogeneous variance, it contained 93% (figure 1.6).

The uncertainty in the calculations of canopy photosynthesis resulted in a Normal distribution, with a standard deviation that increased with the flux. The mean standard deviation was 1.74 µmol CO_2 m^{-2} ground s^{-1}, with a range from 0.9 to 2.7 µmol CO_2 m^{-2} ground s^{-1} and an average coefficient of variation of 15%. There was no clear seasonal effect in the uncertainty, but it varied each day as NEE increased, being maximum during the first half of the day (figure 1.7). The diurnal trends of canopy photosynthesis were similar for most days, with a maximum between 800 and 1000 GMT and a decrease during the rest of the day (figure 1.7). Daily average canopy photosynthesis varied between 7.1-15.9 µmol CO_2 m^{-2} ground s^{-1} whereas the daily average ecosystem respiration varied between 2.4-4.3 µmol CO_2 m^{-2} ground s^{-1}. Ecosystem respiration decreased during the entire experiment, whereas canopy photosynthesis had a minimum around DOY 230.

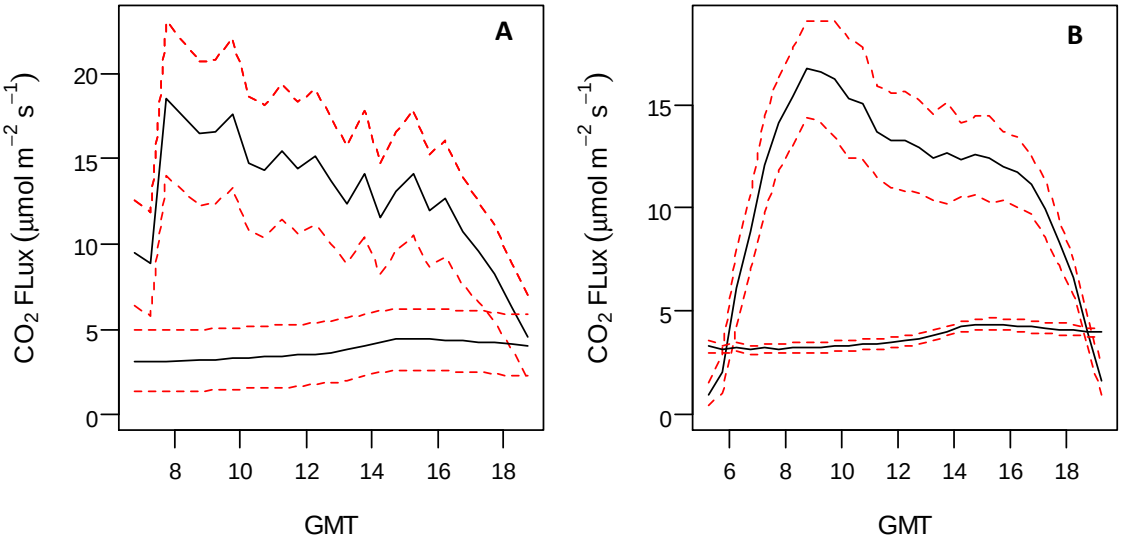

Figure 1.7: A: canopy photosynthesis (P) and ecosystem respiration (R_{eco}) calculated for DOY 191. The solid, black lines are the most probable values; the red, dashed lines are the 95% probability intervals. On the right, the most probable P and R_{eco} (black, solid lines) for every time of the day and envelopes of one standard deviation width (red, dashed lines) showing the seasonal variation of this average.

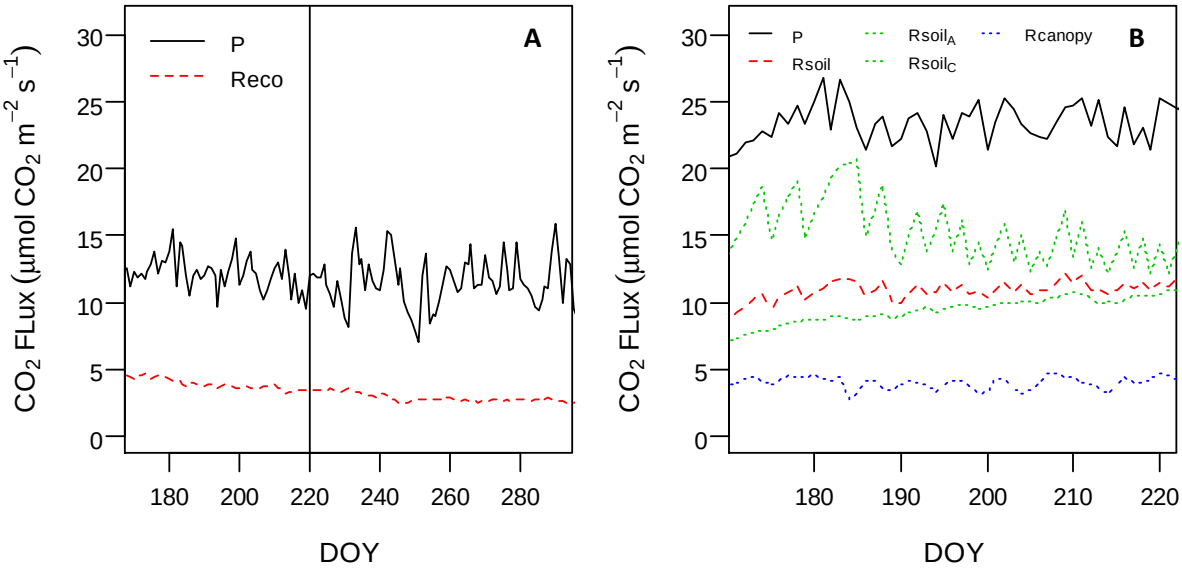

Figure 1.8: A: Daily average canopy photosynthesis (P) calculated following strategy 1 (net ecosystem exchange + ecosystem respiration) and ecosystem respiration (Reco). B: Daily average canopy photosynthesis (P) calculated following strategy 2, average soil respiration (Rsoil), average soil respiration segregated into the locations beneath the canopy ($Rsoil_A$) and in the alley ($Rsoil_B$) and canopy respiration (Rcanopy). Soil respiration in the alleys is the lowest of the two curves describing soil respiration.

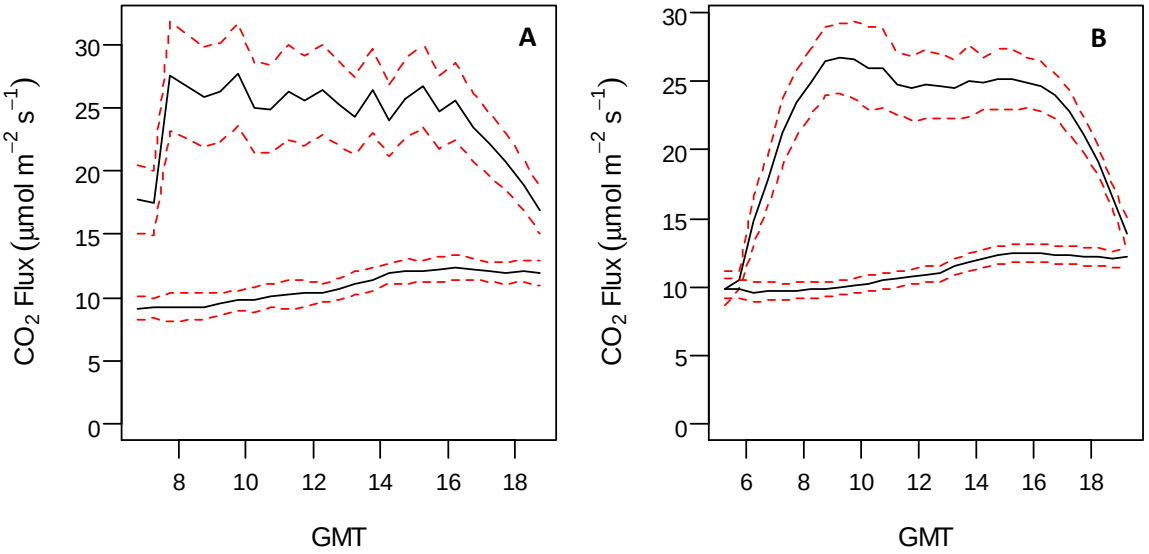

Figure 1.9: A: Canopy photosynthesis calculated following strategy 2 (net ecosystem exchange + soil respiration + canopy respiration) and soil respiration calculated for DOY 191. The solid, black lines are the most probable fluxes; the red, dashed lines are the 95% probability intervals. B: Average most probable canopy photosynthesis (strategy 2) and soil respiration (black, solid lines) for every time of the day and envelopes of one standard deviation width (red, dashed lines) showing the seasonal variation, restricted to the period between DOY 172 and 220.

2.3.3.3. Canopy photosynthesis (Strategy 2)

Given the very high values measured at location 6 in the alley, this location was not included in the predictions of average soil respiration. It was not clear what the frequency of locations with such high fluxes was in the orchard, but it was assumed that it would not be very important and thus it was unwise to include it in the predictions. The predictions of canopy photosynthesis following strategy 2 were restricted to the period between DOY 172 and 220, to avoid their application outside the period in which the models of soil respiration were calibrated.

A Monte Carlo simulation with 1000 samples per location was used to quantify the uncertainty in the estimations of field-level average soil respiration, resulting in a Normal distribution, with a standard deviation of 1.3 µmol CO_2 m^{-2} ground s^{-1}. The uncertainty in the calculations of canopy photosynthesis following strategy 2 also followed a Normal distribution which standard deviation varied between 1.05 and 2.80 µmol CO_2 m^{-2} ground s^{-1}, resulting in an average coefficient of variation of 7%. Soil respiration was systematically higher than ecosystem respiration, which means that either ecosystem respiration was being underestimated or soil respiration was being overestimated. The seasonal and daily variation of soil respiration was higher than in ecosystem respiration. However, the diurnal patterns of canopy photosynthesis based on both strategies were quite similar, because net CO_2 ecosystem exchange still had the most important effect in the dynamics, although the in strategy 2, the diurnal curves tend to be flatter. The aggregated field-level soil respiration in the alleys was lower than beneath the canopies and their seasonal dynamics were very distinctive, as soil respiration in the alley increased whereas it decreased beneath the canopy (figure 1.8).

Daily average canopy photosynthesis varied between 20 and 27 µmol CO_2 m^{-2} ground s^{-1}, whereas daily average soil respiration varied between 9 and 13 µmol CO_2 m^{-2} ground s^{-1}. No clear seasonal trend was observed for soil respiration or canopy photosynthesis, although the period of time considered was restricted and cannot be compared directly with the results obtained with strategy 1.

2.4. Discussion

2.4.1. Soil respiration and eddy covariance measurements

Testi et al. (2008) measured soil respiration beneath the canopy and in the alley and took measurements with an eddy covariance system in an irrigated olive orchard under similar environmental conditions. The average values of soil respiration were 5.7 and 1.1 µmol CO_2 m^{-2} ground s^{-1} beneath the canopy and in the alley, respectively. The measurements beneath the canopy are similar to the ones obtained in this study and the diurnal patterns also showed no response to soil temperature. In the alley, however, measurements in this study are much higher, which can be explained by a higher soil water content compared to their value of 0.05 cm^3 water cm^{-3} soil. Nighttime ecosystem respiration was very similar in their study, with a range of 2.3 to 4.8 µmol CO_2 m^{-2} ground s^{-1}.

As expected, the stratification of the sample into locations beneath the canopy and in the alley allowed detecting two very different dynamics of soil respiration, but also of soil temperature and water content. In the alley, water content and temperature were correlated in time (i.e. as temperature

increased, water content decreased) which generated a situation of confounding factors and, for high soil water contents, soil respiration could be reduced by a decrease in CO_2 production and transport and this effect is difficult to discern from the effect of low temperature. However, the relationship was broken beneath the canopy due to irrigation, in which the dynamics were more complex at both daily and seasonal scale.

The low sensitivity to temperature found at the diurnal scale was not related to the effect of drought (e.g. Reichstein et al., 2002) or supra-optimal temperatures (e.g. Testi et al., 2008). However, recent studies with automatic soil respiration chambers indicate that soil respiration beneath a tree canopy may show a weak response to temperature at the diurnal scale due to they dynamics of root respiration (Baldocchi et al., 2006). Baldocchi et al. (2006) observed that the response to soil temperature increased when moving away from the trees, which was also evident in this study.

None of the environmental variables measured at location 6 in the alley would justify such a high increase of soil respiration as temperature and soil water content were similar to the rest of the locations. A visual analysis of the soil surface revealed that cracks were forming in the soil as it dried. These cracks could increase the availability of oxygen throughout the soil profile and thus increase soil respiration. However, other locations in the orchard also showed these cracks. To the knowledge of the author, no values of soil respiration as high as in location 6 has been published under Mediterranean conditions, even for summer conditions and high water contents. Further research is needed to explain this phenomenon.

As observed by Ruppert et al. (2006), filtering nighttime measurements of eddy covariance with quality tests showed that some fluxes at low friction velocities are still adequate, although most of the rejected fluxes occurred at low friction velocities. However, unlike their observations, in this study , most rejected fluxes were concentrated at the end of the night, sunrise and sunset. This suggests that during the day, well-mixed conditions prevail and that conditions worsen as the night advances. The fact that the consecutive application of the filters always added new fluxes to the rejection list indicates that using one criterion is not enough to detect all fluxes that should be rejected.

2.4.2. Modeling soil and ecosystem respiration

2.4.2.1. Parameter estimation and model selection

The variance in the residuals of the models of soil and ecosystem respiration was not heterogeneous, although the presence of large deviations in the models of soil respiration made the Laplace distribution a better alternative than the Normal distribution. Note that the method of maximum likelihood does not require knowing the distribution of the measurement error but the distribution of the residuals, which may or may not resemble the errors in the measurements, depending on the amount of additional error introduced by the simplifications in the model. However, for the calculation of uncertainty in canopy photosynthesis, it was necessary to quantify the error in the daytime measurements of eddy covariance and, as expected, the variance in the error increased with the flux and the Normal distribution was the one that best described this error. The increase of uncertainty with the flux was similar to the values

reported by Richardson et al. (2008) for different locations in the CarboEurope program, although they were characterized by a Laplace distribution. A description of the measurement error (i.e. plotting the histogram and calculating the moments) does not provide reasonable arguments to choose one or another distribution, as different distribution can produce similar histograms, especially when the variance is heterogeneous (Stauch et al., 2008). A quantitative method, such as the use of corrected Akaike Information Criterion, is required. To the knowledge of the author, a quantitative comparison of different hypotheses concerning the measurement errors and model residuals of eddy covariance and soil respiration measurements has never been published.

The uncertainty in some of the location-specific parameters in model 64 of soil respiration was not properly estimated by the matrix of second partial derivatives as the likelihood function was not smooth in the neighborhood of the maximum likelihood estimate. This could be caused by a non-negligible 3rd and higher order partial derivative. When this is the case, the curvature estimated locally at the maximum likelihood value is not a good approximation of the variance-covariance matrix (see figure A1.4 in Appendix I). The reason why the Normal approximation is less adequate for the location-specific parameters is that these parameters were estimated with a sample size of 60 data points (number of measurements per location), whereas the global parameters were estimated with the full sample (i.e. 360 data points). Thus, the average curvature in the region around the maximum likelihood was estimated by building profiles of the logarithm of the likelihood and fitting a parabola to each profile (Bolker, 2008). However, note that this method does not allow calculating the covariance between each pair of parameters, only the variance of each parameter. Since the uncertainty in the parameter values had a small effect on prediction uncertainty, it was not considered necessary to obtain a more accurate estimation of parameter uncertainty.

Model selection uncertainty was negligible for the models of soil respiration and small for the models of ecosystem respiration. The fact that the most complex model (i.e. model 64 with 17 free parameters) had the lowest AIC_c value in soil respiration for both types of locations suggests that even more complex models (i.e. with more parameters) could be proposed for the data, although the Normal approximation might not hold for such complex models and a rigorous Bayesian integration should be used. Also, the information criterion may eventually fail to recognize adequately the trade-off between goodness of fit and complexity for very complex models. Such abuse of information criteria is known as “model dredging” (Stephens et al., 2005) and should be avoided.

2.4.2.2. Spatial and temporal variability of CO_2 fluxes

The variation in time of soil respiration in different locations was similar in relative terms, but the actual values varied per location. Thus, the location-specific models represented a great improvement over simpler models of aggregated field-level soil respiration. However, the predictions of the aggregated soil respiration could still be biased since only 12 locations were sampled and the exact weights to be associated to respiration beneath the canopy and in the alleys were unknown. Respiration in location 6 in the alley was not included in the predictions because the observed fluxes were much higher than for the rest of the locations.

The systematic differences between soil and ecosystem respiration could be explained by an underestimation of ecosystem respiration during the night, due to non-turbulent transport mechanisms (Aubinet, 2008). In this study, ecosystem respiration underestimated field-level soil respiration, on average, by 65%. Lavigne et al. (1997) observed that respiration based on measurements of eddy covariance underestimated aggregated chamber-based measurements by 27%. Goulden et al. (1996) observed a similar underestimation of 32%. However, Granier et al. (2000) and Wohlfahrt et al. (2005) observed very good agreements between both approaches. Finally, Law et al. (2001) observed that respiration based on eddy covariance measurements was higher than the aggregated chamber-based ecosystem respiration plus plant respiration. The discrepancies in the literature could be related to different meteorological conditions during the measurements, canopy structure and the procedure to scale the chamber measurements to the field level. The difference observed in this study is certainly much higher than what would be expected based on these reports in the literature.

The uncertainty in the calculations of canopy photosynthesis following both strategies were very similar, but the uncertainty for strategy 2 was underestimated as it had not considered the uncertainty due to canopy respiration. Therefore, it is expected that the true uncertainty in strategy 2 is higher that in strategy 1. Approximately, half of the uncertainty was generated by errors in the measurements of net CO_2 ecosystem exchange and the other half was generated by the predictive uncertainty of ecosystem and soil respiration. Note that, since soil respiration was modeled for each location and then aggregated, the uncertainty in the predictions of field-level soil respiration was smaller than for each individual location, due to the effect of averaging independent random variables. Therefore, including location-specific parameters increased both the predictive accuracy and precision.

The predicted average soil respiration in the alleys and beneath canopy had very different temporal dynamics, even if the same model was used to make the predictions in both cases, indicating the high flexibility of model 64. Indeed, the values of the parameters describing the seasonal variation of reference respiration were very different, as soil respiration beneath the canopy decreased while in the alleys it increased. Soil respiration was always lower in the alley compared to beneath the canopy, and oscillations in respiration beneath the canopy were larger than in the alley.

Testi et al. (2008) estimated daily canopy photosynthesis following strategy 1, in an irrigated olive orchard, and observed during the summer a range of 15-25 g CO_2 m^{-2} day^{-1}, which would agree with the values of canopy photosynthesis obtained with strategy 1 in this study. This would suggest that the canopy photosynthesis following strategy 2 is overestimated, which could be explained by an overestimation of soil respiration (which was higher than ecosystem respiration). However, if ecosystem respiration during nighttime was being underestimated due to advection (Aubinet, 2008) this would affect both estimations in this study and in Testi et al. (2008), and both could strongly underestimate the true canopy photosynthesis. Therefore, without a third source of information, this issue cannot be resolved and the estimates with either strategy should be taken with caution.

This means that the methodology presented in this study will not resolve which method is biased (or even if both methods are biased). However, realizing that the two approaches result in such different

estimates is important enough as it cast doubts on previous estimations and highlights the need for a third, independent estimation of the fluxes to decide among the methodologies.

2.5. Conclusions

The following main conclusions have been obtained from the study:

1. The calculation of canopy photosynthesis following strategy 1 was, on average, 50% lower than the calculations following strategy 2 and these differences were not caused by the uncertainties in the calculations, indicating that at least one of the strategies is strongly biased.

2. Canopy photosynthesis following strategy 1 was maximal in the morning and decreased during the rest of the day. Canopy photosynthesis following strategy 2 showed a very small decrease and stay rather constant most of the day.

3. The uncertainty in the estimations of canopy photosynthesis for both strategies was very similar, increasing slightly with the flux with an average standard error of 1.8 µmol CO_2 m^{-2} ground s^{-1} that implies a coefficient of variation of 15 and 6% for strategy 1 and 2, respectively.

4. The variance of the residuals of the models of soil and ecosystem respiration was homogeneous and they were best described by a Laplace distribution, though the advantage was very small for ecosystem respiration. The incorporation of spatial variability in the parameters of soil respiration increased both the predictive accuracy and precision.

3. A three-dimensional model of canopy photosynthesis and radiation interception for olive orchards

Summary

A three-dimensional model of canopy photosynthesis and radiation interception for olive orchards was calibrated with the available scientific literature and tested with two measurements of canopy photosynthesis in a super-high density olive orchard in Cordoba (Spain), using an eddy covariance system and closed soil respiration chambers. The model underestimated canopy photosynthesis by 5% when it was calculated from net ecosystem exchange, soil respiration and canopy respiration, but overestimated canopy photosynthesis by 65% when it was estimated by net ecosystem exchange and ecosystem respiration, indicating a strong underestimation of nighttime measurements of ecosystem respiration with eddy covariance. For a LAI of 2.5, the model predicted an average daily photosynthesis of 46 g CO_2 m^{-2} ground day^{-1} during Spring-Autumn and a radiation use efficiency aboveground of 0.9 g DM MJ^{-1} PAR. The critical parameters in the model were the leaf area density and the parameters associated to the hyperbolic response of photosynthesis to absorbed radiation. The model is able to simulate the interception of radiation and photosynthesis of other olive orchards as long as the structure of the canopy is properly described.

Keywords: Eddy covariance, *Olea europaea*, superintensive olive, super-high density olive, global sensitivity analysis, 3D model, radiation use efficiency, radiation interception.

3.1. Introduction

The assimilation of CO_2 through photosynthesis is the main process that determines the growth and productivity of plants (Goudriaan and van Laar, 1994) and it is an important flux in the global CO_2 cycle (Cox et al., 2000). Photosynthesis is a well-known process under potential conditions (i.e. without limitations due to water or nutrient deficiencies) and the use of leaf-level models has been key in ecophysiological studies (Farquhar et al., 2001). However, the canopy modifies its own microclimate (Goudriaan, 1977) creating strong gradients of environmental conditions which affect leaf photosynthesis. If this gradient is ignored, we obtain a "big leaf" model (Collatz et al., 1991), but this model tends to overestimate canopy photosynthesis (de Pury and Farquhar, 1997). Therefore, an accurate simulation of canopy photosynthesis requires taking into account the three-dimensional spatial heterogeneity of environmental conditions, especially radiation. Due to these gradients, the sensitivity of photosynthesis to environmental conditions and plant traits depend on the scale at which it is studied (Luo et al., 2001).

Olive trees (*Olea europaea* L.) represent an extended horticultural crop in Mediterranean regions, reaching 9.5 Mha worldwide in 2010 (FAO Statistics Division, 2012). The impact of this crop on the regional carbon balance is important, especially in countries were the cultivation of olives is performed in extensive regions such as Spain, Italy or Greece. Olive cropping systems, which include agroforestry systems, traditional groves and intensive

orchards, at high and super-high densities, are of enormous relevance from an economic and ecological perspective. Super-high density olive orchards are planted at a density of 1500-2000 trees ha^{-1} in order to obtain high yields during the first years of establishment and they are pruned to generate a structure suitable for mechanization of all operations (Gomez-del-Campo, 2010). In these orchards, each tree consists of a single main stem and fruits are harvested with modified grape harvesters. When the orchards reach their maximum dimension, the crowns of the trees merge forming continuous, parallel hedgerows.

There exists abundant literature characterizing the photosynthesis of leaves in olive trees (Connor and Fereres, 2005), including the calibration of a mechanistic model of photosynthesis (e.g. Diaz-Espejo et al., 2006) and different models of stomatal conductance (Moriana et al., 2003). The interception of radiation and photosynthesis of isolated olive trees has been modeled in detail (Diaz-Espejo et al., 2002; Diaz-Espejo et al., 2004) using the ray-tracing model proposed by Sinoquet et al. (2001). In high-density olive orchards, Mariscal et al. (2000a) modeled the interception of radiation by the canopy using the radiative transfer equations of Norman and Welles (1983), a method that is easier to parameterize as it only measuring the leaf area density, leaf angle distribution and optical properties and dimensions of the trees.

Although simpler models have been proposed for the interception of radiation by isolated trees (Villalobos, 2008; Sinoquet et al., 2007) and hedgerows (Gijzen and Goudriaan, 1989; Pronk et al., 2003), the three-dimensional approach developed by Norman and Welles (1983) is able to simulate all the different types of olive orchards, allowing a level of generality that cannot be achieved with simpler models. If the different types of olive orchards are to be compared, it should be done with a single, common model, rather than several, simplified models.

The model Maestra (Luo et al., 2001) implements the method of Norman and Welles (1983) and scales photosynthesis and transpiration up from the leaf to the canopy level. In this study, the model is used to simulate the canopy photosynthesis of a typical super-high density olive orchard being calibrated using the relevant scientific literature. The model was tested with measurements of canopy photosynthesis and net CO_2 canopy exchange obtained with an eddy covariance system and soil respiration chambers. A global sensitivity analysis was performed to identify the most influential parameters and environmental variables.

The model may be used to explore the effect of canopy structure on radiation interception and photosynthesis, as well as transpiration and water use efficiency (though the present study will only focus on the first two concepts). For other objectives, summary models could be derived using this model as benchmark. As an example of how to derive simpler expressions, the potential daily dry matter production and radiation use efficiency was calculated by subtracting plant respiration estimated from the scientific literature (Mariscal et al., 2000b; Perez-Priego et al., submitted; Villalobos et al., 2006) from the simulation of photosynthesis.

3.2. Materials & Methods

3.2.1. Site description

The experiment was performed on the farm “La Harina” located in Cordoba, Spain (37° 44' N, 4° 36' W, altitude 170 m) in 2011. The system studied was a 21.5 ha olive orchard (*Olea europaea* cv. Arbequina) planted in 2005,

spaced at 4 x 1.5 m, with rows oriented on the NNW-SSE axis. The soil is a Xerofluvent (IGN, 2011) as described by the Soil Taxonomy classification (NRCS, 2006). The climate in the area is typically Mediterranean, with an average annual rainfall of 600 mm, with almost no rain in the summer, and an average annual reference evapotranspiration of 1390 mm.

The orchard was drip-irrigated with two emitters per tree (total discharge rate of 4.4 l h^{-1} $tree^{-1}$). Irrigation was applied twice every week, with an extent of 7 hours per application. The trees were pruned every two years, with a mechanical topping that reduced height to 2.5 m and lateral, manual pruning. During the period of measurements, the height of the canopy was 3 m. The residues were chipped and spread over the soil surface. No tillage was performed and, during winter, a green cover was allowed to grow in the alleys between the planted rows, being eliminated in spring by mowing. Weeds in the rows were controlled chemically. However, due to extensive rainfall in Spring, at the beginning of the experiment, the green cover grew again, occupying the alleys and was not eliminated until the day 172 of the year (i.e. mid-June).

Measurements of net CO_2 ecosystem exchange using the eddy covariance method were taken from DOY 170 until 290 whereas soil respiration was measured with closed chambers between DOY 170 and 220. The measurements allowed modeling soil respiration and ecosystem respiration using non-linear regression models describing the effect of environmental conditions on respiration. From these models and the daytime measurements of net CO_2 ecosystem exchange, canopy photosynthesis was estimated following two strategies: (i) as the sum of net ecosystem exchange and ecosystem respiration and (ii) as the sum of net ecosystem exchange, soil respiration and canopy respiration. Fluxes calculated with both strategies will be compared with the simulations of the model Maestra. Details about the experiment and the calculation of the fluxes are given in Chapter 1.

It was assumed that photosynthesis in the experiment was not affected by soil water deficit, nutrient deficiency, pests or diseases. A foliar analysis was performed in July on a sample of 100 leaves, resulting in a nitrogen concentration of 1.6 % (referring to dry matter content), approximating the sufficiency threshold[9] of 1.5 % (Fernandez-Escobar et al., 2009). No signs of other deficiencies were observed. There were signs of olive knot (i.e. a disease caused by the bacteria *Pseudomonas savastanoi* consisting of tumors in the branches), but, to the knowledge of the authors, no quantitative effect of this disease on photosynthesis has been reported.

In order to characterize the water status of the trees, predawn leaf water potential was measured in three trees that received the same irrigation as the rest of the orchard and in two additional trees that received a higher amount of irrigation (control trees). The control trees were drip-irrigated with three emitters per tree (total discharge rate of 6.6 l h^{-1} $tree^{-1}$). Irrigation was applied three times a week, with an extent of each application that varied in time (8.00 h in June, 9.00 h in July and August, 6.75 h in September and 5.25 h in October). The irrigation program was designed assuming a crop coefficient[10] of 0.65. This value is slightly higher than the value

[9] The sufficiency threshold is also known as the critical nutrient concentration. By definition, when the concentration falls below the threshold, nutrients will limit plant growth (Ulrich, 1952).

[10] The crop coefficient is the ratio between the reference evapotranspiration (ET_0) calculated from weather measurements and the actual evapotranspiration of the canopy. The concept implies that the reference evapotranspiration takes into account meteorological effects and the crop coefficients integrates the effects of aerodynamic and canopy resistances to

of 0.55 than would be predicted by applying the model of Testi et al. (2004). Due to operational problems, the actual irrigation in the month of August was, on average, 10% lower than the programmed dose.

5 leaves per tree were measured every 10 days just before sunrise, assuming that the different tissues in the tree were in hydraulic equilibrium with the soil. Predawn leaf and soil water potentials are linearly related in olive trees (Ennajeh et al., 2008).

3.2.2. Maestra model

"Maestra" is a three-dimensional model of canopy photosynthesis, transpiration and absorption of radiation and it is based on the model "Maestro", published by Wang and Jarvis (1990a). The canopy is represented as an array of crowns, defined by their location, shape and dimensions. The fluxes are calculated for a target crown in the center of the plot, but additional trees need to be considered around it in order to avoid border effects. The target crown is divided into a grid by defining layers (vertical stratification) and sectors (horizontal stratification). At each grid point, solar radiation absorption, photosynthesis and transpiration are calculated, and scaled up to the canopy level weighted by the leaf area associated to each grid point. The reader is referred to Wang and Jarvis (1990a) and the website of the model (www.maestra.unsw.edu.au) for more details, though the most relevant equations are described in the following paragraphs.

The absorption of solar radiation is calculated based on the method proposed by Norman and Welles (1983). Given a beam of solar radiation, defined by zenith solar angle Z (rad) and azimuth solar angle Ω (rad) and assuming a uniform leaf area density within each crown (LAD, m^2 leaf m^{-3} crown), the probability, P, that the beam is not intercepted by the canopy is given by

$$P(Z,\Omega) = \exp\left(-G(Z,\Omega)S(Z,\Omega)LAD\right) \qquad (2.1)$$

were G is the fraction of foliage projected on the plane perpendicular to the direction of the solar beam and S is the length of the segment (m) that results from the intersection of the direction of the beam and the crown. Leaf area density was assumed uniform within each crown. For the absorption of diffuse radiation, solar beams are integrated over the entire sky hemisphere. Assuming that the leaf angle distribution is uniform with respect to the azimuth angle, the value of G is described by the ellipsoidal model proposed by Campbell (1986)

$$G = \cos Z\sqrt{X^2+\tan^2 Z}\left[X+\frac{1}{2\epsilon_1 X}\log\left(\left(1+\epsilon_1\right)\left(1-\epsilon_1\right)^{-1}\right)\right]^{-1} \qquad (2.2)$$

Where $\epsilon_1 = \sqrt{1-1/X^2}$, so that it only depends on the parameter X and Z. Equation 2.2 was used as X > 1 in this study. See Appendix III for more details on the G function.

Photosynthesis (A, µmol CO_2 m^{-2} leaf s^{-1}) is calculated as the result of a biochemical model of demand of CO_2 (Farquhar et al., 1980) and a model of supply of CO_2 as it diffuses through the stomata (Leuning, 1995). The demand of CO_2 is computed as

---

water vapor flux, and soil evaporation (Testi et al., 2004). Typical values of ET_0 for Cordoba (Spain) were used in the calculations.

$$A = \min\left(A_v, A_q\right) - R_d \quad (2.3)$$

Where A_v and A_q are the rates of gross photosynthesis (µmol CO_2 m^{-2} leaf s^{-1}) limited by Rubisco activity and production of chemical energy in the electron transport chain, respectively. R_d is leaf mitochondrial respiration (µmol CO_2 m^{-2} leaf s^{-1}). Photosynthesis limited by Rubisco activity is calculated as

$$A_v = V_{c,max} \frac{C_i - \Gamma_*}{C_i + k_c\left(1 + o_i / k_o\right)} \quad (2.4)$$

Where $V_{c,max}$ is the maximum activity of Rubisco, C_i (µmol CO_2 mol^{-1} air) is the intercellular CO_2 concentration, Γ_* is the CO_2 compensation point in the absence of mitochondrial respiration, o_i is the intercellular oxygen concentration (assumed constant and equal to 2.05 10^5 µmol O_2 mol^{-1} air), k_c and k_o are the Michaelis coefficients of Rubisco activity for CO_2 and O_2 as substrate (µmol CO_2/O_2 mol^{-1} air). The term $k_c(1 + o_i / k_0)$ represents the assumption that CO_2 and O_2 are competing for the same enzyme locations, thus O_2 lowers the enzyme affinity for CO_2. It was assumed that CO_2 concentration at the carboxylation site of Rubisco was equal to the intercellular CO_2 concentration, that is, mesophyll conductance (Yin and Struik, 2009) was not included, since no model of photosynthesis including mesophyll conductance has been calibrated for olive trees, to the knowledge of the author. Photosynthesis limited by electron transport is calculated as:

$$A_q = \frac{J}{4}\frac{C_i - \Gamma_*}{C_i + 2\Gamma_*} \quad (2.5)$$

Where J (µmol e^- m^{-2} leaf s^{-1}) is the electron transport rate, which increases with the photosynthetic photon flux (Q, µmol photon m^{-2} leaf s^{-1}), defined by the following quadratic equation:

$$\theta J^2 - \left(\alpha Q + J_{max}\right) J + Q\alpha J_{max} = 0 \quad (2.6)$$

Where α is the quantum efficiency (mol e^- (mol photon)$^{-1}$), J_{max} is the maximum electron transport rate (µmol e^- m^{-2} leaf s^{-1}) and θ is the degree of curvature of the parabola. The parameters $V_{c,max}$, J_{max}, k_o, k_c, Γ_* and R_d were assumed to increase with temperature as described by the Arrhenius equation

$$P_T = P_{25}\, e^{H_p\left(T_L - 298.15\right)/\left(298.15 R T_L\right)} \quad (2.7)$$

Where P_T is the value of the parameter P at absolute leaf temperature T_L (K), P_{25} is the value of the parameter P at 25 °C, R is the gas constant (8.31 J mol^{-1} K^{-1}) and H_p is the activation energy of parameter P (J mol^{-1}). The original code of Maestra had to be changed to allow the Arrhenius equation to be applied to R_d. The model of CO_2 supply is

$$A = g_{sc}\left(C_s - C_i\right) \quad (2.8)$$

Where C_s is the CO_2 concentration at the surface of the leaf (µmol CO_2 mol^{-1} air) and g_{sc} (mol air m^{-2} leaf s^{-1}) is the stomatal conductance. Stomatal conductance is simulated as proposed by Leuning (1995):

$$g_{sc} = g_{s0} + \frac{a_1 A}{\left(C_s - \Gamma\right)\left(1 + D_s / D_0\right)} \quad (2.9)$$

Where g_{s0} is the stomatal conductance when A = 0, Γ (µmol CO_2 mol^{-1} air) is the CO_2 compensation point when respiration is present, D_s (kPa) is vapor pressure deficit at the leaf surface and D_0 is the response of g_{sc} to vapor pressure deficit. The parameter a_1 is an empirical parameter where $1/a_1 = 1 - C_i/C_s$ at saturating levels of absorbed radiation (Leuning et al., 1995). It was assumed that these parameters did not vary with the position inside the canopy or leaf age. The coupling of the supply and demand functions is solved analytically as proposed by Leuning (1990). See Appendix IV for more details.

Leaf temperature is needed to calculate the value of the different parameters of the photosynthesis model, as described by equation 2.7. Leaf temperature depends on the temperature of the air within the canopy, the leaf boundary layer conductance for heat fluxes and the leaf energy balance, as described by Leuning et al. (1995). The degree to which a leaf alters the environment around it (i.e. D_s, C_S and T_L) is defined by the degree of coupling of the leaf to the air (Jarvis and McNaughton, 1986). An ideal, perfectly coupled leaf (i.e. a leaf which boundary layer is negligible) will not affect D_s, C_s or T_L and these variables will be equal to VPD, CO_2 concentration in the air and temperature of the air, respectively. Small, hypostomatous leaves in well ventilated canopies such as orchards are highly coupled (Jarvis and McNaughton, 1986). Villalobos et al. (2000) observed that an olive orchard was highly coupled to its environment and the assumption of a perfect coupled canopy was a good approximation. This evidence suggests that it is reasonable to assume perfectly coupled olive leaves. This assumption avoids the need to solve the energy balance and does not require that the distribution of wind velocity be known, which is not well understood for discontinuous canopies such as tree orchards (Lee, 2000). Some initial simulations were performed in Maestra with and without solving the energy balance and for different exponential extinctions of wind velocity. The differences between the results were negligible, supporting the adequacy of the assumption.

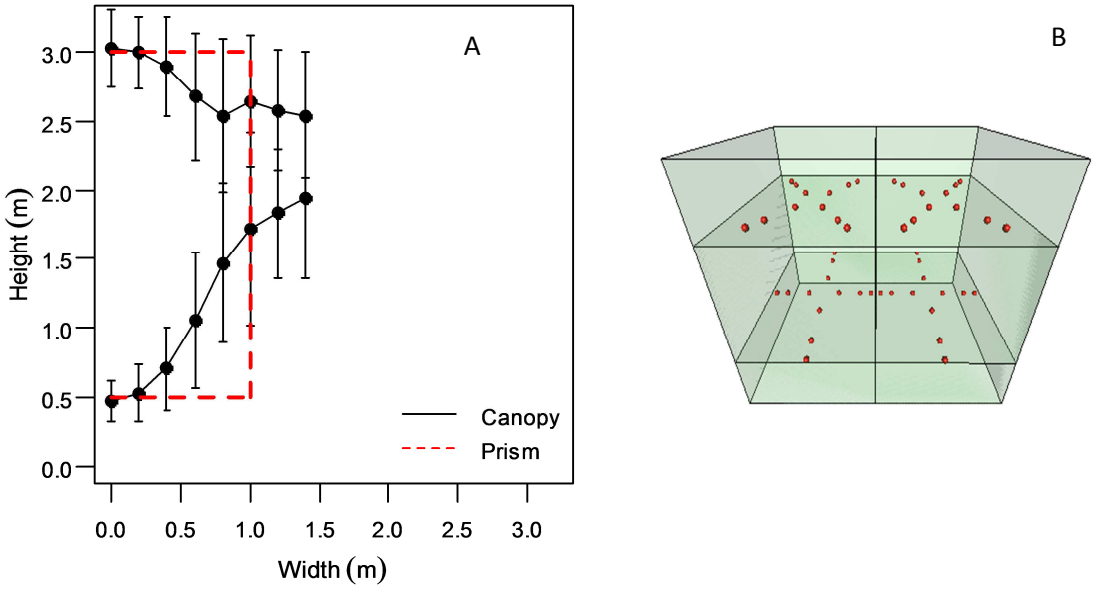

Figure 2.1: A: The transversal half-area of the hedgerow, averaged for 24 transects (4 trees). Solid lines represent the envelope surface of the canopy. The vertical bars represent twice the standard deviation. The dashed, red lines represent the approximation to the canopy as a prism, fixing the height and using the equivalent width. B: 3D sketch of the crowns of two consecutive olive trees as simulated by Maestra. Two layers are represented, with the grid points associated to the different sectors for each layer. The disposition of the grid points is characteristic of even and odd layers.

3.2.3. Radiation Interception

3.2.3.1. Canopy structure and parameters

The dimensions of the crowns[11] were obtained by measuring the intersection of a meter pole with the surface crown at different points in a regular grid. For every point, the upper and lower heights of the crowns were registered (figure 2.1A). The grid was composed of transects perpendicular to the planting row every 0.75 m, while each transect was 2 m long and was divided into 10 intervals of 20 cm. Ten trees were measured and for each tree, three transects were sampled at each side of the hedgerow.

The height of the crowns varied less than their width (figure 2.1A). The crown did not fit exactly any regular shape and out of all the crown shapes used in Maestra, the prism was the one that best resembled the real canopy (figure 2.1B). A first prism was calculated by assuming the same volume and height as the real crowns and calculating the equivalent width. A second prism was calculated by assuming the same volume and width as the real crowns and calculating the equivalent height. The two approaches were compared in their ability to predict measured PAR radiation on the ground and the one that best predicted the measurements was used in the simulations. The orientation of the grid points in Maestra varies for odd and even layers, so that different azimuth orientations can be sampled (figure 2.1B). The code of Maestra was modified to adapt the distribution of the grid points to a rectangular prism.

Measurements of PAR radiation beneath the canopy were taken on DOY 205 with a ceptometer (model SunScan, Delta-T Devices, Cambridge, UK) for the same four trees that were used to calculate crown dimensions. For every tree, measurements were taken on a transect perpendicular to the rows that extended from one row to the next one, to the west side of the trees being studied. Measurements were taken every 20 cm and throughout the first half of the day. A total of 7 repetitions per tree were taken, from 600 GMT until 1400 GMT. For every measurement, a simulation of PAR transmittance at the same locations was simulated using Maestra, with the leaf area and crown dimensions of every individual tree as input.

The average crown height was 2.5 m and the average volume associated to each tree-unit[12] was 7.12 m^3. For the same volume and height, the equivalent width of the regular prism was 1.9 m. Average leaf area index was evaluated with a plant canopy analyzer (model LAI-2000, LI-COR Biosciences, Lincoln, Nebraska, USA) under overcast conditions using a 15° view cap facing the hedgerows, in order to approximate the conditions of Miller's formula (Miller, 1966; in LI-COR Biosciences, 1992)

$$LAI = \int_0^{\pi/2} -\log\left(T(Z)\right)\cos Z \sin Z \, dZ \qquad (2.10)$$

[11] In this study, canopy refers to the aboveground part of the tree orchard. Thus, the canopy is the result of distributing the crowns in the field following a certain planting pattern. For example, leaf area index is a property of the canopy whereas leaf area density refers to the crowns.

[12] A tree-unit in this study refers to a volume of the hedgerow limited by a length of 1.5 m (i.e. the distance between consecutive trees). Note that individual crowns are not distinguishable in a hedgerow.

Where LAI is the leaf area index (m^2 leaf m^{-2} ground), T is the transmittance of the canopy and Z is the zenith angle. Knowing that each tree was associated to a ground surface of 6 m^2, the plant leaf area was derived and by dividing by the volume associated to each tree-unit, the average leaf area density resulted into 2.18 ± 0.12 m^2 leaf m^{-3} crown. The parameter X from the ellipsoidal leaf angle distribution (equation 2.2) was calculated based on data published by Mariscal et al. (2000b) for adult trees (cv. "Picual"). Details about this calculation are presented in Appendix III. Optical properties of the leaves were obtained from Mariscal et al. (2000a) for adult trees (cv. "Arbequina"), averaging values for abaxial and adaxial surfaces. Soil reflectance of PAR was assumed to be 0.2.

3.2.4. Sensitivity Analysis

3.2.4.1. Parameters

A sensitivity analysis of daily integrated canopy photosynthesis (P_g, g CO_2 m^{-2} ground day^{-1}) was performed for 18 parameters (table 2.1). In order to perform this analysis, the relevant scientific literature was used to obtain values for the parameters (i.e. “nominal values” in the analysis). The sensitivity of the model also depends on the environmental conditions, so four different days from the weather series at “La Harina” in 2011 were selected (table 2.1) representing days with high and low temperature and solar radiation. Only daily averages are presented but the original data consisted of averages for periods of 10 min.

The parameters of the stomatal conductance model were obtained from Moriana et al. (2002) for adult trees (cv. "Picual"). The parameters of the model of biochemical demand of CO_2 were retrieved from Diaz-Espejo et al. (2006) for adult and young trees (cv. "Manzanilla"). The activation energy for every parameter in the photosynthesis model was taken from Bernacchi et al. (2001), except for parameters $V_{c,max}$ and J_{max} that were taken from Diaz-Espejo et al. (2006). In Diaz-Espejo et al. (2006), $\Delta H_a = H_p$ and $c = \Delta H_a / (273R)$ so the Arrhenius equation in this work is parameterized only by ΔH_a.

3.2.4.2. Sensitivity Indices

The sensitivity of a model output to changes in the values of the parameters can be defined as the partial derivative of the output of the model with respect to each parameter. In general, the derivative of any function is not constant over time, except for linear models. A local sensitivity analysis evaluates the sensitivity of the model at nominal values of the parameters, whereas a global sensitivity analysis defines the sensitivity for a region of variation of the parameters (Saltelli et al., 2008).

Global sensitivity analysis includes different methodologies, among which the most important are the variance-based analyses and screening methods (Saltelli et al., 2008). In this study, a screening method, based on derivatives (Sobol and Kucherenko, 2009), was used. The derivative of function f with respect to parameter x_i evaluated at the point x_i^* can be approximated numerically as:

$$E_i(x^*) = \frac{f(x_1^*,\ldots,x_i^*(1+\Delta),\ldots,x_k^*) - f(x_1^*,\ldots,x_i^*,\ldots,x_k^*)}{\Delta x_i^*} \qquad (2.11)$$

Table 2.1: Nominal values of parameters considered in the sensitivity analysis. ρ_{soil}, τ_{leaf} and ρ_{leaf} are the soil reflectance, leaf transmittance and reflectance of PAR, respectively. g_{s0} is the stomatal conductance for null net photosynthesis, a_1 is the proportionality factor between net photosynthesis and stomatal conductance, D_0 describes the response of stomatal conductance to VPD, Γ is the CO_2 compensation point, θ describes the degree of curvature of the response to PAR of the electron transport rate, α is the quantum efficiency, J_{max} and $V_{c,max}$ are the maximum rates of electron transport and activity of Rubisco. H_J and H_{Vc} are the activation energies of J_{max} and $V_{c,max}$. R_d and H_{Rd} are the reference leaf respiration at 25 °C and its activation energy. X is the parameter of the ellipsoidal leaf angle distribution, LAD is leaf area density, c' is the ratio between crown height and width. The units in this table correspond to the original units in Maestra and may differ from the ones used in the rest of the text.

Parameters	Units	Nominal value	Source
ρ_{soil}	–	0.2	Assumed
τ_{leaf}	–	0.001	Mariscal et al. (2000a)
ρ_{leaf}	–	0.072	Mariscal et al. (2000a)
g_{s0}	mol m^{-2} leaf s^{-1}	0.045	Moriana et al. (2002)
a_1	–	4.53	Moriana et al. (2002)
D_0	Pa	3500	Moriana et al. (2002)
Γ	µmol CO_2 mol^{-1}	46	Moriana et al. (2002)
θ	–	0.9	Diaz-Espejo et al. (2006)
α	mol e (mol PAR)$^{-1}$	0.2	Diaz-Espejo et al. (2006)
J_{max}	µmol m^{-2} leaf s^{-1}	135.5	Diaz-Espejo et al. (2006)
$V_{c,max}$	µmol m^{-2} leaf s^{-1}	82.7	Diaz-Espejo et al. (2006)
R_d	µmol m^{-2} leaf s^{-1}	1.12	Diaz-Espejo et al. (2006)
H_J	J mol^{-1}	35 350	Diaz-Espejo et al. (2006)
H_{Vc}	J mol^{-1}	73 680	Diaz-Espejo et al. (2006)
H_{Rd}	J mol^{-1}	44 790	Diaz-Espejo et al. (2006)
X	–	2.6	Mariscal et al. (2000a)
LAD	m^2 leaf m^{-3} crown	2.15	Measured
c'	m m^{-1}	1.32	Measured

Table 2.2: Four scenarios chosen from the weather series at La Harina in 2011. T is average air temperature, VPD is average vapor pressure deficit, Rs is daily solar radiation and ΔT is daily temperature amplitude.

Scenario	Day of Year	T (°C)	VPD (kPa)	Rs (MJ m^{-2} ground day^{-1})	ΔT (°C)
1	26	7.9	0.2	5.1	7.8
2	128	18.2	1.0	26.3	18.2
3	266	26.7	2.1	26.4	8.4
4	208	31.0	3.5	29.0	20.0

Where Δ is a small relative variation of parameter i and k is the number of parameters. Δ was defined for each parameter as 10^{-6}. This value was chosen as a balance between the accuracy needed in estimating the derivative and the effects of finite numerical precision in the computation. Since photosynthesis varied throughout the day, it was simulated for steps of 20 min (see Appendix V for details about the simulations settings) and the absolute differences were averaged for every scenario and parameter combination:

$$E_i(x^*) = \frac{\sum_{j=1}^{n} \left| f(x_1^*, \ldots, x_i^*(1+\Delta), \ldots, x_k^*, t_j) - f(x_1^*, \ldots, x_i^*, \ldots, x_k^*, t_j) \right|}{n \Delta x_i^*} \quad (2.12)$$

Where n is the number of 20-min intervals between sunrise and sunset for every scenario and t is every 20-min interval in the simulation. Taking absolute values was necessary as changes in the parameters may increase or decrease photosynthesis at different moments of the day, the results of which would otherwise (partly) level out. The global sensitivity index of a parameter i (μ_i^*) was calculated as:

$$\mu_i^* = \frac{x_i^n}{f^n} \sum_{j=1}^{N} \left| E_i(x_j) \right| \frac{1}{N} \quad (2.13)$$

Where each value of x was generated by a quasi-Monte Carlo sampling procedure (Caflisch, 1998) from the region of variation of each parameter, for a total of N samples (see Appendix V for further details). This index can be interpreted as "the normalized average of the sensitivity of model output to the parameters, when all the parameters are varied at the same time within a nominal region". This index is similar to the one proposed by Campolongo et al. (2007), but normalizing the results by the nominal values and using the quasi-Monte Carlo method to sample parameter space. The local sensitivity coefficient was also calculated:

$$SC_i = E_i(x^n) \frac{x_i^n}{f^n} \quad (2.14)$$

Where the exponent n refers to the nominal values of the parameter or the model output. The interpretation of this index is "the relative variation of model output per relative variation of parameter i around its nominal value".

3.2.5. Simulation of canopy photosynthesis and net CO_2 exchange

Simulations of canopy photosynthesis were performed with the model and compared with the calculations of canopy photosynthesis obtained in the experiment (see Chapter 1) following both strategies. Canopy photosynthesis was simulated every 5 minutes, dividing the canopy into 9 layers and 12 grid points per layer and the flux was averaged in periods of 30 min.

To calculate net primary production, the respiration of the trees was needed. The model of photosynthesis already included leaf respiration, but it was necessary to estimate the respiration for the rest of the organs. Using allometric coefficients and the biomass of leaves, it was possible to estimated the biomass of the rest of the organs. The biomass of leaves was deduced from the specific leaf area. Two samples of 100 leaves were taken, choosing fully expanded leaves distributed throughout the entire canopy. They were sealed into a refrigerated plastic bag to avoid dehydration in the transport and their surface were measured with an area meter (model LI-3000, LI-COR Biosciences, Lincoln, NE). They were dried in an oven for 48 h and weighted again to obtain the dry matter content. The result was a specific leaf area of 50.0 (2.2) 10^{-4} m^2 (g DM)$^{-1}$.

The biomass stored in the wood of the trees was deduced assuming a wood:leaf ratio of 0.7:0.3 based on the data published by Mariscal et al. (2000b) and Villalobos et al. (2006). Out of the total woody tissue, 85% was considered tissue with low metabolic activity and 15% tissue with high metabolic activity (Perez-Priego,

submitted). The respiration of these tissues was simulated using the model of Lloyd and Taylor (1994) with the parameters obtained by Perez-Priego et al. (submitted) from chamber measurements:

$$R_{wood} = W_{wood} R_{w,18} \exp^{E_0\left(\frac{1}{291.15-T_0} - \frac{1}{T+273.15-T_0}\right)} \quad (2.15)$$

Where R_{wood} is the respiration of wood material (µmol CO_2 m^{-2} ground s^{-1}), W_{wood} is wood biomass (kg DM m^{-2} ground), $R_{w,18}$ is respiration per unit of biomass at 18 °C (µmol CO_2 kg DM s^{-1}), and E_0 and T_0 (K) are empirical parameters. $R_{w,18}$ was 0.06 and 0.95 µmol CO_2 m^{-2} ground s^{-1} kg^{-1} DM for low and high activity tissues, E_0 was 200 and 166 K and T_0 was 247 and 256 K, respectively. It was assumed that root biomass represented one third of the total biomass (Mariscal et al., 2000b; Scariano et al., 2008; see Chapter 3), that fine roots represented 2/3 of root biomass and that the respiration per unit of biomass of fine and structural roots was the same as for wood tissues with high and low metabolic activity. The net primary production was calculated by subtracting plant respiration from canopy photosynthesis. Assuming a concentration of 50% of carbon in dry matter, it was possible to calculate the radiation use efficiency (RUE, g DM MJ^{-1} PAR) and potential productivity (g DM m^{-2} ground day^{-1}).

3.3. Results

3.3.1. Radiation Interception

The prism with the same volume and height as the real canopy generated a better prediction of PAR beneath the canopy than the prism with the same volume and width (figure 2.2). The simulations underestimated PAR at the center of the alley and overestimated slightly PAR beneath the canopy on the west side (last 1.5 meters of each transect). The predictions of PAR radiation beneath the canopy were in general very accurate. With the prism that maintained the same volume but fixed the width, PAR on the ground was overestimated beneath the canopy and underestimated in the center of the alley and the predictions were not very accurate. Based on the results, the prism with the same volume and height was used for all the simulations.

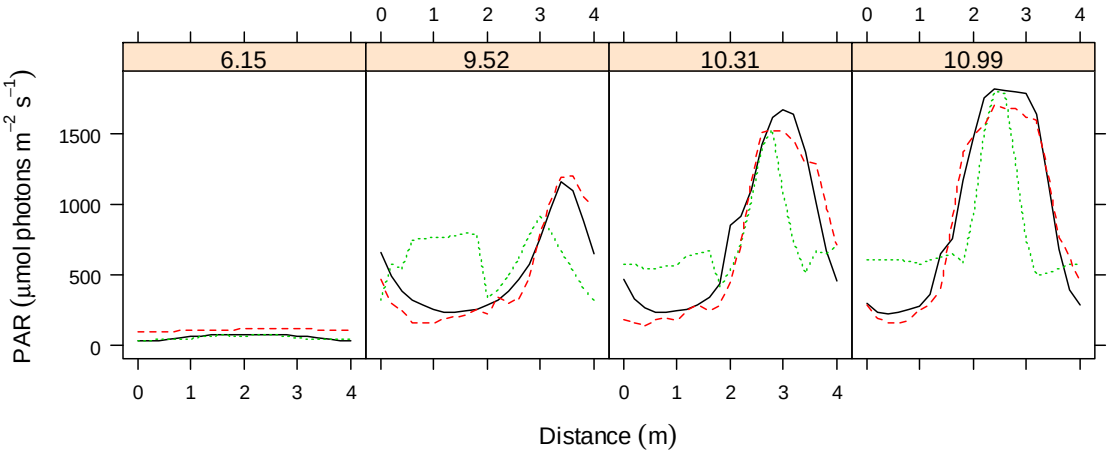

Figure 2.2: PAR on the ground at different distances from the row of trees and times of the day (GMT, indicated in the grey headers). The black solid lines represent the measured values for each distance and time of day, the red dashed lines are the simulations for a prism with the same volume and height as the real canopy and the green dotted lines for a prism with the same volume and width. The east direction corresponds to the left side of the plots.

3.3.2. Sensitivity analysis

To facilitate the interpretation of the results, horizontal bar plots were used to describe the sensitivity to each parameter and for every index (i.e. local sensitivity, SC_i and global sensitivity, μ_i^* for 10% and 20% variation). All the values are given in table AVI.1 in Appendix VI. The global sensitivity did not vary much for the ±10% and ±20% range of variation for most parameters, so only results for ±20% are shown for all the scenarios (figure 2.5). The differences among sensitivity indices are shown for scenario 4 (figure 2.2). The parameters LAD, α, θ, J_{max} and c' had on scenarios 1-3 a much higher influence than Γ, d_{0L}, ρ_{soil}, ρ_{leaf}, τ_{leaf}, g_0, X, H_j, and a_1, V_{cmax}, H_{vc}, H_{rd}. In scenario 4, the differences were smaller and the transition from the most influential 5 parameters to the rest of the parameter was more gradual.

Some parameters showed clear differences in the values of SC_i and μ_i^*, such as θ, α or R_d, where the sensitivity of the model varied greatly with the index being used. In general, the global sensitivity decreased when the range of variation increased, but that was not always the case (e.g. LAD and g_0). The different results generated by the indices did not have a great impact in the ranking of the most influential parameters but it affected the ranking of parameter with lower influence, such as H_{Rd} and R_d. The global index with ±20% variation resulted in a more equilibrated sensitivity to the different parameters (figure 2.5), whereas the local sensitivity showed a sensitivity highly concentrated in the most influential parameters. Differences between local and global sensitivity indices were more important than differences in the range of variation of the global sensitivity indices (figure 2.3). All values of SC_i or μ_i^* were smaller than 1, indicating that changes in any parameter always had a less than proportional effect on photosynthesis. The highest sensitivity was obtained for scenarios 1 and 3 with values of SC_i and μ_i^* up to 0.75.

The parameters of the stomatal conductance model had a very small influence on photosynthesis, which translates into a small effect of VPD (which only acts through parameter D_0). The optical properties of the leaves and soil surface had a negligible effect while canopy structure was very important. As vapor pressure deficit had a small impact on photosynthesis and since CO_2 concentration was assumed constant in the simulations, photosynthesis was determined by leaf temperature and absorbed PAR radiation (figure 2.4A). The average absorbed PAR radiation for each layer was small in all scenarios, due to high leaf area density (figure 2.4B), so that only the outer leaves were exposed to high solar radiation fluxes. For the range of values of absorbed PAR and temperature observed in the simulations, photosynthesis was limited by the rate of electron transport (figure 2.4A). For higher radiation fluxes (e.g. scenario 4), photosynthesis in the upper layer of the canopy and during the central hours of the day became limited by the activity of Rubisco (figure 2.4A), which increased the influence of $V_{c,max}$ in the analysis (figure 2.5), but when all the layers and fluxes during the day are considered, the overall effect was small. The intercellular CO_2 concentration was very stable, with a variation of 240-250 μmol CO_2 mol^{-1} air in the range 15-45 °C and 0-1500 μmol photons m^{-2} leaf s^{-1}.

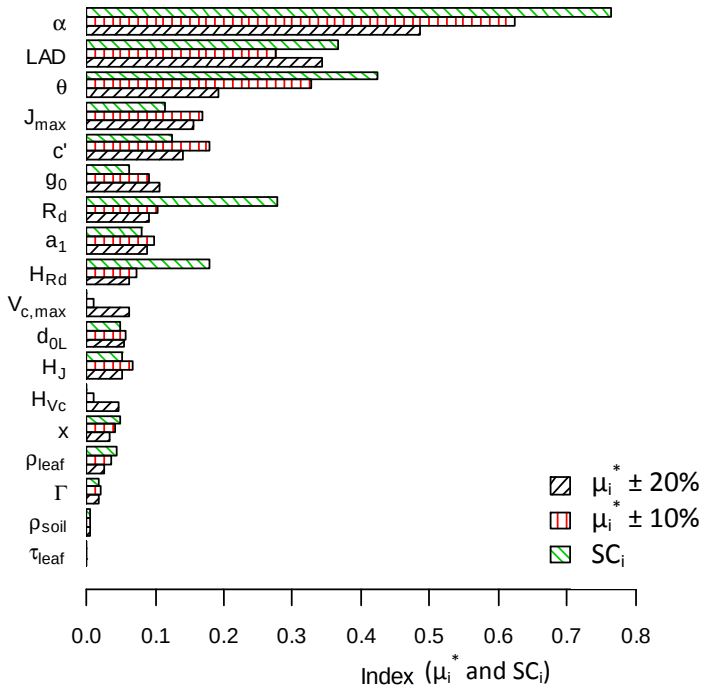

Figure 2.3: Comparison of all sensitivity indices applied to daily canopy photosynthesis for scenario 4. SC_i represents local sensitivity, μ_i^* ± 10% and μ_i^* ± 20% represent global sensitivity for a range of variation 10% and 20%, respectively.

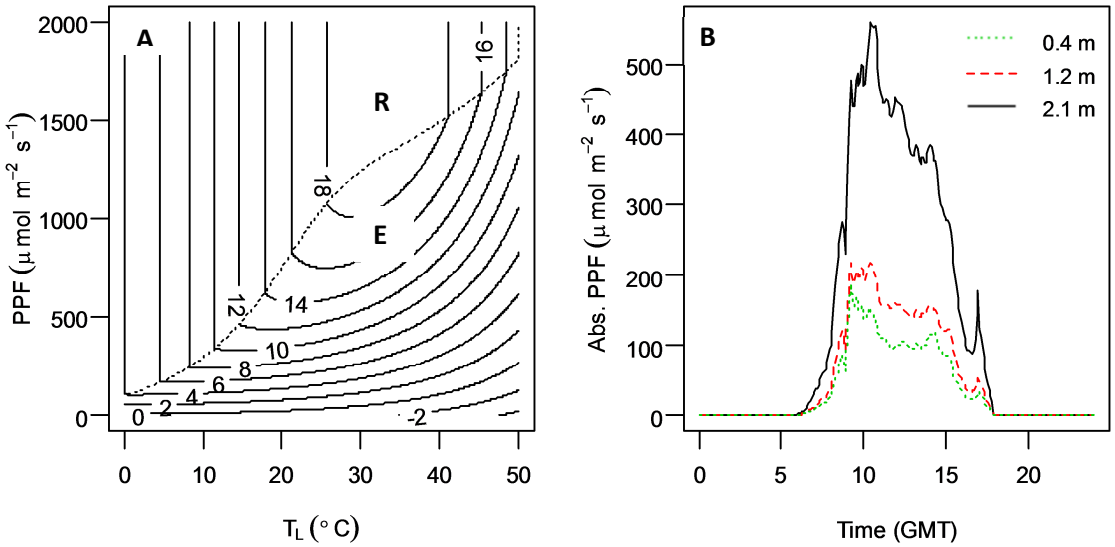

Figure 2.4: A: Contour plot of net leaf photosynthesis (µmol CO_2 m^{-2} leaf s^{-1}) versus photon flux density (PPF) and leaf temperature (T_L), with constant surface CO_2 concentration (360 µmol CO_2 mol^{-1} air) and vapor pressure deficit (VPD, 3 kPa). The dotted line separates Rubisco-limited photosynthesis (upper region, R) and light-limited photosynthesis (lower region, E). B: The average absorbed PPF for each layer in scenario 3 of the sensitivity analysis.

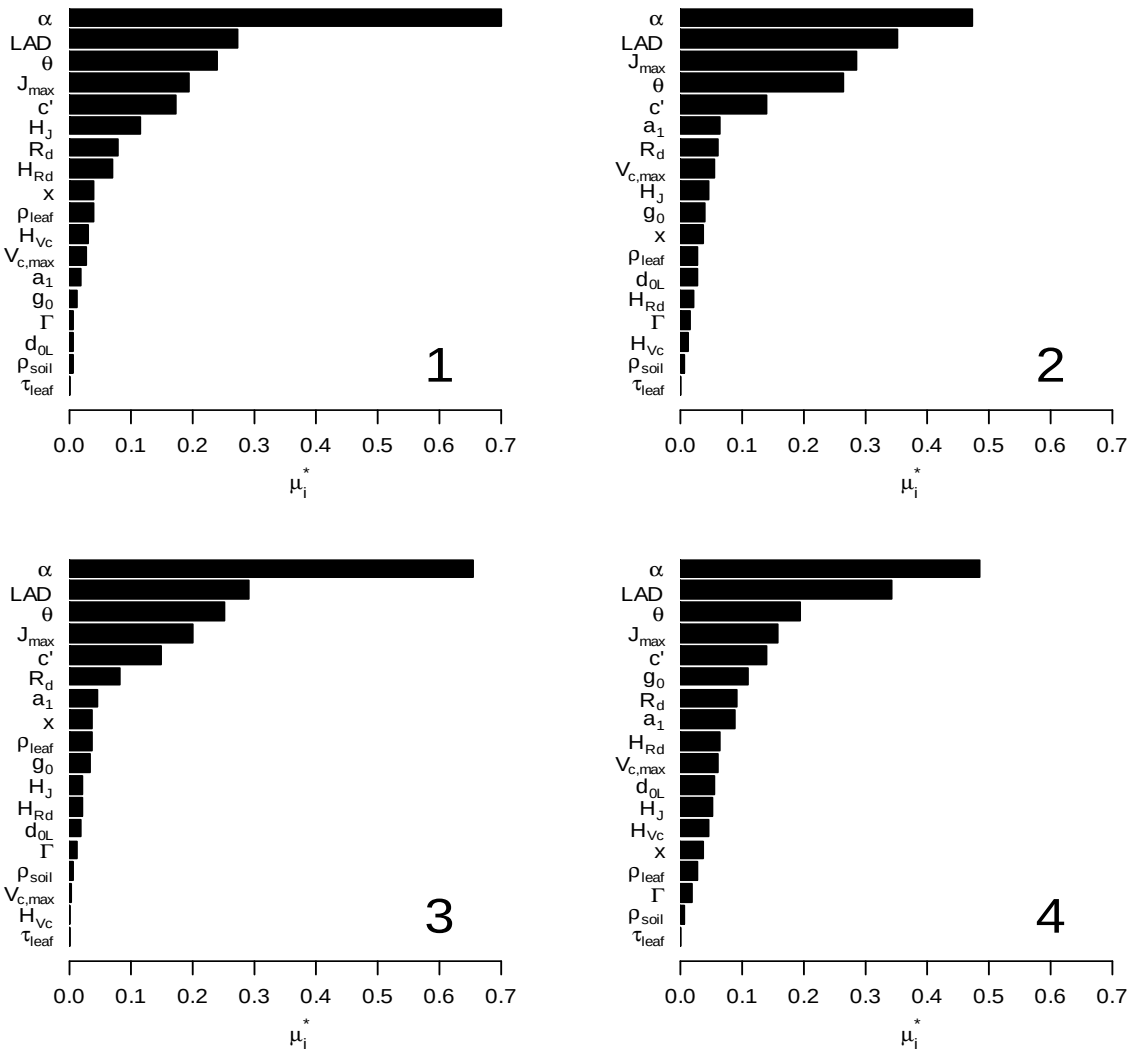

Figure 2.5: Absolute global sensitivity (±20%) of daily photosynthesis for all scenarios (1 through 4). See table 2.1 for the meaning of the parameters.

3.3.3. Simulations

The control treatment and the treatment that received normal farm management had very similar values of predawn leaf water potential at the beginning of the experiment and they both decrease to a minimum value on DOY 220 (figure 2.6). The predawn leaf water potential at the beginning of the experiment was -0.2 MPa for both treatments, whereas the minimum was -1.1 MPa for the treatment under farm management and -0.8 MPa for the control treatment. This means that the irrigation applied to the trees was not sufficient to maintain the soil water potential in the root zone, even for the control treatment. Part of the decrease could be explained by a decrease of irrigation during August due to technical problems (see Materials & Methods).

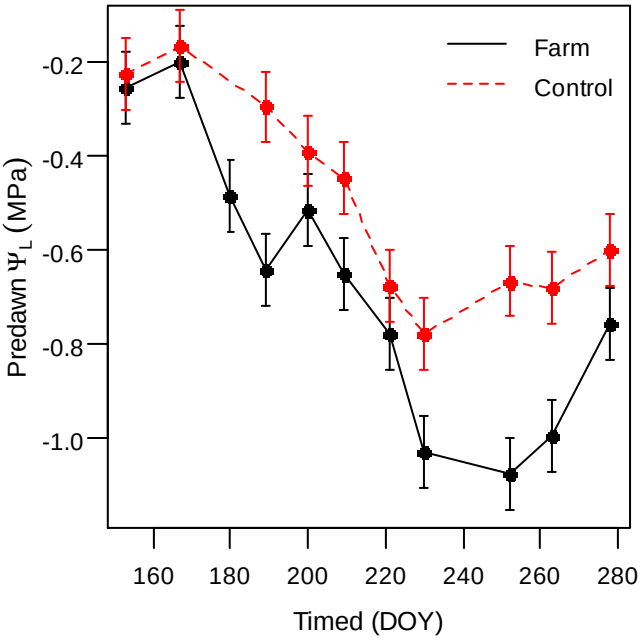

Figure 2.6: Predawn leaf water potential measured in a tree under control irrigation (red, dashed lines) and farm irrigation (black, solid line).

The simulations generated by the model were biased with respect to the calculations obtained in the experiment (figure 2.7B), and the residuals were not distributed symmetrically, with long tails towards lower values. The median of the residuals between the model and calculated canopy photosynthesis based on strategy 1 was +7.48 (+40%) µmol CO_2 m^{-2} ground s^{-1} and for strategy 2 it was -3.66 (-15%) µmol CO_2 m^{-2} ground s^{-1} (figure 2.7B). The standard deviation of the residuals was 4.45 and 4.61 µmol CO_2 m^{-2} ground s^{-1} for strategy 1 and 2, respectively. The average standard error of both measurements was 1.8 µmol CO_2 m^{-2} ground s^{-1} (see Chapter 1), which indicated that over half of the variance in the residuals was due to structural error in the model. There was some seasonal variation in the residuals (figure 2.7B), which is represented by in the figure by a loess regression. A loess regression fits a polynomial to each point in the dataset using weighted least squares, where the weight for each point is the distance to the point where the fit is being calculated. The loess curve is the combination of the loess curve for all points. It is a robust method to represent the mean trend of a cloud of points (Cleveland, 1979).

The seasonal trend of simulated canopy photosynthesis was very similar to the seasonal trend of canopy photosynthesis calculated following strategy 1 (figure 2.7A), once they were divided by the average flux during the period 170-190 to remove the systematic deviation between the model and the experiment (figure 2.7B). The gaps in the measurements due to rejection of low quality eddy covariance fluxes explain part of the very low relative values in the period between DOY 275 and 300 (i.e. without gaps the decrease of relative photosynthesis is not so abrupt).

The integration of photosynthesis and plant respiration to the daily scale indicated that the estimated plant respiration was, on average, 40 ± 0.07% of canopy photosynthesis with an average net primary production of 22.2 g CO_2 m^{-2} ground day^{-1}. Maximum and minimum photosynthesis was 45.0 and 13.9 g CO_2 m^{-2} ground day^{-1},

on days 165 and 297 of the year, respectively. Maximum and minimum plant respiration was 22.1 and 6.7 g CO_2 m^{-2} ground day^{-1}, on days 231 and 298 of the year, respectively. When the net primary production is converted into production of dry matter aboveground, an average of 7.3 g DM m^{-2} ground day^{-1} is obtained. Note that trees intercepted, on average, 61% of total incoming PAR and the vertical projection of the canopy covered 47.5% of the soil. Assuming a hypothetical orchard that intercepted all the radiation and had the same radiation use efficiency, the daily production of dry matter aboveground will increase to 12.0 g DM m^{-2} ground day^{-2}.

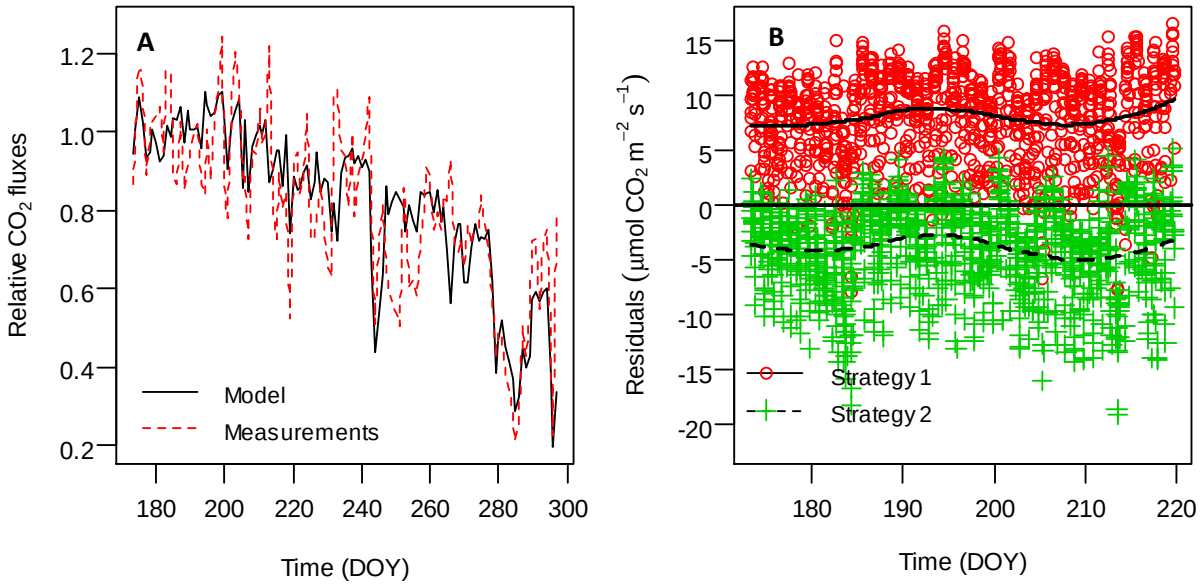

Figure 2.7: A: Relative daily canopy photosynthesis simulated with Maestra and calculated from the experiment with strategy 1 (net ecosystem exchange + ecosystem respiration). The original daily values were divided by the average during the period 170-190. B: Residuals between simulated fluxes and calculated fluxes from the experiment versus time. Green crosses represent the residuals for strategy 1. Red circles represent the residuals for strategy 2 (net ecosystem exchange + soil respiration + canopy respiration).

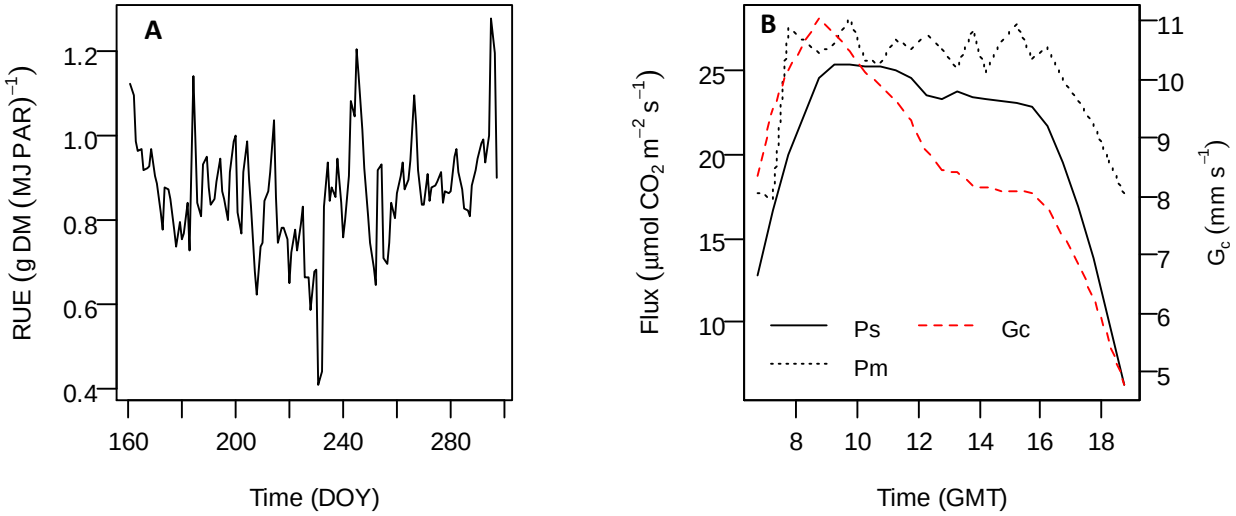

Figure 2.8: Daily radiation use efficiency calculated with the output of the model (RUE, g DM $(MJ\ PAR)^{-1}$) of the aboveground part of the trees (A) and an example of the diurnal trend of simulated canopy photosynthesis (Ps, µmol CO_2 m^{-2} ground s^{-1}), photosynthesis calculated with strategy 2 (Pm = net ecosystem exchange + soil respiration + canopy respiration) and simulated canopy conductance (G_c, mm s^{-1}) for DOY 191 (B). This example is representative of clear-sky summer days in the simulation.

The daily radiation use efficiency decreased during the summer (figure 2.8A) to a minimum of 0.40 g DM (MJ PAR)$^{-1}$ on DOY 231, though this minimum was much lower than the other values observed in the simulation. After this minimum, the radiation use efficiency rapidly recovered and increased throughout autumn, with a maximum over 1.42 g DM (MJ PAR)$^{-1}$. This variation was linearly related to daily average temperature (R^2 = 0.65)

The diurnal trend of canopy photosynthesis simulated by the model and calculated with strategy 2 were quite similar (figure 2.8B), for clear-sky summer days. Canopy photosynthesis varied little during most of the day with an average value of 25 µmol CO_2 m^{-2} ground s^{-1}. This pattern was explained by the diurnal evolution of radiation interception (not shown, but a similar curve to that for photosynthesis in figure 2.8B). The model always underestimated photosynthesis at the end of the day, which caused the asymmetry in the residuals (figure 2.7B).

The simulated canopy conductance, however, presented a very different diurnal pattern, with an asymmetric curve that peaked early in the morning, decreasing during the rest of the day. In some days, canopy conductance recovered partially at the end of the day, and the midday decrease varied from day to day. However, the maximum value was very constant, with an average of 11.25 ± 1.1 mm s^{-1}. This pattern is very characteristic of olive orchards (Testi et al., 2008; Villalobos et al., 2000). The variations in canopy conductance among days were mainly related to vapor pressure deficit whereas the variations in canopy photosynthesis were mainly related to radiation interception.

3.4. Discussion

3.4.1. Sensitivity analysis

For parameters with high influence, the differences in sensitivity measured by the difference indices were notable. The choice of the range of variation in the global sensitivity analysis was not as important as choosing to use a global or local sensitivity analysis. The more extended approached, proposed by Saltelli et al. (2000), combines sensitivity analysis with uncertainty analysis and the range of each parameter is different and it depends on the prior uncertainty on the value of each parameter (e.g. Campolongo and Braddock, 1999; Confalonieri et al., 2010; Richter et al., 2010). However, when that approach is applied, the results depends both on the sensitivity of the model and the prior uncertainty. In this study, it was preferred to fix the same relative range of variation for each parameter. However, in order for this approach to be useful one should adjust the range of variation based on the expectation on how much the parameter might change if calibrated with the data.

It is clear that the most influential parameters were θ, α, J_{max}, c' and LAD, and that there were small differences among scenarios. These results were obtained even for conditions of low vapor pressure deficits (VPD) and high solar radiation (i.e. scenario 2 or 3). These results can be explained by the fact that the hedgerows in the orchard had a high leaf area density and thus most of the leaves were exposed to a small photon flux, below the saturating levels associated to the hyperbola in equation 2.6. This would also explain the higher sensitivity in scenarios 1 and 3, which represent days with a higher fraction of diffuse radiation, than in scenarios 2 and 4,

since diffuse radiation penetrates more efficiently into the canopy allowing shaded leaves to increase their contribution to canopy photosynthesis.

Leaf optical properties and the angle distribution had a very small influence in the output, as opposed to leaf area density. Similar results were obtained by Wang and Jarvis (1990b) when simulating a stand of Sitka spruce with the model Maestro. Using the model Maestra, Luo et al. (2001) reported that canopy photosynthesis of a loblolly pine stand was more sensitive to α and leaf area than other parameters. Ibrom et al. (2006) also detected a higher sensitivity to α and a non-linear response of photosynthesis to this parameter when simulating with Maestra stands of Sitka and Norway spruce.

The results of the sensitivity analysis would suggest that the photosynthesis model used in this study could be simplified into a non-rectangular hyperbola, without great loss of predictive accuracy. However, this approximation is only valid, in principle, for the canopy structure studied in this work, as canopies with lower LAD or lower volume will expose a higher fraction of their leaves to a higher radiation flux and limitations due to Rubisco activity will become more important. Especially on clear-sky summer days with high incoming solar radiation. The effect of different canopy structures on the sensitivity of photosynthesis to different environmental factors requires further research.

3.4.2. Simulations

The low predawn leaf water potentials observed in the second half of the experiment could have affected canopy photosynthesis. Sofo et al. (2008) estimated that the predawn leaf water potential needs to fall below a threshold of -1.0 MPa before any physiological process starts to be affected. Xiloyannis et al. (1999) reported a threshold value of -0.9 MPa. However, Ennajeh et al. (2008) observed a decrease in gas exchange already with predawn leaf water potential of -0.5 MPa.

Photosynthesis is one of the first processes to be affected by water deficit (Sofo et al., 2008), which implies that some minor water stress may have occurred at the end of the summer, especially on days with high evaporative demand. Since the model does not account for the effect of water stress, this could be a source of error, though it would not affect the analysis of model residuals (figure 2.7B) as water potentials were all above -0.7 MPa during that period of time. The fact that the relative seasonal variation of canopy photosynthesis was similar in the model and in the measurements suggests that the possible effect of water stress on canopy photosynthesis was not very important in this experiment.

Given that the simulations of the model were much closer to canopy photosynthesis based on strategy 1, it is likely that the measurement of nighttime respiration were being greatly underestimated. As discussed in Chapter 1, the evidence in the literature with respect to this problem is highly diverse, but the presence of advection during the night could explain the underestimation generated by the method (Baldocchi, 2003). However, advection fluxes are very site-dependent (Aubinet, 2008) so that a generalization cannot be made from the results of this study. Indeed, Luo et al. (2001) found a good agreement between simulations with the model "Maestra" and canopy photosynthesis of a loblolly pine forest calculated with strategy 1. The fact that the seasonal dynamics were captured adequately by the model indicates that the underestimation of daytime

ecosystem respiration may be defined as a fixed fraction. Therefore, the underestimation could be corrected by multiplying by a correction factor which, in this case, has a value of 2 for daily integrated fluxes.

The radiation use efficiency of aboveground growth that has been reported should be taken with caution as it is influenced by the estimation (not measurement) of the biomass of the different components, and the assumption that the respiration per unit of biomass is constant throughout the experiment, which could affect the seasonal dynamics in figure 2.8A. However, Villalobos et al. (2006) observed in a high-density olive orchard cv. "Arbequina" an average aboveground radiation use efficiency of the aboveground part of the trees of 0.86 g DM MJ^{-1} PAR in fruit-bearing trees using measurements of cumulative biomass, very similar as the average value of 0.91 g DM MJ^{-1} PAR in this study. Using measurements of gas exchange at the tree level, Villalobos et al. (2012) obtained a radiation use efficiency of 0.98 g DM MJ^{-1} PAR for a high-density olive orchard. The daily value of aboveground biomass production is below the range of 15-25 g DM m^{-2} ground day^{-1} described for crops in the summer by Goudriaan and van Laar (1994) indicating a lower potential productivity for olive trees, even when assuming a hypothetical full cover. This agrees with the conclusions of Villalobos et al. (2006) that the potential production of olive trees is below that of typical C3 crops.

The seasonal and diurnal patterns of canopy photosynthesis agree with the results of a high sensitivity to absorbed PAR. The diurnal pattern of canopy conductance agrees with previous studies (Testi et al., 2008; Villalobos et al., 2000) that reported similar values and diurnal pattern. Similar patterns of canopy conductance have been reported for other tree species (e.g. forest of *Nothofagus*, Schulze et al., 1995; forest of *Pinus pinaster*, Gash et al., 1989).

However, the diurnal pattern of canopy photosynthesis is very different from the one reported by Testi et al. (2008), which presented a peak in the morning and a strong asymmetry (i.e. the same "shape" as the curve of canopy conductance). Based on their result, they hypothesized that photosynthesis in olive canopies is limited by radiation at the beginning of the day and by stomatal conductance during the rest of the day. The results of the experiment at "La Harina" and the simulations in this study are in contradiction with that hypothesis.

It is then assumed, that the aggregation of soil respiration and plant respiration (i.e. strategy 2) gave a more realistic estimation of canopy photosynthesis than the extrapolation of nighttime ecosystem respiration (i.e. strategy 1). Still, the model underestimated the observed fluxes by 15% and the residuals were more than twice the measurement error (see Chapter 1). Also, the fluxes during the two hours before sunset were always underestimated by the model. The possible sources of these errors are:

1. Canopy photosynthesis may have been underestimated by the model. The results from the comparison of PAR transmittance suggest that this underestimation should be generated by an underestimation of leaf photosynthesis, as simulated and measured PAR on the ground of the orchard were very similar. A strong reduction of the residuals can be expected by modification of θ, α or J_{max}, as indicated by the sensitivity analysis. These modifications could be explained by the following causes:

1.1. A possible vertical variation of specific leaf area and nitrogen concentration that has not been taken into account in the model. The parameters used in this study were calibrated for leaves exposed to

the sun (Diaz-Espejo et al., 2006) which would also result into an underestimation of photosynthesis, if acclimation is an important factor.

1.2. Mesophyll conductance is known to have an effect on photosynthesis of leaves in olive trees (Diaz-Espejo et al., 2007). The parameters obtained by Diaz-Espejo et al. (2006) did not consider the effect of mesophyll conductance, and this can cause an underestimation of calibrated J_{max} and $V_{c,max}$ (Niinemets et al., 2001; Flexas et al., 2008). The modification of the model of photosynthesis incorporating the effect of mesophyll conductance (e.g. Yin and Struik, 2009) could improve the predictions of the model, once all the parameters are re-estimated.

1.3. Genotype variations may cause a change in the values of the parameters of photosynthesis (Bernacchi et al., 2001). The parameters used in this study had been estimated for cv. "Manzanilla" and not cv. "Arbequina". Niinemets et al. (2001) used a value for α of 0.24 and for θ of 0.85, in simulations of leaf photosynthesis in a sclerophyllous evergreen Mediterranean tree species (*Quercus ilex* L.), which indicates that the values reported by Diaz-Espejo et al. (2006) could be rather low.

2. The overestimation of wood and leaf respiration could explain an underestimation of canopy photosynthesis following strategy 2. The response to temperature observed by Perez-Priego et al. (submitted) was taken for cv. “Arbequina” under the same climate. Also, the estimation of respiration of non-photosynthetic organs in this study is rather conservative, as respiration of fruits was not considered. Leaf respiration measured by Diaz-Espejo et al. (2006) and used in this study was very similar to the one observed by Perez-Priego et al. (submitted). The ratio of total plant respiration to canopy photosynthesis was within the range typically observed in plants (van Oijen et al., 2010). Thus, at least at the beginning of the experiment, plant respiration was most likely not overestimated.

3. The aggregation of soil respiration to the field level could be biased due to the spatial variability of the soil. The sampling of soil respiration and the calibration of the models was designed to minimize this bias, by accounting for location-specific variation of parameters and nonlinear responses to environmental conditions (see Chapter 1). Since soil respiration differed in the alleys and beneath the canopy, a higher weight of soil respiration in the alley in the spatial average would reduce the differences between the simulations and the estimated net canopy exchange.

In summary, the most likely explanations for the differences between the model and the calculations from the experiment are a possible underestimation of leaf photosynthesis and/or overestimation of soil respiration. Because it is not clear which is the cause of the systematic error, plus the good agreement with published values of radiation use efficiency and the correct simulation of the relative seasonal variation, it was considered that the model of photosynthesis and radiation interception presented in this study performs satisfactorily.

3.5. Conclusions

The following main conclusions have been reached in this study:

1. Simulations with the model "Maestra" agree with measurements of radiation interception, independent estimations of radiation use efficiency and canopy photosynthesis calculated as the sum of net ecosystem exchange, soil and canopy respiration (strategy 2).

2. Canopy photosynthesis calculated from the sum of net ecosystem exchange and ecosystem respiration was underestimated (strategy 2).

3. The simulations showed that canopy photosynthesis was mainly limited by radiation interception, though the radiation use efficiency varied seasonally. The average radiation use efficiency, defined for the aboveground organs, was 0.9 g DM MJ^{-1} PAR.

4. The diurnal curve of canopy photosynthesis was very symmetric in typical clear-sky days and followed the pattern of absorbed PAR.

References

Akaike, H., 1973. Information Theory and an Extension of the Maximum Likelihood Principle, International Symposium on Information Theory, Tsahkadsor, Armenian SSR, pp. 267-281.

Almagro, M., López, J., Querejeta, J.I. and Martínez-Mena, M., 2009. Temperature dependence of soil CO_2 efflux is strongly modulated by seasonal patterns of moisture availability in a Mediterranean ecosystem. Soil Biology and Biochemistry, 41(3): 594-605.

Amthor, J.S., 2000. The McCree-de Wit-Penning de Vries-Thornley respiration paradigms: 30 years later. Annals of Botany, 86(1): 1-20.

Aubinet, M., 2008. Eddy covariance CO_2 flux measurements in nocturnal conditions: An analysis of the problem. Ecological Applications, 18(6): 1368-1378.

Baldocchi, D. D., 1994. An analytical solution for coupled leaf photosynthesis and stomatal conductance models. Tree Physiology 14(7-9): 1069-1079.

Baldocchi, D. D., 2003. Assessing the eddy covariance technique for evaluating carbon dioxide exchange rates of ecosystems: past, present and future. Global Change Biology, 9: 479-492.

Baldocchi, D.D., Tang, J. and Xu, L., 2006. How switches and lags in biophysical regulators affect spatial-temporal variation of soil respiration in an oak-grass savanna. Journal of Geophysical Research G: Biogeosciences, 111(2): G02008.

Ball, J. T., Woodrow, I. E., and Berry, J. A., 1987. A model predicting stomatal conductance and its contribution to the control of photosynthesis under different environmental conditions. In: Biggins, J. (Editors), Progress in Photosynthesis Research Vol. IV. Nijhoff, Dordrecht. 4: 221-224.

Bélisle, C.J.P., 1992. Convergence Theorems for a Class of Simulated Annealing Algorithms on R^d. Journal of Applied Probability, 29(4): 885-895.

Bernacchi C. J, Singsaas, E. L., Pimentel, C., Portis, A. R. and Long, S. P. 2001. Improved temperature response functions for models of Rubisco-limited photosynthesis. Plant, Cell and Environment, 24, 253–259.

Bernardo, J. M. and Smith, A. F. M., 2007. Bayesian theory. John Wiley & Sons Inc. pp. 640.

Billesbach, D.P., 2011. Estimating uncertainties in individual eddy covariance flux measurements: A comparison of methods and a proposed new method. Agricultural and Forest Meteorology, 151(3): 394-405.

Bolker, B.M. and R Development Core Team, 2012. bbmle: Tools for general maximum likelihood estimation. http://cran.r-project.org/web/packages/bbmle/

Bolker, B.M., 2008. Ecological models and data in R. Princeton University Press, Princeton, NJ. 408 pp.

Brown, J.D., 2010. Prospects for the open treatment of uncertainty in environmental research. Progress in Physical Geography, 34(1): 75-100.

Burnham, K.P. and Anderson, D.R., 2002. Model Selection and Multimodel Inference: A Practical Information-Theoretic Approach. Springer, New York. 448 pp.

Cable, J., Ogle, K., Lucas, R., Huxman, T., Loik, M., Smith, S., Tissue, D., Ewers, B., Pendall, E., Welker, J., Charlet, T., Cleary, M., Griffith, A., Nowak, R., Rogers, M., Steltzer, H., Sullivan, P. and van Gestel, N., 2011. The temperature responses of soil respiration in deserts: a seven desert synthesis. Biogeochemistry, 103(1): 71-90.

Caflisch, R.E., 1998. Monte Carlo and quasi-Monte Carlo methods. Acta Numerica, 7: 1-49.

Campbell, G. S. 1986. Extinction coefficients for radiation in plant canopies calculated using an ellipsoidal inclination angle distribution. Agricultural and Forest Meteorology, 36: 317--321

Campolongo, F. and Braddock, R., 1999. Sensitivity analysis of the IMAGE Greenhouse model. Environmental Modelling & Software, 14(4): 275-282.

Campolongo, F., Cariboni, J. and Saltelli, A., 2007. An effective screening design for sensitivity analysis of large models. Environmental Modelling & Software, 22(10): 1509-1518.

Caticha, A. and Preuss, R., 2004. Maximum entropy and Bayesian data analysis: Entropic prior distributions. Physical Review E, 70(4): 046127.

Cleveland, W.S., 1979. Robust Locally Weighted Regression and Smoothing Scatterplots. Journal of the American Statistical Association, 74(368): 829-836.

Collatz, G. J. 1991. Physiological and environmental regulation of stomatal conductance, photosynthesis and transpiration: a model that includes a laminar boundary layer. Agricultural and Forest Meteorology, 54: 107-136.

Confalonieri, R., Bellocchi, G., Tarantola, S., Acutis, M., Donatelli, M. and Genovese, G., 2010. Sensitivity analysis of the rice model WARM in Europe: Exploring the effects of different locations, climates and methods of analysis on model sensitivity to crop parameters. Environmental Modelling & Software, 25(4): 479-488.

Connor, D. J., Fereres, E. 2005. The physiology of adaptation and yield expression in olive. Horticultural Reviews, 31: 155-229.

Cox, P. M., Betts, R. A., Jones, C. D., Spall, S. A. and Totterdell, I. J., 2000. Acceleration of global warming due to carbon-cycle feedbacks in a coupled climate model. Nature, 408: 184-187.

Davidson, E.A., Richardson, A.D., Savage, K.E. and Hollinger, D.Y., 2006. A distinct seasonal pattern of the ratio of soil respiration to total ecosystem respiration in a spruce-dominated forest. Global Change Biology, 12(2): 230-239.

de Pury, D. G. G., Farquhar, G. D. 1997. Simple scaling of photosynthesis from leaves to canopies without the errors of big-leaf models. Plant, Cell and Environment, 20: 537–557.

Desai, A.R., Richardson, A.D., Moffat, A.M., Kattge, J., Hollinger, D.Y., Barr, A., Falge, E., Noormets, A., Papale, D., Reichstein, M. and Stauch, V.J., 2008. Cross-site evaluation of eddy covariance GPP and RE decomposition techniques. Agricultural and Forest Meteorology, 148(6-7): 821-838.

Diaz-Espejo, A. Hafidi, B., Fernandez, J. E., Palomo, M. J. 2002. Transpiration and Photosynthesis of the Olive Tree: a Model Approach. Acta Horticulturae, 586: 457-460.

Díaz-Espejo, A., Fernández, J.E., Durán, P.J., Girón, I.F., Sinoquet, H., Sonohat, G., Phattaralerphong, J., Infante, J.M., Chamorro, V., Villagarcía, L. and Palomo, M.J. 2004. Canopy architecture and radiation interception measurements in olive. Acta Horticulturae (ISHS) 791: 531-538

Diaz-Espejo, A., Nicolás, E. and Fernández, J.E., 2007. Seasonal evolution of diffusional limitations and photosynthetic capacity in olive under drought. Plant, Cell and Environment, 30(8): 922-933.

Diaz-Espejo, A., Walcroft, A. S., Fernandez, J. E., Hafidi, B., Palomo, M. J. and Giron, I. F. 2006. Modeling photosynthesis in olive leaves under drought conditions. Tree Physiology, 26: 1445–1456

Draper, D. 1997. Model uncertainty in “stochastic” and “deterministic” systems. Proceedings of the 12th International Workshop on Statistical Modeling, Vienna. pp. 43-59.

Dutang, C. and Savicky, P., 2010. randtoolbox: Generating and Testing Random Numbers. http://cran.r-project.org/web/packages/randtoolbox/

Ennajeh, M., Tounekti, T., Vadel, A. M., Khemira, H. and Cochard, H. Water relations and drought-induced embolism in olive (Olea europaea) varieties 'Meski' and 'Chemlali' during severe drought. Tree Physiology, 28: 971–976

Falge, E., Baldocchi, D.D., Olson, R., Anthoni, P., Aubinet, M., Bernhofer, C., Burba, G., Ceulemans, R., Clement, R., Dolman, H., Granier, A., Gross, P., Grünwald, T., Holinger, D.Y., Jensen, N., Katul, G., Keronen, P., Kowalski, A., Ta Lai, C., Law, B. E., Meyers, T., Moncrieff, J., Moors, E., Munger, J. W., Pilegaard, K., Rannik, U., Rebmann, C., Suyker, A., Tenhunen, J., Tu, K., Verma, S., Vesala, T., Wilson, K., Wofsy, S., 2001. Gap filling strategies for defensible annual sums of net ecosystem exchange. Agricultural and Forest Meteorology, 107(1): 43-69.

FAO Statistics Division, 2012. FAOSTAT, http://faostat.fao.org

Farquhar, G. D. von Caemmerer, S. and Berry, J. A. 1980. A Biochemical Model of Photosynthetic CO2 Assimilation in Leaves of C3 Species. Planta, 149: 78-90.

Farquhar, G. D., von Caemmerer, S. and Berry, J. A. 2001. Models of Photosynthesis. Plant Physiology, 125: 42–45.

Fernandez, J.E., Moreno, F., Cabrera, F., Arrue, J.L. and Martin-Aranda, J., 1991. Drip irrigation, soil characteristics and the root distribution and root activity of olive trees. Plant and Soil, 133(2): 239-251.

Fernandez-Escobar, R., Marin, L., Sánchez-Zamora, M.A., García-Novelo, J.M., Molina-Soria, C. and Parra, M.A., 2009. Long-term effects of N fertilization on cropping and growth of olive trees and on N accumulation in soil profile. European Journal of Agronomy, 31(4): 223-232.

Fisher, R.A., 1922. On the Mathematical Foundations of Theoretical Statistics. Philosophical Transactions of the Royal Society of London. Series A, 222: 309-368.

Flexas, J., Ribas-Carbo, M., Diaz-Espejo, A., Galmes, J. and Medrano, H. 2008. Mesophyll conductance to CO2: current knowledge and future prospects. Plant, Cell and Environment, 31: 602–621.

Foken, T. Gockede, M., Mauder, M., Lahrt, L., Amiro, B., Munger, W., 2004. Post-Field Data Quality Control. In: X. Lee, W. Massman and B. Law (Editors), Handbook of Micrometeorology. Atmospheric and Oceanographic Sciences Library. Springer Netherlands, pp. 181-208.

Foken, T., 2008. Micrometeorology. Springer-Verlag, Berlin.

Gash, J. H. C., Shuttleworth, W. J., Lloyd, C. R., Andre, J. C., Goutorbe, J. P. and Gelpe, J. Micrometeorological mesaurements in Les Landes forest during Hapex-Mobilhy. Agricultural and Forest Meteorology, 46: 131-147.

Gaumont-Guay, D., Black, T.A., Griffis, T.J., Barr, A.G., Jassal, R.S. and Nesic, Z., 2006. Interpreting the dependence of soil respiration on soil temperature and water content in a boreal aspen stand. Agricultural and Forest Meteorology, 140(1-4): 220-235.

Gijzen, H. and Goudriaan, J. 1989. A flexible and explanatory model of light distribution and photosynthesis in row crops. Agricultural and Forest Meteorology, 48: 1-20.

Gockede, M., Foken, T., Aubinet, M., Aurela, M., Banza, J., Bernhofe, C., Bonnefond, J.M., Brunet, Y., Carrara, A., Clement, R., Dellwik, E., Elbers, J., Eugster, W., Fuhrer, J., Granier, A., Grunwald, T., Heineschm B., Janssens, I. A., Knohl, A., Koeble, R., Laurila, T., Longdoz, B., Manca, G., Marek, M., Markkanen, T., Mateus, J., Matteucci, G., Mauder, M., Migliavacca, M., Minerbi, S., Moncrieff, J., Montagnani, L., Moors, E., Ourcival, J. M., Papale, D., Pereira, J., Pilegaard, K., Pita, G., Rambal, S., Rebmann, C., Rodrigues, A., Rotenberg, E., Sanz, M.J., Sedlak, P., Seufert, G., Siebicke, L., Soussana, J.F., Valentini, R., Vesala, T.,

Verbeeck, H. and Yakir, D., 2008. Quality control of CarboEurope flux data - Part 1: Coupling footprint analyses with flux data quality assessment to evaluate sites in forest ecosystems. Biogeosciences, 5(2): 433-450.

Gomez-del-Campo, M. 2010. Physiological and Growth Responses to Irrigation of a Newly Established Hedgerow Olive Orchard. Hortscience, 45(5): 809–814.

Goudriaan, J. 1977. Crop Micrometeorology: a simulation study. Centre for Agricultural Publishing and Documentation, Wageningen, the Netherlands, 262 pp.

Goudriaan, J. and van Laar, H. H., 1994. Modelling Potential Crop Growth Processes: Textbook with exercises. Kluwer Academic Publisher, Dordrecht, Netherlands, 251 pp.

Goulden, M.L., Munger, J.W., Fan, S.M., Daube, B.C. and Wofsy, S.C., 1996. Measurements of carbon sequestration by long-term eddy covariance: Methods and a critical evaluation of accuracy. Global Change Biology, 2(3): 169-182.

Granier, A., Ceschia, E., Damesin, C., Dufrene, E., Epron, D., Gross, P., Lebaube, S., Le Dantec, V., Le Goff, N., Lemoine, D., Lucot, E., Ottorini, J.M., Pontailler, J.Y. and Saugier, B., 2000. The carbon balance of a young Beech forest. Functional Ecology, 14(3): 312-325.

Heinemeyer, A. and McNamara, N., 2011. Comparing the closed static versus the closed dynamic chamber flux methodology: Implications for soil respiration studies. Plant and Soil, 346(1): 145-151.

Højstrup, J., 1981. A simple model for the adjustment of velocity spectra in unstable conditions downstream of an abrupt change in roughness and heat-flux. Boundary-Layer Meteorology, 21(3): 341-356.

Hollinger, D.Y. and Richardson, A.D., 2005. Uncertainty in eddy covariance measurements and its application to physiological models. Tree Physiology, 25(7): 873-885.

Houghton, J., Filho, L., Callander, B., Harris, N., Kattenberg, A., Maskel, E., 1996. Climate Change. The Science of Climate Change. Contributionof Working Group I to the Second Assessment Report of the Intergovernemental Panel on Climate Change. Technical Summary. Cambridge University Press, Cambridge.

Hsiao, R.G., 1973. Plant responses to water stress. Annual Review of Plant Physiology, 24: 519-570.

Ibrom, A., Jarvis, P. G., Clement, R. Morgenstern, K., Oltchev, A., Medlyn, B. E., Wang, Y. P., Wingate, L., Moncrieff, J. B., Gravenhorst, G. A comparative analysis of simulated and observed photosynthetic CO2 uptake in two coniferous forest canopies. Tree Physiology, 26: 845–864

IGN, 2011. Mapa de Suelos 1:1000000. Instituto Geográfico Nacional. http://www2.ign.es/signa/

Jarvis, P. G. and McNaughton, K. G., 1986. Stomatal control of transpiration - scaling up from leaf to region. Advances in Ecological Research, 15: 1-49.

Jaynes, E. T. and Bretthorst, L., 2003. Probability theory: the logic of science. Cambridge University Press, pp. 727.

Kaimal, J.C., Izumi, Y., Wyngaard, J.C. and Cote, R., 1972. Spectral characteristics of surface layer turbulence. Quarterly Journal of the Royal Meteorological Society, 98(417): 563.

Kirkpatrick, S., Gelatt, C. D. and Vecchi, M. P., 1983. Optimization by Simulated Annealing. Science 220(4598): 671-680.

Koch, K.R., 2007. Introduction to Bayesian Statistics. Springer-Verlag Berlin Heidelberg, New York.

Kormann, R. and Meixner, F.X., 2001. An analytical footprint model for non-neutral stratification. Boundary-Layer Meteorology, 99(2): 207-224.

Kucherenko, S., Rodriguez-Fernandez, M., Pantelides, C. and Shah, N., 2009. Monte Carlo evaluation of derivative-based global sensitivity measures. Reliability Engineering & System Safety, 94(7): 1135-1148.

Kullback, S. and Leibler, R., 1951. On Information and Sufficiency. The Annals of Mathematical Statistics, 22(1): 79-86.

Lavigne, M.B., Ryan, M.G., Anderson, D.E., Baldocchi, D.D., Crill, P.M., Fitzjarrald, D.R., Goulden, M.L., Gower, S.T., Massheder, J.M., McCaughey, J.H., Rayment, M. and Striegl, R.G., 1997. Comparing nocturnal eddy covariance measurements to estimates of ecosystem respiration made by scaling chamber measurements at six coniferous boreal sites. Journal of Geophysical Research-Atmospheres, 102(D24): 28977-28985.

Law, B.E., Ryan, M.G. and Anthoni, P.M., 1999. Seasonal and annual respiration of a ponderosa pine ecosystem. Global Change Biology, 5(2): 169-182.

Lee, X., 2000. Air motion within and above forest vegetation in non-ideal conditions. Forest Ecology and Management, 135(1-3): 3-18.

Lele, S.R., 2004. Evidence functions and the optimality of the law of likelihood In: M.L. Taper and S.R. Lele (Editors), The Nature of Scientific Evidence: Statistical, Philosophical and Empirical considerations. The University of Chicago Press, Chicago, USA.

Leuning, R., 1990. Modelling stomatal behavior and photosynthesis of Eucalyptus grandis. Australian Journal of Plant Physiology 17(2): 159-175.

Leuning, R., 1995. A critical appraisal of a combined stomatal-photosynthesis model for C3 plants. Plant, Cell and Environment, 18: 339-355.

Leuning, R., Kelliher, F.M., Depury, D.G.G. and Schulze, E.D., 1995. Leaf nitrogen, photosynthesis, conductance and transpiration - scaling from leaves to canopies. Plant Cell and Environment, 18(10): 1183-1200.

Lewis, R. M., Torczon, V. and Trosset, M. W., 2000. Direct search methods: then and now. Journal of Computational and Applied Mathematics 124(1-2): 191-207.

LI-COR, I., 1992. LAI-2000. Plant Canopy Analyzer. Operating Manual.

Liu, Q., Edwards, N.T., Post, W.M., Gu, L., Ledford, J., Lenhart, S., 2006. Temperature-independent diel variation in soil respiration observed from a temperate deciduous forest. Global Change Biology, 12(11): 2136-2145.

Lloyd, J. and Taylor, J.A., 1994. On the temperature-dependence of soil respiration. Functional Ecology, 8(3): 315-323.

Luo, Y. and Zhou, X., 2006. Soil Respiration and the Environment. Elsevier, Inc, San Diego, CA, USA.

Luo, Y., Medlyn, B., Hui, D., Ellsworth, D., Reynolds, J. and Katul, G., 2001. Gross primary productivity in Duke forest: Modelling synthesis of CO_2 experiment and eddy-flux data. Ecological Applications, 11(1): 239-252.

Mariscal, M.J., Orgaz, F. and Villalobos, F.J., 2000a. Modelling and measurement of radiation interception by olive canopies. Agricultural and Forest Meteorology, 100(2-3): 183-197.

Mariscal, M.J., Orgaz, F. and Villalobos, F.J., 2000b. Radiation-use efficiency and dry matter partitioning of a young olive (Olea europaea) orchard. Tree Physiology, 20(1): 65-72.

Mauder, M. and Foken, T., 2011. Eddy-Covariance Software Package TK3. University of Bayreuth. http://www.bayceer.uni-bayreuth.de/mm/de/software/software/software_dl.php

Migliavacca, M., Reichstein, M., Richardson, A.D., Colombo, R., Sutton, M.A., Lasslop, G., Tomelleri, E., Wohlfahrt, G., Carvalhais, N., Cescatti, A., Mahecha, M.D., Montagnani, L., Papale, D., Zaehle, S., Arain, A., Arneth, A., Black, A.T., Carrara, A., Dore, S., Gianelle, D., Helfter, C., Hollinger D., Kutsch, W.L., Lafleur, P.M., Nouvellon, Y., Rebmann, C., da Rocha, H.R., Rodeghiero, M., Roupsard, O., Sebastia, M.T., Seufert, G., Soussana, J.F. van der Molen, M.K., 2011. Semiempirical modeling of abiotic and biotic factors controlling ecosystem respiration across eddy covariance sites. Global Change Biology, 17(1): 390-409.

Miller, J.B., 1966. A formula for average foliage density. Australian Journal of Botany, 15(1): 141.

Mittelbach, H., Casini, F., Lehner, I., Teuling, A.J. and Seneviratne, S.I., 2011. Soil moisture monitoring for climate research: Evaluation of a low-cost sensor in the framework of the Swiss Soil Moisture Experiment (SwissSMEX) campaign. Journal of Geophysical Research-Atmospheres, 116.

Monin, A.S., Obukhov, A.M., 1954. Osnovnye zakonomernosti turbulentnogo peremesivanija v prizemnom sloe atmosfery (Basic laws of turbulent mixing in the atmosphere near the ground). Trudy geofizinst AN SSSR 24 (151): 163–187

Moore, C.J., 1986. Frequency-response corrections for eddy-correlation systems. Boundary-Layer Meteorology, 37(1-2): 17-35.

Moriana, A., Orgaz, F. Pastor, M. and Fereres, E. 2003. Yield Responses of a Mature Olive Orchard to Water Deficits. Journal of the American Society of Horticultural Science. 128 (3): 425–431.

Moriana, A., Villalobos, F. J., Fereres, E. 2002. Stomatal and photosynthetic responses of olive (Olea europaea L.) leaves to water deficits. Plant, Cell and Environment, 25: 395–405.

Morris, M. D. 1991. Factorial sampling plans for preliminary computational experiments. Technometrics, 33(2), 161-174.

Niinemets, U., Dıaz-Espejo, A., Flexas, J., Galmes, J. and Warren, C. R. 2009. Importance of mesophyll diffusion conductance in estimation of plant photosynthesis in the field. Journal of Experimental Botany, 60 (8): 2271–2282

Norman, J. M., Campbell, C. L., 1998. Chapter 15. The light environment of plant canopies. In: Norman, J. M., Campbell, C. L. An Introduction Environmental Biophysics. New York, Springer-Verlag, Inc.

Norman, J.M. and Welles, J.M., 1983. Radiative Transfer in an Array of Canopies1. Agron. J., 75(3): 481-488.

NRCS, 2006. Keys to soil taxonomy. Natural Resources Conservation Service, Washington, D.C., 332 pp.

Owen, A.B., 1998. Scrambling Sobol' and Niederreiter–Xing Points. Journal of Complexity, 14(4): 466-489.

Perez-Priego, O., Testi, L., Orgaz, F. and Villalobos, F., Submitted. Plant respiration of an olive orchard. Functional Plant Biology.

Perez-Priego, O., Testi, L., Orgaz, F. and Villalobos, F.J., 2010. A large closed canopy chamber for measuring CO2 and water vapour exchange of whole trees. Environmental and Experimental Botany, 68(2): 131-138.

Phillips, C.L., Nickerson, N., Risk, D. and Bond, B.J., 2011. Interpreting diel hysteresis between soil respiration and temperature. Global Change Biology, 17(1): 515-527.

Press, W.H., Teukolsky, S.A., Vetterling, W.T. and Flannery, B.P., 2007. Numerical Recipes: The Art of Scientific Computing. Cambridge University Press.

Pronk, A.A., Goudriaan, J., Stilma, E. and Challa, H., 2003. A simple method to estimate radiation interception by nursery stock conifers: a case study of eastern white cedar. NJAS - Wageningen Journal of Life Sciences, 51(3): 279-295.

Reichstein, M. and Beer, C., 2008. Soil respiration across scales: The importance of a model–data integration framework for data interpretation. Journal of Plant Nutrition and Soil Science, 171(3): 344-354.

Reichstein, M., Tenhunen, J.D., Roupsard, O., Ourcival, J.M., Rambal, S., Miglietta, F., Peressotti, A., Pecchiari, M., Tirone, G. and Valentini, R., 2002. Severe drought effects on ecosystem CO_2 and H_2O fluxes at three Mediterranean evergreen sites: revision of current hypotheses? Global Change Biology, 8(10): 999-1017.

Reicosky, D.C., Wagner, S.W. and Devine, O.J., 1990. Methods of calculating carbon-dioxide exchange-rates for maize and soybean using a portable field chamber. Photosynthetica, 24(1): 22-38.

Richardson, A.D. and Hollinger, D.Y., 2005. Statistical modeling of ecosystem respiration using eddy covariance data: Maximum likelihood parameter estimation, and Monte Carlo simulation of model and parameter uncertainty, applied to three simple models. Agricultural and Forest Meteorology, 131(3-4): 191-208.

Richardson, A.D., Braswell, B.H., Hollinger, D.Y., Burman, P., Davidson, E.A., Evans, R.S., Flanagan, L.B., Savage K., Urbanski, S.P. and Wofsy, S.C., 2006. Comparing simple respiration models for eddy flux and dynamic chamber data. Agricultural and Forest Meteorology, 141(2-4): 219-234.

Richardson, A.D., Mahecha, M.D., Falge, E., Kattge, J., Moffat, A.M., Papale, D., Reichstein, M., Stauch, V.J., Braswell, B.H., Churkina, G., Kruijt, B. and Hollinger, D.Y., 2008. Statistical properties of random CO_2 flux measurement uncertainty inferred from model residuals. Agricultural and Forest Meteorology, 148(1): 38-50.

Richter, G.M., Acutis, M., Trevisiol, P., Latiri, K. and Confalonieri, R., 2010. Sensitivity analysis for a complex crop model applied to Durum wheat in the Mediterranean. European Journal of Agronomy, 32(2): 127-136.

Ruppert, J., Mauder, M., Thomas, C. and Luers, J., 2006. Innovative gap-filling strategy for annual sums of CO_2 net ecosystem exchange. Agricultural and Forest Meteorology, 138(1-4): 5-18.

Saltelli, A., Ratto, M., Andres, T., Campolongo, F., Cariboni, J., Gatelli, D., Saisan, M., Tarantola and S., 2008. Global Sensitivity Analysis: The Primer. John Wiley & Sons, Ltd., 292 pp.

Savage, K., Davidson, E.A. and Richardson, A.D., 2008. A conceptual and practical approach to data quality and analysis procedures for high-frequency soil respiration measurements. Functional Ecology, 22(6): 1000-1007.

Savage, K., Davidson, E.A., Richardson, A.D. and Hollinger, D.Y., 2009. Three scales of temporal resolution from automated soil respiration measurements. Agricultural and Forest Meteorology, 149(11): 2012-2021.

Scariano, L., Lo Bianco, R., Di Marco, L. and Policarpo, M., 2008. Dynamics of dry matter partitioning in young 'Nocellara del Belice' olive trees. In: Özkaya, M. T., Lavee, S., Ferguson, L., Proceedings of the Fifth International Symposium on Olive Growing, Vols 1 and 2. Acta Horticulturae, pp. 397-401.

Schotanus, P., Nieuwstadt, F.T.M. and Debruin, H.A.R., 1983. Temperature measurement with a sonic anemometer and its application to heat and moisture fluxes. Boundary-Layer Meteorology, 26(1): 81-93.

Schulze, E.D. , Leuning, R. and Kelliher, F. M. 1995. Environmental Regulation of Surface Conductance for Evaporation from Vegetation. Vegetatio, 121: 79-87.

Searles, P.S., Saravia, D.A. and Rousseaux, M.C., 2009. Root length density and soil water distribution in drip-irrigated olive orchards in Argentina under arid conditions. Crop and Pasture Science, 60(3): 280-288.

Shannon, C. E., 1948. A Mathematical Theory of Communication. The Bell System Technical Journal, 27: 379–423.

Sinoquet, H., Le Roux, X., Adam, B., Ameglio, T., Daudet, F. A. 2001. RATP: a model for simulating the spatial distribution of radiation absorption, transpiration and photosynthesis within canopies: application to an isolated tree crown. Plant, Cell and Environment, 24(4): 395-406.

Sinoquet, H., Stephan, J., Sonohat, G., Lauri, P. E. and Monney, Ph. 2007. Simple equations to estimate light interception by isolated trees from canopy structure features: assessment with three-dimensional digitized apple trees. New Phytologist, 175: 94–106.

Smith, R. L., 1999. Bayesian and frequentist approaches to parametric predictive inference. In: Bernardo, J. M., Berger, J. O., Dawid, A. P. and Smith, A. F. M. Bayesian Statistics. Oxford University Press.

Sobol, I. M. and Kucherenko, S. 2009. Derivative based global sensitivity measures and their link with global sensitivity indices. Mathematics and Computers in Simulation, 79, 3009–3017.

Sofo, A., Manfreda, S., Fiorentino, M., Dichio, B., Xiloyannis, C. 2008. The olive tree: a paradigm for drought tolerance in Mediterranean climates. Hydrology Earth System Sciences, 12: 293–301.

Stauch, V.J., Jarvis, A.J. and Schulz, K., 2008. Estimation of net carbon exchange using eddy covariance CO_2 flux observations and a stochastic model. Journal of Geophysical Research, 113(D3).

Sugiura, N., 1978. Further analysts of the data by Akaike' s information criterion and the finite corrections. Communications in Statistics - Theory and Methods, 7(1): 13-26.

Tang, J. and Baldocchi, D.D., 2005. Spatial-temporal variation in soil respiration in an oak-grass savanna ecosystem in California and its partitioning into autotrophic and heterotrophic components. Biogeochemistry, 73(1): 183-207.

Testi, L., Orgaz, F. and Villalobos, F., 2008. Carbon exchange and water use efficiency of a growing, irrigated olive orchard. Environmental and Experimental Botany, 63(1-3): 168-177.

Testi, L., Villalobos, F. J. and Orgaz, F. 2004. Evapotranspiration of a young irrigated olive orchard in southern Spain. Agricultural and Forest Meteorology, 121: 1–18.

Ulrich, A., 1952. Physiological bases for assessing the nutritional requirements of plants. Annual Plant Physiology, 3: 207 - 228.

van Oijen, M., Schapendonk, A. and Hoglind, M. 2010. On the relative magnitudes of photosynthesis, respiration, growth and carbon storage in vegetation. Annals of Botany 105: 793 –797

van Wijk, M.T., van Putten, B., Hollinger, D.Y. and Richardson, A.D., 2008. Comparison of different objective functions for parameterization of simple respiration models. Journal of Geophysical Research G: Biogeosciences, 113(3).

Van't Hoff, J.H., 1898. Lectures on Theoretical and Physical Chemistry. Part I. Chemical Dynamics (translated by R. A. Lehfeldt). Edward Arnold, London, 268 pp.

Venables, W.N. and Ripley, B.D., 2002. Modern Applied Statistics with S. Statistics and Computing. Springer. 495 pp.

Verhoef, A., 1995. Surface energy balance of shrub vegetation in the Sahel. Wageningen UR. 247 pp.

Vickers, D. and Mahrt, L., 1997. Quality control and flux sampling problems for tower and aircraft data. Journal of Atmospheric and Oceanic Technology, 14(3): 512-526.

Villalobos, F. J. 2008. Comment on ''Relationships between single tree canopy and grass net radiations''. Agricultural and Forest Meteorology, 148: 693–695

Villalobos, F.J., Orgaz, F., Testi, L. and Fereres, E., 2000. Measurement and modeling of evapotranspiration of olive (*Olea europaea* L.) orchards. European Journal of Agronomy, 13(2-3): 155-163.

Villalobos, F.J., Perez-Priego, O., Testi, L., Morales A. and Orgaz, F., 2012. Effects of water supply on carbon and water exchange of olive trees. European Journal of Agronomy, 40: 1-7.

Villalobos, F.J., Testi, L., Hidalgo, J., Pastor, M. and Orgaz, F., 2006. Modelling potential growth and yield of olive (Olea europaea L.) canopies. European Journal of Agronomy, 24(4): 296-303.

Vossen, P. 2007. Olive oil: History, production, and characteristics of the world's classic oils. Hortscience, 42 (5): 1093-1100.

Walker, A.M., 1969. On the Asymptotic Behaviour of Posterior Distributions. Journal of the Royal Statistical Society. Series B (Methodological), 31(1): 80-88.

Wang, Y. P. and Jarvis, P. G., 1990b. Influence of crown structural-properties on PAR absorption, photosynthesis and transpiration in Sitka spruce - Application of a model (Maestro). Tree Physiology 7(1-4): 297-316.

Wang, Y.P. and Jarvis, P.G., 1990a. Description and validation of an array model - Maestro. Agricultural and Forest Meteorology, 51(3-4): 257-280.

Webb, E.K., Pearman, G.I. and Leuning, R., 1980. Correction of flux measurements for density effects due to heat and water vapor transfer. Quarterly Journal of the Royal Meteorological Society, 106(447): 85-100.

Wilczak, J.M., Oncley, S.P. and Stage, S.A., 2001. Sonic anemometer tilt correction algorithms. Boundary-Layer Meteorology, 99(1): 127-150.

Wohlfahrt, G., Anfang, C., Bahn, M., Haslwanter, A., Newesely, C., Schmitt, M., Drosler, M., Pfadenhauer, J. and Cernusca, A., 2005. Quantifying nighttime ecosystem respiration of a meadow using eddy covariance, chambers and modelling. Agricultural and Forest Meteorology, 128(3-4): 141-162.

Xiloyannis, C., Dichio, B., Nuzzo, V., Celano, G., 1999. Defense strategies of olive against water stress. Acta Horticulturae (ISHS) 474: 423-426.

Yin, X. and Struik, P. C., 2009. C3 and C4 photosynthesis models: An overview from the perspective of crop modelling. NJAS - Wageningen Journal of Life Sciences 57(1): 27-38.

Zucchini, W. 2000. An introduction to model selection. Journal of Mathematical Psychology, 44: 41 61.

Appendix I. Additional Figures and Tables

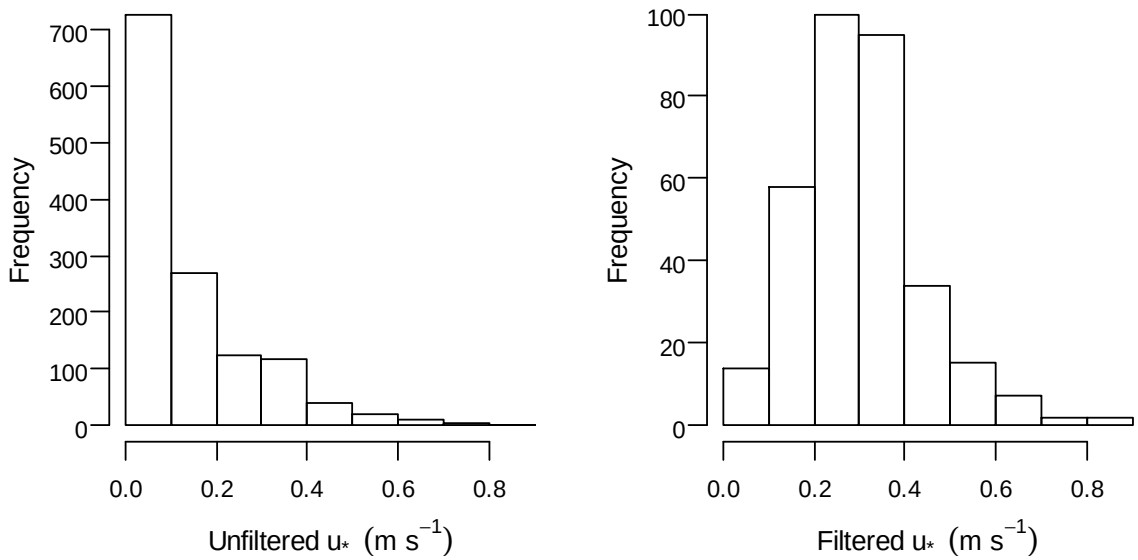

Figure A1.1: Frequency histogram of nighttime friction velocity before and after applying the filters. It shows that most fluxes at low friction velocities were eliminated by the filters.

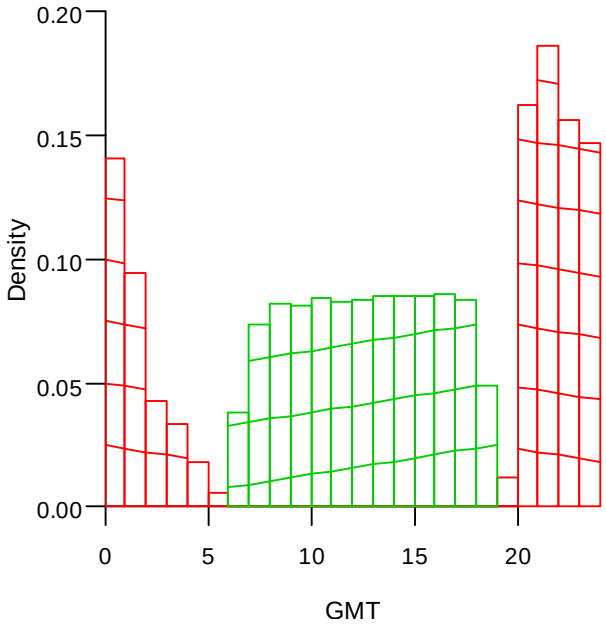

Figure A1.2: Probability density histogram of filtered fluxes during daytime (green, lines from bottom-left to top-right) and nighttime (red, lines from top-left to bottom-right). The probability density is calculated independently for nighttime and daytime data, so that the bar height is not in the same scale. The major gaps during the day occur at sunrise and sunset, whereas during the night the proportion of rejected fluxes increases from sunset to sunrise.

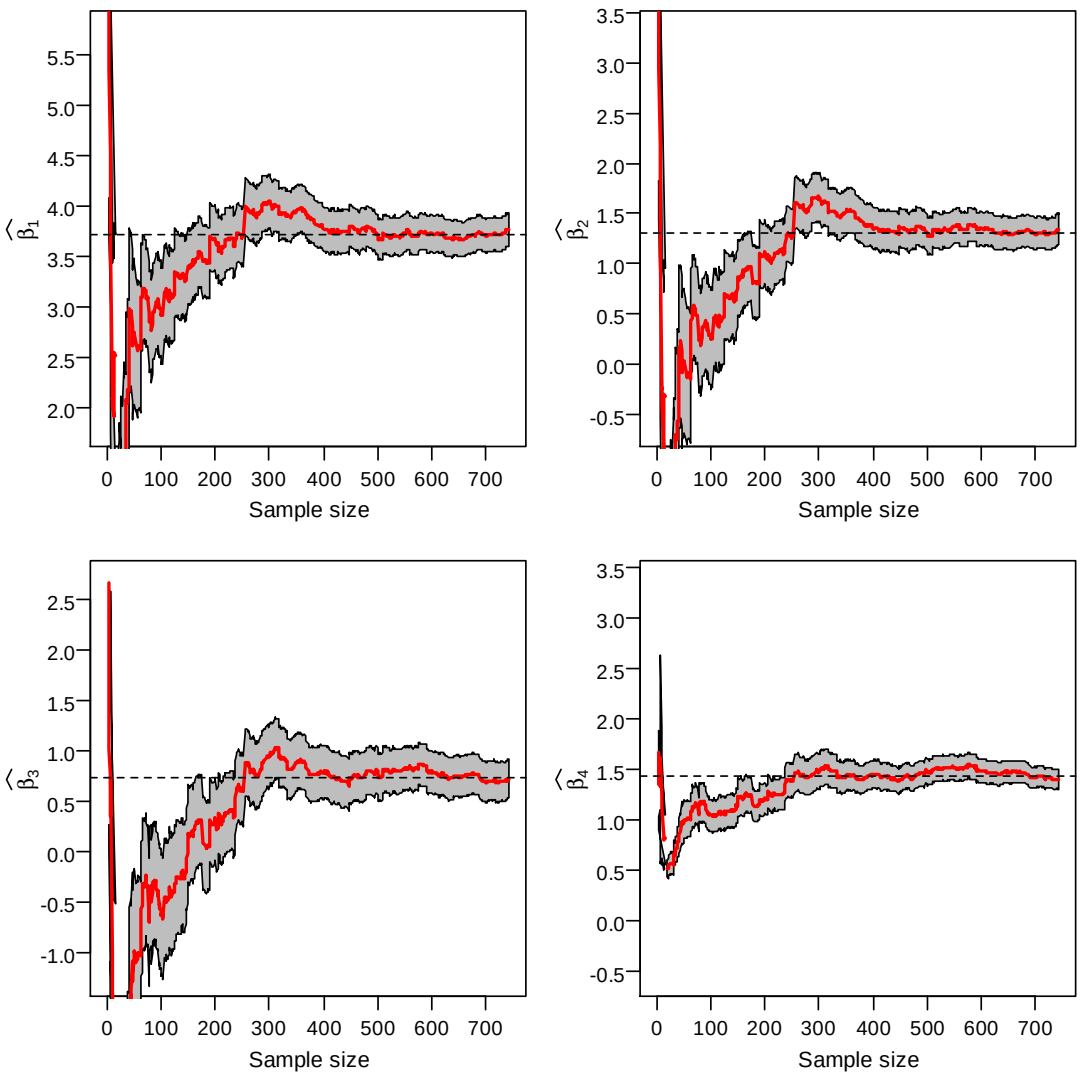

Figure A1.3: Maximum likelihood estimation of the parameters of the descriptive model 5 of ecosystem respiration combined with a Normal probability distribution with homogeneous variance, for increasing sample sizes. The grey areas represent ±σ around the maximum likelihood estimation. The samples were selected by a Sobol low-discrepancy sequence without scrambling, using the R package "randtoolbox" (Dutang and Savicky, 2010). Each sample n+1 contains all the elements of the sample n, plus an additional datum not contained in sample n, selected as to ensure that the sample was always evenly distributed in time. This figure represents an example of the convergence of the maximum likelihood estimator towards β_0, which is approximated by the dashed line. The uncertainty in the estimation of each parameter also decreases as sample size increases. It can be observed that for samples bigger than 400 data points, the values of the parameters (and their uncertainties) barely change.

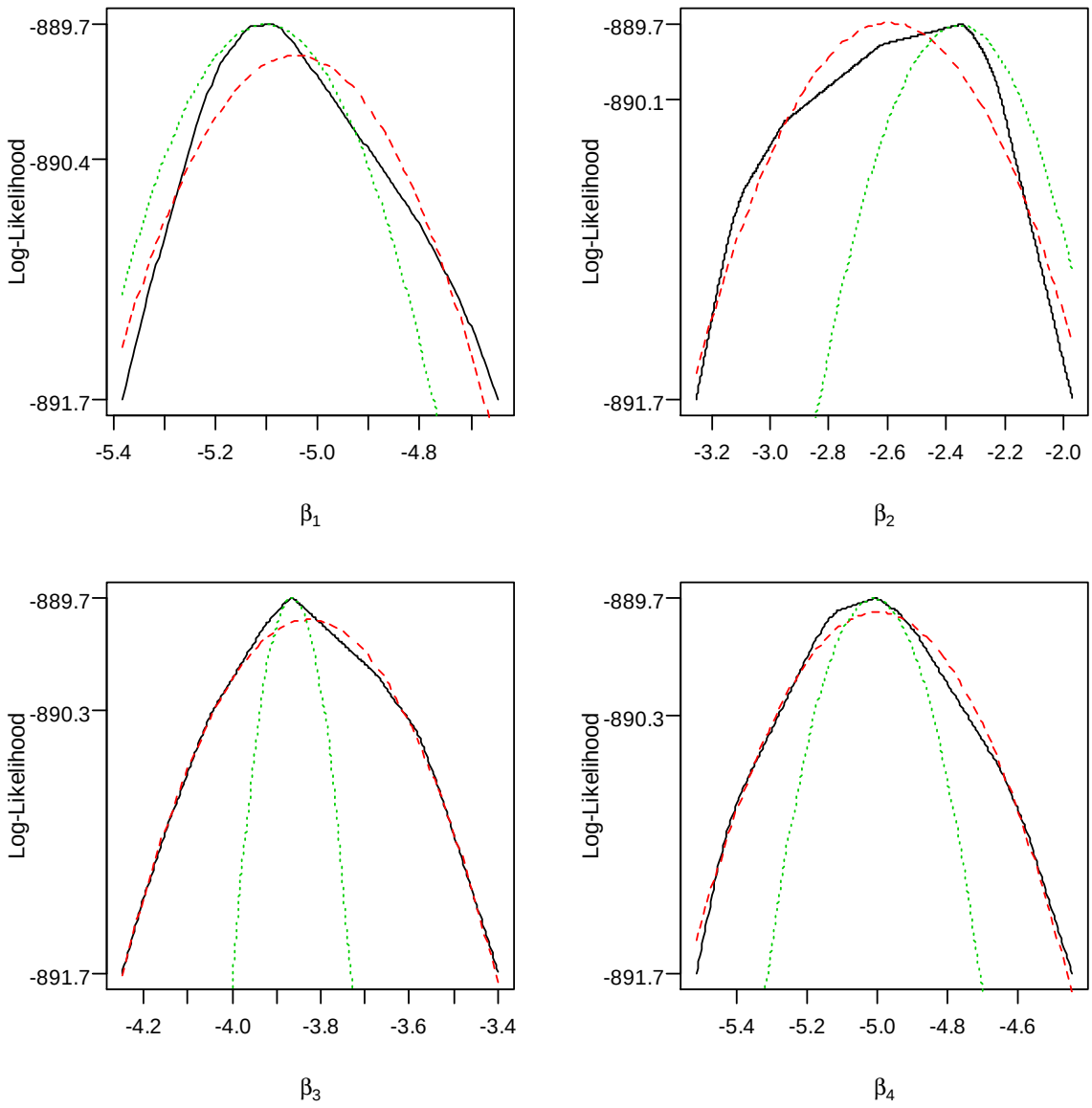

Figure A1.4: Quadratic approximation to log-likelihood profiles of the first four parameters of model 64 of soil respiration in the alley[13], bounded for a log-likelihood of 2 units (equivalent to a 95% probability interval with the Normal approximation). The black solid line is the likelihood profile, the red dashed line the quadratic function approximated to the log-likelihood and the green, dotted line the curvature predicted by the second partial derivative at the maximum. The quadratic function is a more accurate approximation to the log-likelihood function than the approximation based on the derivative at the maximum likelihood. For example, the local derivative will predict a 95% interval for β_{13} of -4.00 to -3.87, as opposed to -4.25 to -3.40 predicted by the more accurate quadratic approximation. The intervals for each parameter can always be determined directly from the likelihood functions, but to evaluate the effect of parameter uncertainty on predictive uncertainty, a probability density function needs to be estimated from the likelihood function in order to apply Bayesian integration (i.e. equation 1.17).

[13] Model 64 that includes the effect of soil water content on temperature sensitivity and a seasonal effect on reference respiration and defines the parameters of reference respiration for each location

Appendix II. Original formulations of published models

Model 1 is equivalent to equation 1.11 in Lloyd and Taylor (1994)

$$R = R_{10} e^{E_0\left(\frac{1}{283.15 - T_0} - \frac{1}{T_{soil} + 273.15 - T_0}\right)} \quad \text{(A2.1)}$$

Where R_{10}, E_0 and T_0 are equivalent to β_1, β_2 and β_3, respectively. Note however that in this study the reference temperature was set to 20 °C instead of 10 °C which means that 293.15 should be used instead of 283.15 in the exponent.

Model 2 is equivalent to the model D2 in Richardson et al. (2006)

$$R = \theta_1 \left(\theta_2 + \theta_3 \sin JD_\pi + \theta_4 \cos JD_\pi\right)^{(T - T_{ref})/10} \quad \text{(A2.2)}$$

Where θ is used instead of β to describe the empirical parameter and the reference temperature is not predefined. JD_π is equivalent to D in this study.

Model 3 is equivalent to equation A2 and A3 combined in Reichstein et al. (2002) but soil water content was used instead of relative soil water content and the independent effect of soil water content was taken out

$$R_{eco} = R_{eco,ref}\, f\left(T_{soil}, RSWC\right) g\left(RSWC\right) \quad \text{(A2.3)}$$

$$f\left(T_{soil}, RSWC\right) = e^{E_0(RSWC)\left(\frac{1}{T_{ref} - T_0} - \frac{1}{T_{soil} - T_0}\right)} \quad \text{(A2.4)}$$

$$E_0 = a + b \cdot RSWC \quad \text{(A2.5)}$$

Where $R_{eco,ref}$, a, b, and T_0 are equivalent to β_1 through β_4. The function g described an effect of soil water content on the reference ecosystem respiration. Note that using soil water content instead of relative soil water content implies dividing RSWC by a constant (range of soil water content in the soil) which would modify proportionally parameter b (β_3) without affecting the calculations of the model.

Appendix III. Ellipsoidal leaf angle distribution

The G function is defined as the ratio between the projection of leaf area on the plane perpendicular to the direction of solar beam and the leaf area, and it depends on the leaf angle distribution and solar zenith angle (Z). The ellipsoidal model assumes that the distribution of leaf angles is equivalent to the distribution of area elements on the surface of a spheroid[14] (Norman and Campbell, 1998), so that the average leaf projections can be substituted by the projections of the spheroid.

Campbell (1986) used the solar elevation angle (β) in the original formulation of the ellipsoidal leaf angle distribution, but in this study, the solar zenith angle is used, knowing that sin β = cos Z and cos β = sin Z. Also, in the original formulation the extinction coefficient was calculated, which is equivalent to the G function but projecting the leaf area on the horizontal plane.

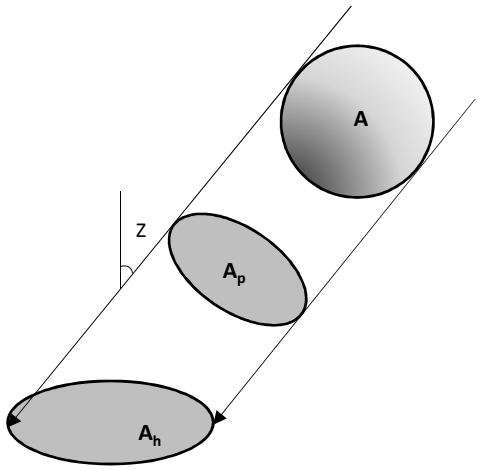

Figure AIII.1: Projection of a sphere (A) on the horizontal plane (A_h) and the plane perpendicular to the direction of solar beams (A_p), for a zenith angle Z. A sphere is a special case of spheroid and it is used for simplicity.

The extinction coefficient is defined as

$$k = \frac{A_h}{A} \qquad \text{(A3.1)}$$

Where A is the surface of the spheroid and A_h is the projection on the horizontal plane (figure AIII.1). The G function is

$$G = \frac{A_p}{A} \qquad \text{(A3.2)}$$

Where A_p is the projection on the plane perpendicular to the solar beam. It follows from trigonometry that

[14] A spheroid is a surface obtained by rotating an ellipse around one of its axis.

$$A_p = A_h \cos Z \tag{A3.3}$$

Thus, the relationship between the extinction coefficient and G is

$$G = k \cos Z \tag{A3.4}$$

Being aware of these relations, equation A3.2 is transformed into

$$G = \frac{\pi b^2 \cos Z \sqrt{1 + \frac{a^2}{b^2} \tan^2 Z}}{A} \tag{A3.5}$$

Where a and b are the horizontal and vertical radii of the spheroid. For Z = 0 rad, the value of G is

$$G_0 = \frac{\pi b^2}{A} \tag{A3.6}$$

And for Z = π/2, the value of G is

$$G_{\pi/2} = \frac{\pi a b}{A} \tag{A3.7}$$

Developing further equation A3.5 gives

$$G = \sqrt{\left(\frac{\pi b^2}{A}\right)^2 \cos^2 Z + \left(\frac{\pi a b}{A}\right)^2 \sin^2 Z} \tag{A3.8}$$

And substituting equations A3.6 and A3.7 in equation A3.8 results into

$$G = \sqrt{{G_0}^2 \cos^2 Z + {G_{\pi/2}}^2 \sin^2 Z} \tag{A3.9}$$

This expression is valid for any type of spheroid (i.e. any value of a and b) and is much simpler than the original formulation (equation 2.2). By definition, the parameter X is the ratio between a and b, which in the new formulation can be expressed as

$$X = \frac{a}{b} = \frac{G_0}{G_{\pi/2}} \tag{A3.10}$$

This formulation allows calculating the parameter X directly from empirical values of G_0 and $G_{\pi/2}$, as done in this study with the values published by Mariscal et al. (2000a). For a value of G_0 = 0.78 and $G_{\pi/2}$ = 0.30 in Mariscal et al. (2000), X = 2.6.

Appendix IV. Coupling of stomatal conductance and photosynthesis

Maestra solves the coupling of stomatal conductance and photosynthesis by applying the method of Leuning (1990) which can be adapted to any stomatal conductance model based on the model of Ball et al. (1987). This method yields a quadratic equation that enables calculating A_v and A_q in equation 2.3 and then the value of A may be derived. To show the link between the quadratic equation and equations 2.3 through 2.9 in the main text, the derivation of the analytical solution will be shown in this appendix.

Photosynthesis limited by Rubisco activity (equations 2.3 and 2.4) and photosynthesis limited by electron transport (equations 2.3 and 2.5) can be expressed in a general form as follows

$$A = \gamma\left[\frac{C_i - \Gamma_*}{C_i + \beta}\right] - R_d \qquad \text{(A4.1)}$$

Which is equivalent to equation 2.3-2.4 for $\gamma = V_{c,max}$ and $\beta = k_c\left(1 + o_i / k_o\right)$ and to equation 2.3-2.5 for $\gamma = J/4$ and $\beta = 2\,\Gamma_*$. The only unknown term in the right-hand side of equation A4.1 is C_i, as the rest is either known, given the environmental inputs, or a parameter of the model. Substituting equation 2.8 (supply function) and 2.9 (stomatal conductance) of the main text yields

$$\frac{A}{C_s - C_i} = g_{s0} + \frac{a_1 A}{C_s - \Gamma} f \qquad \text{(A4.2)}$$

Where $f = \left(1 + D_s / D_0\right)^{-1}$ (whereas $f = h_s$ in Leuning (1990)). Stomatal conductance has been defined for CO_2 fluxes in this study, but it was defined for H_2O in fluxes in Leuning (1990), being the latter 1.6 times higher due to higher diffusivity of H_2O molecules. To facilitate the comparison with the original formulation, the constants that multiply A in the right hand side of equation A4.2 are grouped into the term X

$$X = \frac{a_1 f}{C_s - \Gamma} \qquad \text{(A4.3)}$$

This is equivalent to equation 16 in Leuning (1990). Rearranging equation A4.2 and considering equation A4.3, we obtain

$$A\left(\frac{1}{C_s - C_i} - X\right) - g_{s0} = 0 \qquad \text{(A4.4)}$$

So far we have a function of A and C_i, both unknown, but A is a function of C_i. Substituting A4.4 for equation A4.1 and expanding the product it results into

$$\frac{\gamma(C_i-\Gamma_*)}{(C_i+\beta)(C_s-C_i)}-\frac{R_d}{C_s-C_i}-\frac{\gamma X(C_i-\Gamma_*)}{C_i+\beta}+(XR_d-g_{s0})=0 \qquad \text{(A4.5)}$$

Where the only unknown is C_i and thus we do not need additional equations. The following steps are taken to arrive at an expression equivalent to the original equation given by Leuning (1990). Multiplying all terms by $(C_i+\beta)(C_s-C_i)$ results in

$$\gamma(C_i-\Gamma_*)-R_d(C_i+\beta)-\gamma X(C_i-\Gamma_*)(C_s-C_i)+(R_dX-g_{s0})(C_i+\beta)(C_s-C_i)=0 \qquad \text{(A4.6)}$$

and when the expression is expanded it leads to

$$\begin{aligned}&\gamma C_i-\gamma\Gamma_*-R_dC_i-R_d\beta-\gamma C_iC_sX+\gamma C_i^2X+\gamma\Gamma_*C_sX-\\&\gamma\Gamma_*C_iX+XR_dC_sC_i+XR_dC_s\beta-XR_dC_i^2-XR_dC_i\beta-\\&g_{s,0}C_sC_i-g_{s,0}C_s\beta+g_{s,0}C_i^2+g_{s,0}C_i\beta=0\end{aligned} \qquad \text{(A4.7)}$$

This can be reorganized into a more generic form

$$aC_i^2+bC_i+c=0 \qquad \text{(A4.8)}$$

Where

$$\begin{aligned}a&=g_{s0}+X(\gamma-R_d)\\b&=(1-C_sX)(\gamma-R_d)+g_{s0}(\beta-C_s)-X(R_d\beta+\gamma\Gamma_*)\\c&=(C_sX-1)(\gamma\Gamma_*+\beta R_d)-g_{s0}\beta C_s\end{aligned} \qquad \text{(A4.9)}$$

Equations A4.8 and A4.9 are equivalent to equations 14 and 15 in Leuning (1990) with the difference that the first term of b and c in the original formula is $(1.6-C_sX)$, because stomatal conductance was defined for H_2O fluxes.

Equation A4.8 is applied twice to calculate C_i for the cases of photosynthesis limited by Rubisco activity and electron transport. Then, applying equation A4.1, A_v and A_q are obtained. The larger root is always used. Leaf temperature influences photosynthesis through the temperature response of the parameters, D_s through the value of X and C_s appears in the terms b and c. Note that, when the assumption of perfect coupling is not made, one should recalculate iteratively the leaf temperature with the energy balance (i.e. net absorbed solar radiation must be equal to the sum of sensible and latent heat fluxes). Also, C_s and D_s should be calculated from CO_2 concentration, VPD in the air and the boundary layer conductance.

Baldocchi (1994) derived a cubic equation that included the effect of boundary layer conductance, with a similar procedure as Leuning (1990), but the approach in model Maestra is to include the effect of the boundary layer conductance in the energy balance algorithm.

Appendix V. Quasi-Monte Carlo Integration

Given a continuous function f(x), where x varies in the range [a, b], the average value of I_f is

$$I_f = \frac{\int_a^b f(x)\,dx}{b-a} \tag{A5.1}$$

If the primitive of the function is unknown, it can be approximated numerically using quadrature methods (Press et al., 2007). Different methods exist, but they will always differ from the true value by an integration error. An efficient quadrature method is the Monte Carlo integration method, as the integration error does not depend on the dimensions of the function (in this study, the dimensions are the different parameters considered in the sensitivity analysis). The Monte Carlo method defines the average of f (a function of parameter x) as:

$$I_N = \frac{1}{N}\sum_{i=1}^{N} f(x_i) \tag{A5.2}$$

Where x_i are independent and equally distributed random samples from a uniform distribution defined by the range [a, b] and N is the number of samples. The integration error, ε, is defined as

$$\varepsilon = \left| I_f - I_N \right| \tag{A5.3}$$

Which cannot be evaluated directly as we do not know the value of I_f. However, applying the Central Limit Theorem, the estimation of the integration error is

$$\varepsilon_N = \frac{\sigma(f)}{N^{1/2}} \tag{A5.4}$$

Where σ(f) is the standard deviation of function values generated by the method. Equation A5.4 shows that the error decreases with the size of the sample and increases with the variability of the function, but does not depend on the number of parameters. Note that equation A5.2 can be extended to any number k of parameters

$$I_N = \frac{1}{N}\sum_{i=1}^{N} f(x_{1,i},\ldots,x_{k,i}) \tag{A5.5}$$

Where each value $x_{j,I}$ is sampled from an uniform distribution with limits b_j and a_j. Although the convergence rate (i.e. how fast does ε_N decrease) of the Monte Carlo method does not depend on the dimensions of the problem, it can still be too slow, requiring too many function evaluations before achieving a desired level of numerical accuracy (Caflisch, 1998). The reason for this is that random samples tend to cluster, leaving regions of the parameter space unexplored.

Empirical evidence shows that, for problems with a high number of dimensions, and when the variation generated by some of the dimensions is small (in the sensitivity analysis, it means a model where some of the parameters are non-influential); an algorithm with faster convergence rate is the quasi-Monte Carlo method (Caflisch, 1998). This method uses deterministic sequences of numbers, known as "low discrepancy sequences" that try to explore the region of variation of each parameter by maximizing uniformity rather than sampling than drawing samples from an uniform distribution.

Kucherenko et al. (2009) showed that, when calculating derivative-based global sensitivity indices, Sobol low discrepancy sequences converged faster than the Monte Carlo method or the trajectory-based method of Morris (1991). However, with a low discrepancy sequence one cannot calculate the integration error (ε_N), as the samples are not random. However, a small random perturbation of each value, that still maintains a high uniformity, allows calculating the integration error. This perturbation is known as "scrambling" and the method used in this study is that of Owen (1998) as implemented in the R package "randtoolbox" (Dutang and Savicky, 2010).

In this study, a value of N = 200 was used, to reach a relative integration error (i.e. ε_N/I_N) lower than 5% for all parameters, except for leaf reflectance, were the relative error varied between 15 and 20% in different scenarios. However, given the small sensitivity of the model to this parameter, it was not considered necessary to increase the size of the sample.

Prior to the sensitivity analysis, simulations were done with the nominal values of the parameters to determine the optimal time and spatial resolution of the model, so that a good numerical accuracy in the diurnal integration of photosynthesis flux was achieved but maintaining computational time within reasonable limits, as a global sensitivity analysis requires to perform many simulations with the model. The optimal settings were:

- The target crown was divided into three layers, with 12 sectors per layer.

- Diffuse radiation was simulated by integrating for the whole sky hemisphere using 9 zenith angles and 12 azimuth angles.

- Fluxes were calculated every 20 min, using weather data obtained at a time resolution of 10 min.

- To avoid the border effect, a virtual plot with 7 rows and 17 trees per row was created and photosynthesis was calculated in the tree at the center of the virtual plot.

Appendix VI. Results of the sensitivity analysis

Table AVI.1: Results of the sensitivity analysis. SC_i is the absolute local sensitivity coefficient, μ_i^* 10% and μ_i^* 20% is the global sensitivity index for variations of 10% and 20% of the parameters. ρ_{soil}, τ_{leaf} and ρ_{leaf} are the soil reflectance and leaf transmittance and reflectance for PAR radiation, respectively. g_{s0} is the stomatal conductance for null net photosynthesis, a_1 is the proportionality factor between net photosynthesis and stomatal conductance, D_0 describes the response of stomatal conductance to VPD, Γ is the CO_2 compensation point, θ describes the degree of curvature of electron transport response to absorbed PAR, α is the quantum efficiency, J_{max} and $V_{c,max}$ are the maximum rate of electron transport and activity of Rubisco, respectively. H_J and H_{Vc} are the activation energies of J_{max} and $V_{c,max}$. x is the parameter of the ellipsoidal leaf angle distribution, LAD is leaf area density and c' is the ratio between vertical and horizontal dimensions of the hedgerow.

	Scenario 1			Scenario 2			Scenario 3			Scenario 4		
	SC_i	μ_i^* 10%	μ_i^* 20%	SC_i	μ_i^* 10%	μ_i^* 20%	SC_i	μ_i^* 10%	μ_i^* 20%	SC_i	μ_i^* 10%	μ_i^* 20%
ρ_{soil}	0.00	0.00	0.00	0.01	0.01	0.01	0.00	0.00	0.00	0.00	0.01	0.00
τ_{leaf}	0.00	0.00	0.00	0.00	0.00	0.00	0.00	0.00	0.00	0.00	0.00	0.00
ρ_{leaf}	0.03	0.04	0.04	0.04	0.04	0.03	0.03	0.04	0.03	0.05	0.04	0.03
g_{s0}	0.01	0.01	0.01	0.02	0.03	0.04	0.02	0.03	0.03	0.06	0.09	0.11
a_1	0.02	0.02	0.02	0.04	0.06	0.06	0.03	0.04	0.04	0.08	0.10	0.09
D_0	0.01	0.01	0.01	0.02	0.02	0.03	0.01	0.01	0.02	0.05	0.06	0.05
Γ	0.01	0.01	0.01	0.02	0.01	0.01	0.01	0.01	0.01	0.02	0.02	0.02
θ	0.29	0.33	0.24	0.58	0.42	0.26	0.37	0.36	0.25	0.42	0.33	0.19
α	0.86	0.75	0.70	0.66	0.56	0.47	0.88	0.74	0.65	0.76	0.62	0.49
J_{max}	0.08	0.18	0.19	0.27	0.31	0.28	0.10	0.18	0.20	0.12	0.17	0.16
$V_{c,max}$	0.06	0.03	0.03	0.01	0.02	0.05	0.00	0.00	0.00	0.00	0.01	0.06
R_d	0.16	0.08	0.08	0.15	0.06	0.06	0.24	0.09	0.08	0.28	0.10	0.09
H_J	0.06	0.12	0.12	0.06	0.06	0.05	0.02	0.03	0.02	0.05	0.07	0.05
H_{Vc}	0.08	0.04	0.03	0.01	0.01	0.01	0.00	0.00	0.00	0.00	0.01	0.05
H_{Rd}	0.16	0.07	0.07	0.06	0.03	0.02	0.17	0.02	0.02	0.18	0.07	0.06
X	0.03	0.04	0.04	0.04	0.04	0.04	0.03	0.04	0.04	0.05	0.04	0.03
LAD	0.22	0.21	0.27	0.29	0.30	0.35	0.27	0.22	0.29	0.37	0.28	0.34
c'	0.09	0.20	0.17	0.12	0.17	0.14	0.07	0.19	0.15	0.12	0.18	0.14